Fall 12-20-2017

Fabrication and Characterization of Intricate Nanostructures

Treva T. Brown
University of New Orleans, ttbrown1@uno.edu

Fabrication and Characterization of Intricate Nanostructures

A Dissertation

Submitted to the Graduate Faculty of the
University of New Orleans
in partial fulfillment of the
requirements for the degree of

Doctor of Philosophy
in
Chemistry
Nanomaterials

by

Treva Tarnese Brown

B.Sc., Louisiana State University, 2011

December, 2017

To …

My parents,

Leslie and Gwen Brown

And my family, friends, and mentors who believed in me

Acknowledgements

The accomplishment of this work would not be possible if it were not for the continuous help, support, and mentorship of various faculty, family, and friends. I would first like to thank my advisor and mentor Professor John B. Wiley for allowing me to spread my creative research wings and embark on an enlightening and fulfilling microscopy journey that has opened doors to endless possibilities. I would also like to thank Professor Wiley for letting me be my true self which paved the way for me to impact various students on many levels in the chemistry department at the University of New Orleans as well as in the scientific community. Furthermore, I would like to graciously thank my committee members: Professor Matthew Tarr, Professor Mark Trudell, Professor Viktor Poltavets, and Professor Weilie Zhou for being supportive while challenging me to think in new, innovative ways to make my project come full circle.

Many thanks also to Professor Jayne Garno at Louisiana State University in Baton Rouge, LA for graciously opening the doors of her lab and allowing me to work on her atomic force microscopy instruments. Special thanks also go to the members of the Garno group that helped with imaging techniques as well as in understanding acquired data - Dr. Zachary Highland, Dr. Ashley Taylor, and Neepa Kuruupu. Moreover, I would also like to acknowledge Dr. Jibao He at Tulane University in New Orleans, LA for his help in Tulane's School of Science and Engineering electron microscopy lab to acquire FEG-transmission electron microscopy images.

To my current groupmates: Alexis Blanco, Clare Davis-Wheeler Chin, Shahid Khan, Pramathesh Maji, Anamika Poduval - I would like to thank all of you for you for your continuous motivation and friendship along with allowing me to be a part of your successes along your different journeys. And to my former groupmates: Dr. Sara Akbarian-Tefaghi, Dr. Elisha Josepha, Dr. Léa Gustin, Dr. Taha Rostamzadeh, Dr. Jagnyaseni Tripathy, Dr. Dariush Montasserasadi, Dr.

Shivaprasad Reddy Adireddy, Sarah Gauthier, Mayra Franco, and, Mark Granier - thank you for the continuous motivation during your time here in the Wiley Group as well as continuously checking in after completing your degrees. Your wisdom and knowledge has helped me in succeeding in my research endeavors.

I would also like to thank other colleagues at the University of New Orleans who have played tremendous roles in various stages of my Ph.D. journey. Dr. Kristen Williams, thank you for being my mentor and friend. Your constant motivation and determination for me to reach my goals has and always will be greatly appreciated. Also, a special thanks to Dr. Richard Prevost for always going above and beyond for anything I may have needed inside and outside of the lab. More gratitude goes to Dr. Zhi Zheng and Shuke Yan for electron microscopy assistance and to Daniel Adams for help in understanding acquired physical data.

Most important, I would not be where I am without keeping my faith in God and constantly being motivated by my parents, Mr. and Mrs. Leslie and Gwen Brown, to which this work is dedicated. I thank God for leading my way through this Ph.D. journey as well as for blessing me with loving, caring and supportive parents who have stood by me and helped in every capacity needed since day one. Moreover, I am truly thankful for the plethora of family, friends and mentors who make up my ever-encouraging support system. It has been through your motivational words of encouragement and wisdom that I have made it as the first in my family to earn a doctoral degree. It is my hope and prayer that my story of determination and perseverance through this scientific Ph.D. journey will inspire the next young woman or little girl to pursue a career in the Science, Technology, Engineering, and Mathematics area no matter what odds are placed against them. Remember to keep the faith and all else will be set in place for your success too.

Lastly, I would like to gratefully acknowledge financial support from the Louisiana Board of Regents Graduate Fellowship and the National Science Foundation (CHE-1412670).

Table of Contents

List of Figures

Abstract

Encapsulation of nanoparticles within hexaniobate nanoscrolls presents interesting advances in the formation of nanocomposites exhibiting unique multi-dimensional properties. Building upon previous successes, facile yet versatile wet-chemical and microwave-irradiation synthetic protocols for the fabrication of a series of hexaniobate composites are presented herein. Solvothermal and, more recently, microwave-assisted methods have been developed that allow for the fabrication of peapod-like structures. During solvothermal treatment, exfoliated hexaniobate nanosheets scroll around highly ordered chains of preformed nanoparticles (NPs) to produce nanopeapods (NPPs). This approach offers versatility and high yields, in addition to the potential for advanced functional device fabrication.

For the characterization of these materials, advanced techniques in atomic force microscopy (AFM) were used for investigating the surface of materials at the nanometer scale. Extensive physical, dynamic, and force modulation studies were performed on novel oxide nanocomposites by implementing particular scanning techniques to determine information such as topology, stress-induced behavior at the nanoscale, magnetic behavior, and frictional forces of the nanoscale materials. These composites were then analyzed by topological intermittent contact studies in tapping and contact mode, as well as with derivative techniques of these commonly used scanning probe approaches.

In addition to studying surfaces using conventional modes of AFM, the mechanical properties of these nanocomposites were measured via dynamic lateral force modulation (DLFM) and magnetic properties of functionalized magnetic nanosheets were mapped via magnetic sampling modulation (MSM). By utilizing the capabilities of the DLFM imaging mode, elastic

properties such as Young's Modulus were measured from force-distance curves. In addition to this modulation mode, MSM was used to selectively map the vibrating magnetic nanomaterials from a modulated electromagnetic field. The information obtained from these AFM techniques can be helpful in determining the relative structural behavior of these nanocomposites and gauge their use in various applications such as structural engineering of nanoarchitectures as well as studying magnetic characteristics of metal oxide nanocomposites that exhibit characteristics different from their bulk counterparts.

Keywords: Nanocomposites, nanopeapods, microwave-assisted reactions, solvothermal synthesis, nanoparticle encapsulation, layered inorganic nanostructures, atomic force microscopy, dynamic lateral force modulation, magnetic sampling modulation, transmission electron microscopy

Chapter 1 Introduction

1.1 One-Dimensional Nanomaterials

One-dimensional nanostructures have been of great interest in recent years because they show great promise in various scientific applications due to their inherent properties, one of which is their encapsulation potential.[1] Structures such as nanotubes, nanorods, and nanowires make up this classification of materials. Interest in these materials began with the discovery of carbon nanotubes (CNTs).[2] These materials were used in applications related to solar cells, catalysis, and hydrogen storage. In the late 1990s, these materials began to get exploited for their encapsulation potential. These structures became known as nanopeapods (NPPs) that consist of a linear array of nanoparticles, the "peas", encapsulated within the hollow space of a nanotube or nanoscroll, the "pod". The first peapod structure, C60@Carbon Nanotube (CNT), was discovered in 1998 by B. W. Smith.[3]

1.2 Layered Inorganic Nanomaterials

Two-dimensional nanomaterials are also important in nanomaterial applicability. These materials are usually produced by liquid-phase exfoliation methods, some of which will be discussed in later chapters of this dissertation.[4–6] Once exfoliated, these 2D nanomaterials can form 1D nanostructures with applications in solar cells, electronics, and catalysis.[5,6] This phenomena can occur in various 2D layered compounds such as graphene, $K_4Nb_6O_{17}$, and WS_2 in which their individual lamellae can be transformed from a nanosheet to a nanotube or nanoscroll.[7–10]

1.2.1 Potassium Hexaniobate

Potassium hexaniobate has a stacked structure consisting of edge and corner -sharing NbO_6 octahedra and negatively charged layers which contain cations in the interlayer.[11]

Moreover, potassium hexaniobate consists of two distinct layers, Interlayer I and Interlayer II, with different ion exchange capabilities.[12,13] It is much easier to have guest species exchange within Interlayer I, however, in Interlayer II, the exchange rarely occurs.

Hexaniobate serves many applications on the environmental and energy forefront. As a photocatalyst, researchers are developing ways to use hexaniobate in the photodegradation of toxic organics.[14] Also, hexaniobate nanostructures can have applications in intercalation and ion exchange, as well as exploiting hexaniobate nanoscrolls for the encapsulation of nanoparticles (NPs) and other materials.[15–18]

1.2.2 Hexaniobate Nanocomposites

Hexaniobate nanoscrolls are derived from the exfoliation of hexaniobate nanosheets and are extensively reviewed in Chapter 2 of this dissertation. Hexaniobate nanoscrolls were synthesized using previously reported methods from the Wiley group (Figure 1.1).[1] The focus in this chapter is on microwave assisted fabrication of nanoscrolls. This approach is facile and quick without compromising the structural integrity of the scrolls. Figure 1.2 shows the uniform morphologies of nanoscrolls created via this method. Furthermore, nanopeapods can be formed by simply adding as-synthesized nanoparticles to the above-mentioned synthetic scheme.

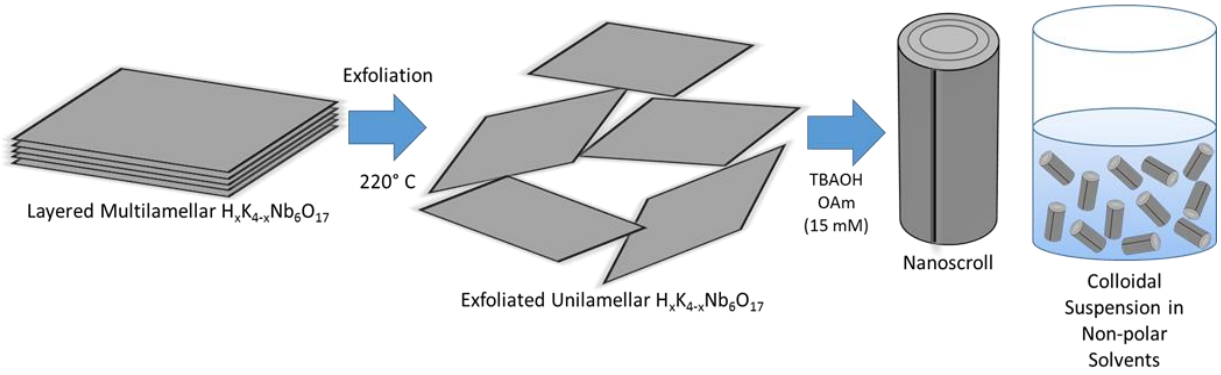

Figure 1.1. Synthetic scheme for hexaniobate nanoscrolls

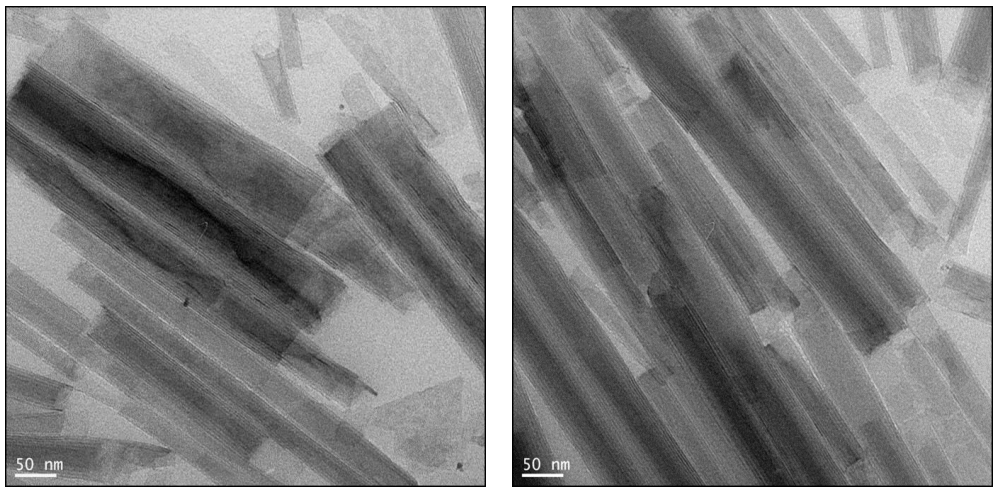

Figure 1.2.TEM images of hexaniobate nanoscrolls.

1.3 Atomic Force Microscopy Characterization

The atomic force microscope was developed in 1986 by Binning, Quate, and Gerber, and the concept for this type of scanning probe microscope was based off of principles of the scanning tunneling microscope.[19,20] The AFM instrument uses a sharp tip to "feel" along the surface at sub-nanometer scale (vertical resolution ~1 nm), to be able to "see" the surface in its entirety.[21] Observation of various surfaces is achieved by raster scanning a sharp tip along the surface of the specimen being studied. Simultaneously, a beam from a diode laser shines down on the cantilever which is attached to the tip, and as the cantilever bends due to forces acting upon it, the laser light is deflected back to four-quadrant photo-diode detector as shown in Figure 1.3. The signals obtained from the detector are then translated into digital output signals which in turn give a visual image of the surface relative to surface height.

Typically, characterization of nanoscrolls and nanopeapods has been based on results from Transmission Electron Spectroscopy (TEM) and X-Ray Diffraction (XRD) analysis. Currently, there is very little research that focuses on Atomic Force Microscopy (AFM) as a characterization method for these nanomaterials. Based on literature research of nanoscrolls, AFM has only been used to investigate the topography and height of these nanomaterials, and

most times, the topography is the only qualitative piece of information from AFM that is reported. However, with the advancement of atomic force microscopes, there is much more information that can be extrapolated qualitatively and quantitatively.

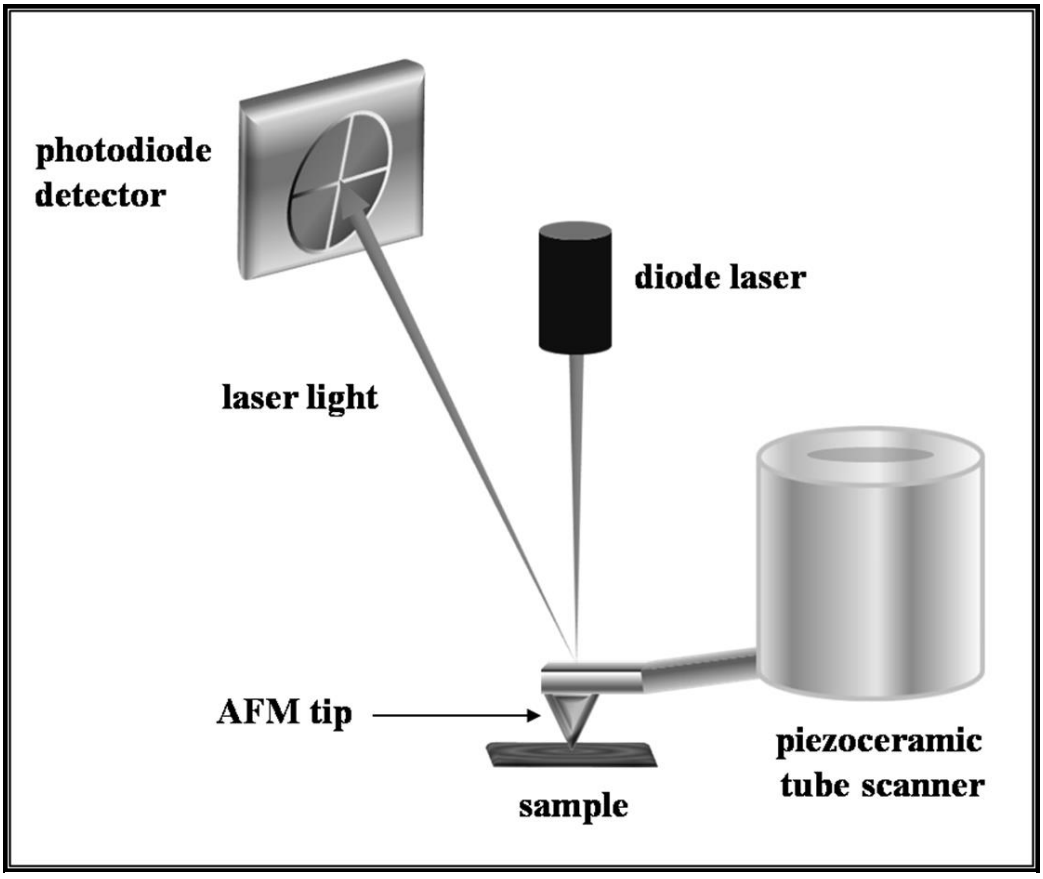

Figure 1.3 Schematic of Atomic Force Microscope scanning components.

1.3.1 Contact Mode Atomic Force Microscopy Imaging

With contact mode AFM (Figure 1.4), the tip stays in constant contact with the sample, and it is in this mode in which one can use a computer software program, such as NanoManipulator, to control the tip in attempts to deliberately deform the surface.[22]

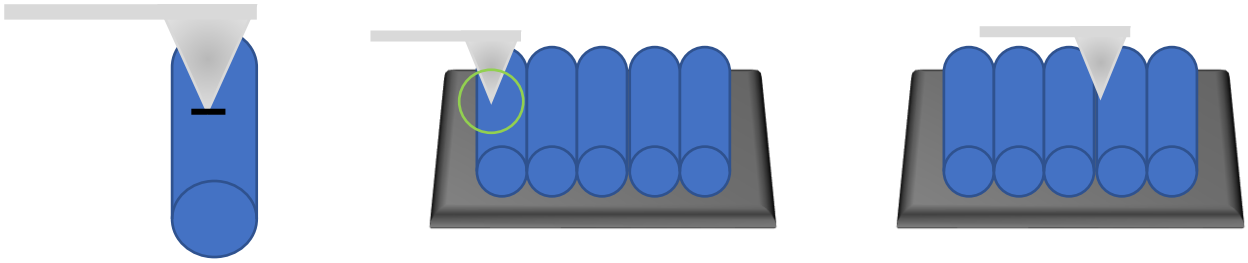

Figure 1.4. Schematic diagram of contact mode AFM in which the tip stays in constant contact with the sample as it is raster scanned across the surface.

1.3.2 Tapping Mode Atomic Force Microscopy Imaging

In intermittent "tapping" mode as depicted schematically in Figure 1.5, the tip comes in intermittent contact with the sample. The phase is tracked sinusoidally, depicting the motion of the tip as it approaches and reproaches the sample. The topography image is constructed by showing the difference of heights as a variation of colors, with darker areas showing lower topographic details opposed to brighter areas showing higher topographical details of the surface. The color scale bars are arbitrarily produced by the software to give a perspective of the height variation of the surface of the sample. The phase image is an enhanced image that shows viscoelasticity, [23] but more so, the phase image allows us to clearly see defined features that are unable to be seen in topography images. Furthermore, the phase image can show variants of composition, adhesion, friction, chemical composition, as well as other factors, which will be explored in DLFM mode. [21,24] The 3-D topography image is a three-dimensional representation

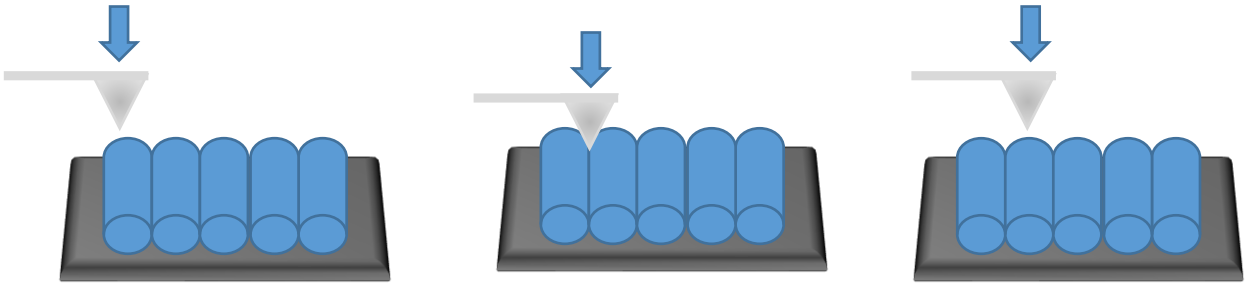

Figure 1.5. Schematic of tip motion across surface of a nanoscroll sample in tapping mode. The tip oscillates at a frequency near its resonance, and as it is raster scanned across the surface, the tip comes in contact intermittently with the surface.

of the topography image, and its difference in color is attributed to the lighting representation that the software uses to enhance the features of these types of images.

1.3.3 Dynamic Lateral Force Modulation

By utilizing the characteristic features of tapping mode and alternating the force exerted by the tip, deformation of these scrolls can be explored. It has previously been shown how AFM could be used to identify individual single-wall and multi-wall carbon nanotubes by "squeezing" the tube between the tip and substrate.[25] The compressions of these tubes were then measured using force-distance curves and the difference in these measurements were compared to already known interlayer spacing of the nanotubes.[25] Based on this knowledge, interest was geared towards applying a similar method to investigate the investigation of mechanical properties of hexaniobate nanoscrolls.

In dynamic operation modes of scanning probe microscopy, the cantilever is mounted onto a piezoceramic scanning tube to allow an external excitation of an oscillation and is deliberately vibrated.[26] When the tip approaches the sample, elastic and inelastic interactions cause a change in both the amplitude and the phase of the cantilever, and are interpreted by the feedback signal. Using force-distance curves taken at the time of scanning, elastic, plasto-elastic and frictional properties (adhesion) can be measured.[27,28]

1.3.4 Magnetic Sample Modulation

With magnetic sample modulation (MSM), it is possible to detect magnetic nanomaterials with increased spatial resolution and sensitivity.[29] In this mode, magnetic nanomaterials can physically move due to an electromagnetic field of alternating current created by flux.[29] A soft, non-magnetic tip is scanned slowly across the vibrating sample and as the changes in tip deflection changes, the frequency and amplitude are able to be tracked and allows for the

mapping of the vibrational response of the sample. This imaging mode could further magnetic based nanocomposite studies by having the ability to track magnetic vibrations of nanomaterials used within the system.[29]

1.4 References

(1) Adireddy, S.; Carbo, C. E.; Yao, Y.; Vargas, J. M.; Spinu, L.; Wiley, J. B. High-Yield Solvothermal Synthesis of Magnetic Peapod Nanocomposites via the Capture of Preformed Nanoparticles in Scrolled Nanosheets. *Chem. Mater.* **2013**, *25* (19), 3902–3909 DOI: 10.1021/cm402352k.

(2) Baughman, R. H.; Zakhidov, A. A.; De Heer, W. A. Carbon nanotubes--the route toward applications. *science* **2002**, *297* (5582), 787–792.

(3) Smith, B. W.; Monthioux, M.; Luzzi, D. E. Encapsulated C60 in carbon nanotubes. *Nature* **1998**, *396* (6709), 323–324 DOI: 10.1038/24521.

(4) Sun, Y.; Wu, Q.; Shi, G. Graphene based new energy materials. *Energy Environ. Sci.* **2011**, *4* (4), 1113–1132.

(5) Cui, X.; Zhang, C.; Hao, R.; Hou, Y. Liquid-phase exfoliation, functionalization and applications of graphene. *Nanoscale* **2011**, *3* (5), 2118–2126.

(6) Dias, A. S.; Lima, S.; Carriazo, D.; Rives, V.; Pillinger, M.; Valente, A. A. Exfoliated titanate, niobate and titanoniobate nanosheets as solid acid catalysts for the liquid-phase dehydration of D-xylose into furfural. *J. Catal.* **2006**, *244* (2), 230–237.

(7) Kosynkin, D. V.; Higginbotham, A. L.; Sinitskii, A.; Lomeda, J. R.; Dimiev, A.; Price, B. K.; Tour, J. M. Longitudinal unzipping of carbon nanotubes to form graphene nanoribbons. *Nature* **2009**, *458* (7240), 872–876.

(8) Saupe, G. B.; Waraksa, C. C.; Kim, H.-N.; Han, Y. J.; Kaschak, D. M.; Skinner, D. M.; Mallouk, T. E. Nanoscale Tubules Formed by Exfoliation of Potassium Hexaniobate. *Chem. Mater.* **2000**, *12* (6), 1556–1562 DOI: 10.1021/cm981136n.

(9) Li, Y. D.; Li, X. L.; He, R. R.; Zhu, J.; Deng, Z. X. Artificial lamellar mesostructures to WS2 nanotubes. *J. Am. Chem. Soc.* **2002**, *124* (7), 1411–1416.

(10) Dai, H. Carbon nanotubes: synthesis, integration, and properties. *Acc. Chem. Res.* **2002**, *35* (12), 1035–1044.

(11) Domen, K.; Kudo, A.; Shibata, M.; Tanaka, A.; Maruya, K.-I.; Onishi, T. Novel photocatalysts, ion-exchanged K 4 Nb 6 O 17, with a layer structure. *J. Chem. Soc. Chem. Commun.* **1986**, No. 23, 1706–1707.

(12) Maeda, K.; Eguchi, M.; Lee, S.-H. A.; Youngblood, W. J.; Hata, H.; Mallouk, T. E. Photocatalytic Hydrogen Evolution from Hexaniobate Nanoscrolls and Calcium Niobate

Nanosheets Sensitized by Ruthenium(II) Bipyridyl Complexes. *J. Phys. Chem. C* **2009**, *113* (18), 7962–7969 DOI: 10.1021/jp900842e.

(13) Maeda, K.; Eguchi, M.; Youngblood, W. J.; Mallouk, T. E. Niobium Oxide Nanoscrolls as Building Blocks for Dye-Sensitized Hydrogen Production from Water under Visible Light Irradiation. *Chem. Mater.* **2008**, *20* (21), 6770–6778 DOI: 10.1021/cm801807b.

(14) Kudo, A.; Sayama, K.; Tanaka, A.; Asakura, K.; Domen, K.; Maruya, K.; Onishi, T. Nickel-loaded K4Nb6O17 photocatalyst in the decomposition of H2O into H2 and O2: Structure and reaction mechanism. *J. Catal.* **1989**, *120* (2), 337–352.

(15) Viculis, L. M.; Mack, J. J.; Kaner, R. B. A Chemical Route to Carbon Nanoscrolls. *Science* **2003**, *299* (5611), 1361 DOI: 10.1126/science.1078842.

(16) Feng, S.; Xu, R. New materials in hydrothermal synthesis. *Acc. Chem. Res.* **2001**, *34* (3), 239–247.

(17) Yao, Y.; Chaubey, G. S.; Wiley, J. B. Fabrication of Nanopeapods: Scrolling of Niobate Nanosheets for Magnetic Nanoparticle Chain Encapsulation. *J. Am. Chem. Soc.* **2012**, *134* (5), 2450–2452 DOI: 10.1021/ja206237v.

(18) Kobayashi, Y.; Hata, H.; Salama, M.; Mallouk, T. E. Scrolled Sheet Precursor Route to Niobium and Tantalum Oxide Nanotubes. *Nano Lett.* **2007**, *7* (7), 2142–2145 DOI: 10.1021/nl0708260.

(19) Binnig, G.; Quate, C. F.; Gerber, C. Atomic Force Microscope. *Phys. Rev. Lett.* **1986**, *56* (9), 930–933.

(20) Binnig, G.; Rohrer, H. Scanning tunneling microscopy. *IBM J. Res. Dev.* **2000**, *44* (1/2), 279.

(21) Eaton, P.; West, P. *Atomic force microscopy*; Oxford University Press, 2010.

(22) Requicha, A. A.; Arbuckle, D.; Mokaberi, B.; Yun, J. Algorithms and software for nanomanipulation with atomic force microscopes. *Int. J. Robot. Res.* **2009**, *28* (4), 512–522.

(23) Tamayo, J.; García, R. Deformation, Contact Time, and Phase Contrast in Tapping Mode Scanning Force Microscopy. *Langmuir* **1996**, *12* (18), 4430–4435 DOI: 10.1021/la960189l.

(24) Brown, T. T.; LeJeune, Z. M.; Liu, K.; Hardin, S.; Li, J.-R.; Rupnik, K.; Garno, J. C. Automated scanning probe lithography with n-alkanethiol self-assembled monolayers on Au (111): Application for teaching undergraduate laboratories. *JALA J. Assoc. Lab. Autom.* **2011**, *16* (2), 112–125.

(25) DeBorde, T.; Joiner, J. C.; Leyden, M. R.; Minot, E. D. Identifying individual single-walled and double-walled carbon nanotubes by atomic force microscopy. *Nano Lett.* **2008**, *8* (11), 3568–3571.

(26) Giessibl, F. J. Advances in atomic force microscopy. *Rev. Mod. Phys.* **2003**, *75* (3), 949–983.

(27) Cappella, B.; Baschieri, P.; Frediani, C.; Miccoli, P.; Ascoli, C. Improvements in AFM imaging of the spatial variation of force-distance curves: on-line images. *Nanotechnology* **1997**, *8* (2), 82.

(28) http://www.parkafm.com/index.php/park-spm-modes/91-standard-imaging-mode/222-lateral-force-microscopy-lfm.

(29) Li, J.-R.; Lewandowski, B. R.; Xu, S.; Garno, J. C. Detecting the Magnetic Response of Iron Oxide Capped Organosilane Nanostructures Using Magnetic Sample Modulation and Atomic Force Microscopy. *Anal. Chem.* **2009**, *81* (12), 4792–4802 DOI: 10.1021/ac900369v.

Chapter 2 Utilizing Microwave Irradiation for the Rapid Synthesis of Hexaniobate Nanoscrolls*

2.1 Introduction

Advanced materials synthesis of nanostructures is an ever-growing area of study with increasing interest in the exploitation of various properties at the nanoscale. Moreover, the onset of discovering structures with unique anisotropic physical properties as found in lamellar solids, layered transition oxides, and layered oxides has sparked ever-growing interest leading to promising advancements in materials syntheses and assemblies.[1–5] Recently, one-dimensional nanostructures have been of great interest because they show great promise in various scientific applications due to their intrinsic properties, and most notably, their scrolling potential. One such material possessing these properties is potassium hexaniobate, $K_4Nb_6O_{17}$, which is well-known for its scrolling capabilities of exfoliated lamellae,[6] photocatalytic properties,[7] and encapsulation of host materials for the fabrication of nanocomposites with enhanced features.[6,8]

Potassium hexaniobate ($K_4Nb_6O_{17}$), is a layered oxide structure which consists of layers of NbO_6 octahedra with cations that are ion exchangeable within the interlayer spacings.[9] The layers of Nb_6O_{17} can go through a process of exfoliation following the intercalation of bulky ions. After intercalation, the layers spontaneously roll up into nanoscrolls, to relieve the strain intrinsic to the asymmetric Nb_6O_{17} layers.[2,10,11]

Several groups have reported on various synthetic route to form nanoscrolls from hexaniobate. [2,5,7,9,12–14] Most common synthetic routes rely on benchtop methods that can take days for the reaction to take place. However, with the recent advances in microwave-assisted (MA) reactions,[15] production of the same hexaniobate nanostructures can be synthesized at a

*This chapter will be adapted for: Brown, T.T., Akbarian-Tefaghi, S., Mitton, B., Moore, K., Veiga,E., Wiley, J.B., "Rapid Preparation of Hexaniobate Nanoscrolls and Nanopeapods via Microwave Assisted Reactions". *Manuscript in Preparation.*

more rapid rate. In this chapter, an extensive comparison of each synthetic step in the nanoscroll manufacturing process has been studied. It has been shown that microwave-assisted reactions for producing hexaniobate nanostructures produces high quality nanoscrolls in a little over an 1 h, which makes this technological advance significant in nanoscroll formation in comparison to previous reports of solvothermal[2] (6 hours) and benchtop[12,13,16] (> 4 days) methods.

2.2 Experimental

Starting Materials. K_2CO_3 (Alfa Aesar, 99%) and Nb_2O_5 (Alfa Aesar, 99%), tetrabutylammonium hydroxide 30-hydrate (TBAOH, Sigma Aldrich), oleylamine (Sigma Aldrich, 70%), toluene (Sigma Aldrich, anhydrous, 99.8%), distilled water, and ethanol (200 Proof, absolute).

2.2.1 Preparation of $K_4Nb_6O_{17}$ Nanostructures

$K_4Nb_6O_{17}$ Starting Material

$K_4Nb_6O_{17}$ was synthesized by two separate solid-state reactions (SSR) of K_2CO_3 and Nb_2O_5 (molar ratio of both syntheses was 1.1:1.5). The first reaction (SSR1) was carried out in air at 900º C for 1 h with an intermediate grinding before further heating at 1050 º C for 48 h, and the second reaction (SSR2) was carried out in air at 550 º C for 12 h and 900 º C for 1 h with intermediate grinding between both heating steps before finally heating at 1100 ºC for 24 h. In both reactions, 10% excess of K_2CO_3 was present due to the volatilization of potassium oxide during the heating process.[2,10] The resulting products were then washed with distilled water to remove any excess reagents before centrifuging twice for 10 minutes each followed by one 5-minute centrifugation with 15 mL of acetone. The products were then dried overnight at 70 ºC. Both reactions were subjected to the following methods of acid exchange and scrolling reactions.

Acid exchange of $K_4Nb_6O_{17}$

The proton-exchange of $K_4Nb_6O_{17}$ to form $H_xK_{4-x}Nb_6O_{17}$ was carried out by three different methods: benchtop, solvothermal, and microwave protonation techniques. For the benchtop method, 0.25 g of $K_4Nb_6O_{17}$ was treated with 25 mL of 3 M HCl solution for 4 days at 50 ºC with stirring in a fume hood. In the solvothermal method 0.5 g of hexaniobate mixed treated with 5 mL of 6 M HNO_3 and placed into a Teflon-lined stainless-steel autoclave (Parr, model 4749, 1800 psi, 23 mL). The autoclave was then heated to 90 ºC and held at that temperature for 48 h then cooled to room temperature. Microwave protonation was achieved by treating 0.5 g hexaniobate with 5 mL of 6 M HNO_3 solution in a StartSYNTH Microwave Synthesis Labstation. The reaction mixture was contained inside a quartz pressure reaction vessel (<15 bar) and placed in a rotor within the instrument. After a 10 minute warmup, the sample was heated for 3 h at 60 ºC with constant stirring at a power level of 300W.[15] All synthesized products were washed with distilled water and centrifuged twice for 10 minutes, followed by one 5-minute centrifugation with 15 mL of acetone. The products were then dried overnight at 70 ºC.

Preparation of Intercalated Multi-Walled Nanoscrolls (INS)

Nanoscroll formation was achieved by solvothermal synthesis, similar to what has been previously reported by our group[2], as well as microwave-irradiated synthesis. Solvothermally, a solution of $H_xK_{4-x}Nb_6O_{17}$ (0.1 g), TBAOH (19 mmol), and 5 mL oleylamine (~15 mmol) in 9 mL toluene was prepared and magnetically stirred for 1 h before transferring into a Teflon-lined stainless-steel autoclave (Parr, model 4749, 1800 psi, 23 mL). The autoclave was then kept at 220 ºC for 6 h and cooled to room temperature thereafter. Conversely, microwave formation of nanoscrolls was performed by combining 0.05 g $H_xK_{4-x}Nb_6O_{17}$, 0.15 g TBAOH (9.5 mmol), and 2.5 mL oleylamine (7.5 mmol), and 4.5 mL toluene in. The mixture was placed in a quartz pressure

reaction vessel (<15 bar) in a rotor within a StartSYNTH Microwave Synthesis Labstation. After a 30-minute warmup, the sample was heated at 130 ºC for 1 h with a maximum power maintained at 700W. The products of both syntheses were centrifuged, and the supernatant was decanted. The samples were then washed with ethanol and centrifugated in 30 mL of ethanol for 20 minutes with intermediate cycles of ultrasonic treatment. The nanoscrolls were then re-dispersed in toluene.

2.2.2 Characterization

Transmission electron microscopy (TEM) images were acquired on a JEOL 2010 high-resolution microscope powered by an operating voltage of 200 keV and equipped with a Gatan slow scan charge-coupled device (CCD) camera. Interlayer spacings were obtained on a FEI TECNAI G2 F30 FEG TEM (300 kV) at Tulane University. TEM sample preparation was carried out by drop-casting a dilute dispersion of nanoscrolls onto a 200 mesh copper grid. X-Ray powder diffraction (XRD) data for phase purity was gathered from a Philips X'Pert system equipped with a curved graphite monochromator and Cu Kα radiation (λ = 1.5418 Å). Atomic Force Microscopy (AFM) images were acquired by an Asylum Research MFP-3D Atomic Force Microscope in intermittent contact mode powered by dual amplitude resonance tracking (DART). Dilute dispersions of nanoscrolls were drop cast onto silica substrates for AFM imaging.

2.3 Results and Discussion

Recent developments in nanocomposite syntheses have played a pivotal role in the time it takes to make quality nanostructures such as nanoscrolls. Previously, nanoscrolls have been synthesized by numerous synthetic routes which have led to quality sturctures.[2,9,12,17] However, previously recorded work had reaction times that have required an excess of time to complete. The study presented in this chapter was developed to investigate the formation of hexaniobate nanoscrolls and to determine the best routes to obtain structurally rigid nanostructures in the least

amount of time. Figure 2.1 shows the reaction template used to study each step of the nanoscroll formation process. Parameters taken into consideration were the solid-state reaction of the starting material, the protonation of hexaniobate via benchtop, solvothermal, and microwave methods, and the scrolling of hexaniobate via previously reported solvothermal methods versus the newly developed microwave scrolling methods.

2.3.1 Solid State Reactions of $K_4Nb_6O_{17}$ Starting Material

Two different synthetic routes of forming the layered oxide starting materials consisted of a modified method previously reported in our group,[2] which added an extra day to the heating time of the starting material in experiment 1(SSR1), whereas in experiment 2 (SSR2), an extra grinding step was incorporated. The resulting XRD patterns are shown in Figure 2.2 comparing both SSR1 and SSR2.

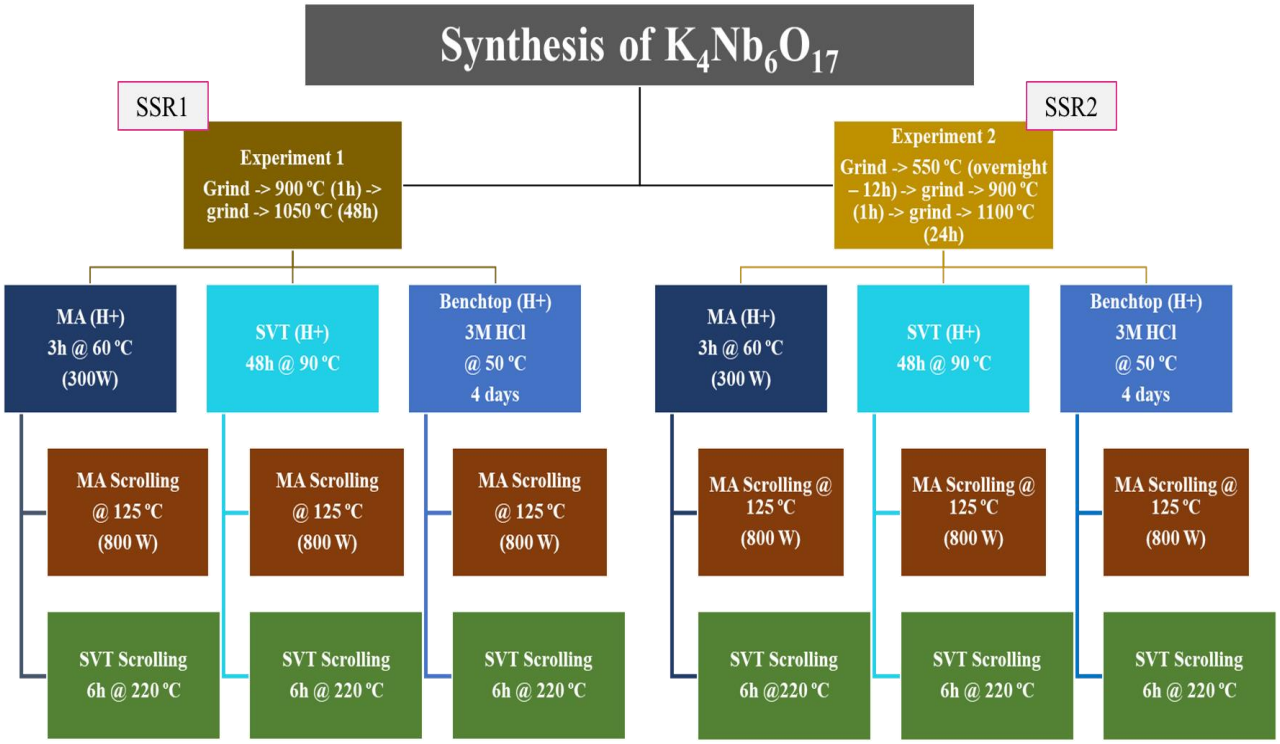

Figure 2.1. Reaction schematic to study formation of hexaniobate nanoscrolls.

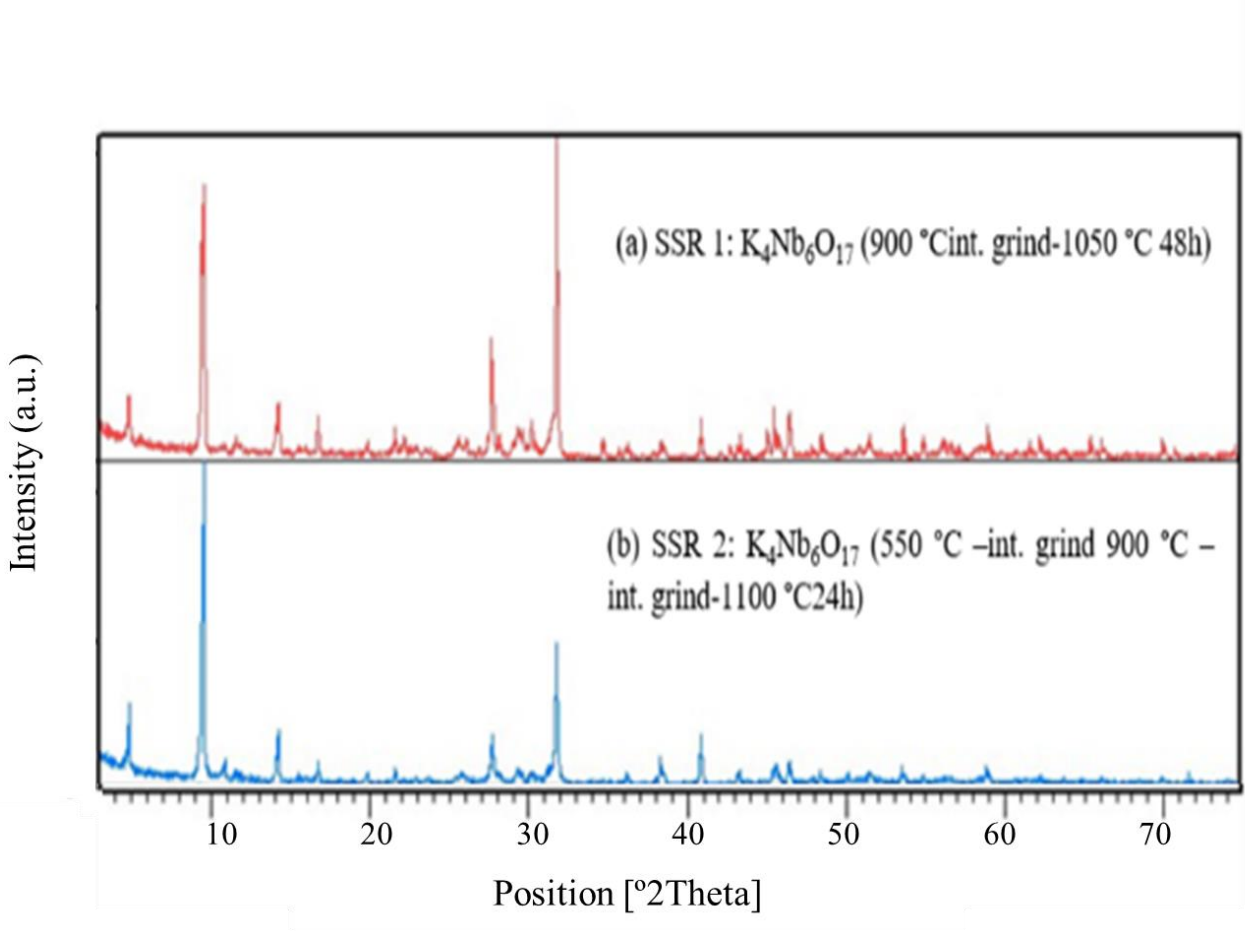

Figure 2.2. XRD patterns for the solid-state reactions (SSR) of potassium hexaniobate A) SSR 1 heated 900 °C for 1h, re-ground, then heated at 1050 °C for 48h and B) SSR 2 heated 550 °C for 16h, re-ground, heated at 900 °C for 1h, re-ground, then heated at 1100 °C.

2.3.2 Protonation of $K_4Nb_6O_{17}$

Experimental parameters for protonation of $K_4Nb_6O_{17}$ to form $H_xK_{4-x}Nb_6O_{17}$ were studied from previously reported synthetic protocols for benchtop (BT) protonation[2,10,18] However, more recently, our group has developed two protonation reaction methods to decrease the time of protonation from 4 d (BT) to 2 d via a solvothermal (SVT) protonation method and even further time decrease to 3 h via microwave assisted (MA) protonation.[19] Figure 2.3 shows the resulting XRD patterns for the three different protonation syntheses. It is readily observed that the high angle reflections in the 0*k*0 planes have shifted to the right of the original peaks from the two solid state reactions of the starting material, which indicates proton exchange has occurred with

placement of H^+ ions in the interlayers of the niobate. It is also significant to note that the high angle reflection peaks of the protonated products, no matter which protonation method was used, shifts to higher angle indicating protonation, though the extent of in the MA method does not appear to be as extensive as in the other two techniques. As will be highlighted below, this small difference is not significant in that it does not interfere with subsequent steps of the scroll fabrication.

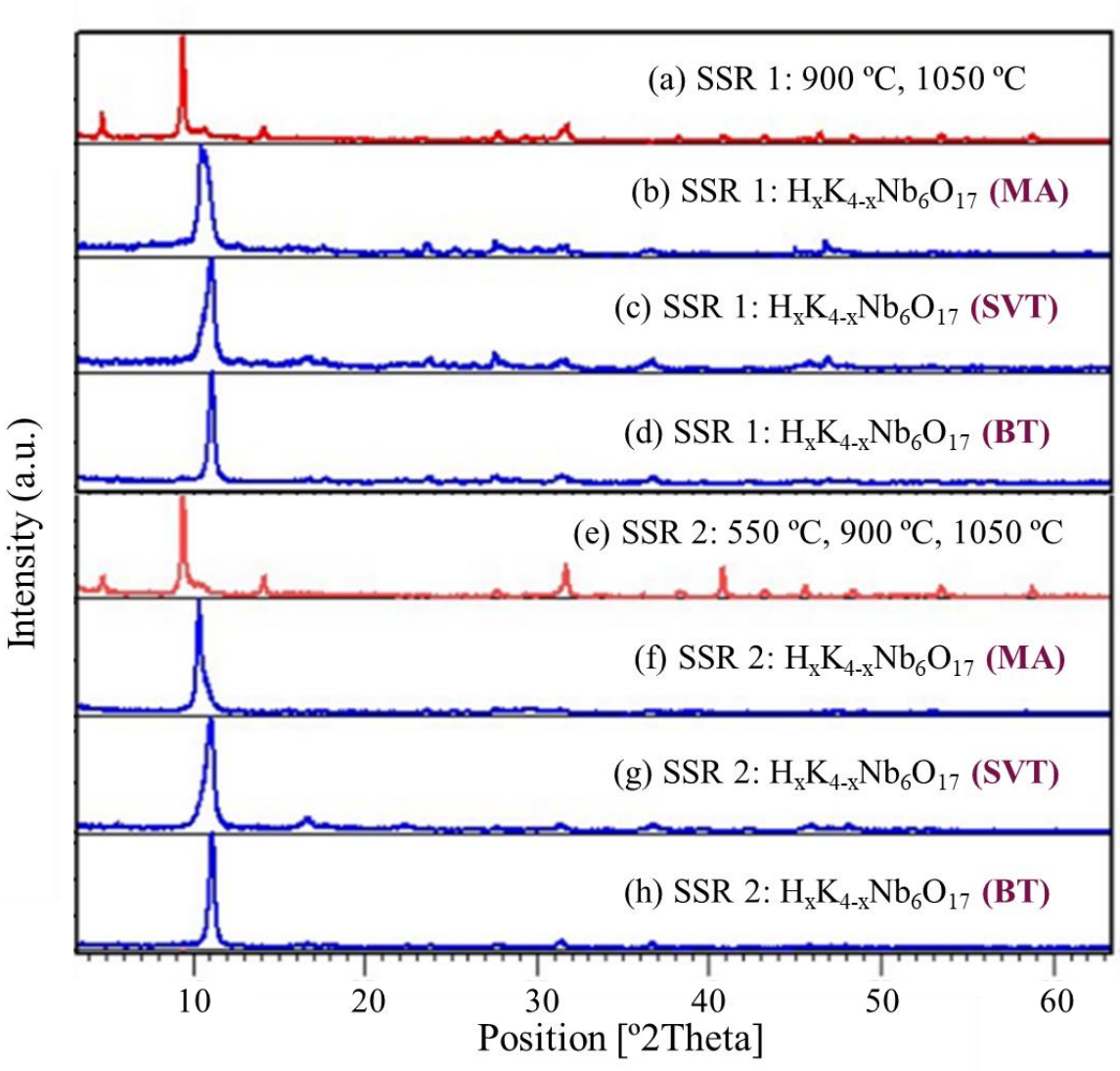

Figure 2.3. XRD patterns of A and E) Starting material solid state reactions (SSR) 1 and 2, B) Microwave-protonated hexaniobate from SSR 1, C) Solvothermally- protonated hexaniobate from SSR 1, D) Benchtop-protonated hexaniobate from SSR 1, F) Microwave-protonated.

2.3.3 Synthesis of Intercalated Hexaniobate Nanoscrolls

Microwave protonation and scrolling. Protonation and scrolling of intercalated nanoscrolls has been achieved at a much faster rate than previously recorded in literature. TEM images (Figures 2.4 and 2.5) show much similar structural features as observed previously in other recorded methods for hexaniobate protonation and scrolling.[1,2,9,10,17,19,20] The microwave-assisted reaction is adapted from a previously reported solvothermal method[2] developed in our group, which consists of combining ~0.5 times the amount of reagents into a quartz reaction vessel and heated to 130 ºC for 1h at 700 W.[19] After centrifugation and purification, microwave synthesized nanoscrolls were readily obtained and akin to the intercalated nanoscrolls obtained by benchtop protonated, solvothermal nanoscrolls synthesized previously by our group.

Combining solvothermal and microwave methods in both protonation and scrolling. Controlled experiments were performed to investigate the combination of ST protonation and MA scrolling methods. Figures 2.6 and 2.7 show TEM images of resulting nanoscrolls combining solvothermal protonation with microwave scrolling (Figure 2.6) and microwave protonation with solvothermal scrolling (Figure 2.7). When compared to previously mentioned microwave scrolling with microwave protonation syntheses (Figures 2.4 and 2.5) or solvothermal scrolling with solvothermal syntheses (Figure 2.8), an excess of un-scrolled or partially scrolled hexaniobate lamellae was observed throughout the samples in Figure 2.8 and Figure 2.9a. Therefore, it can be inferred that combining different methodologies may result in low nanoscroll yields.

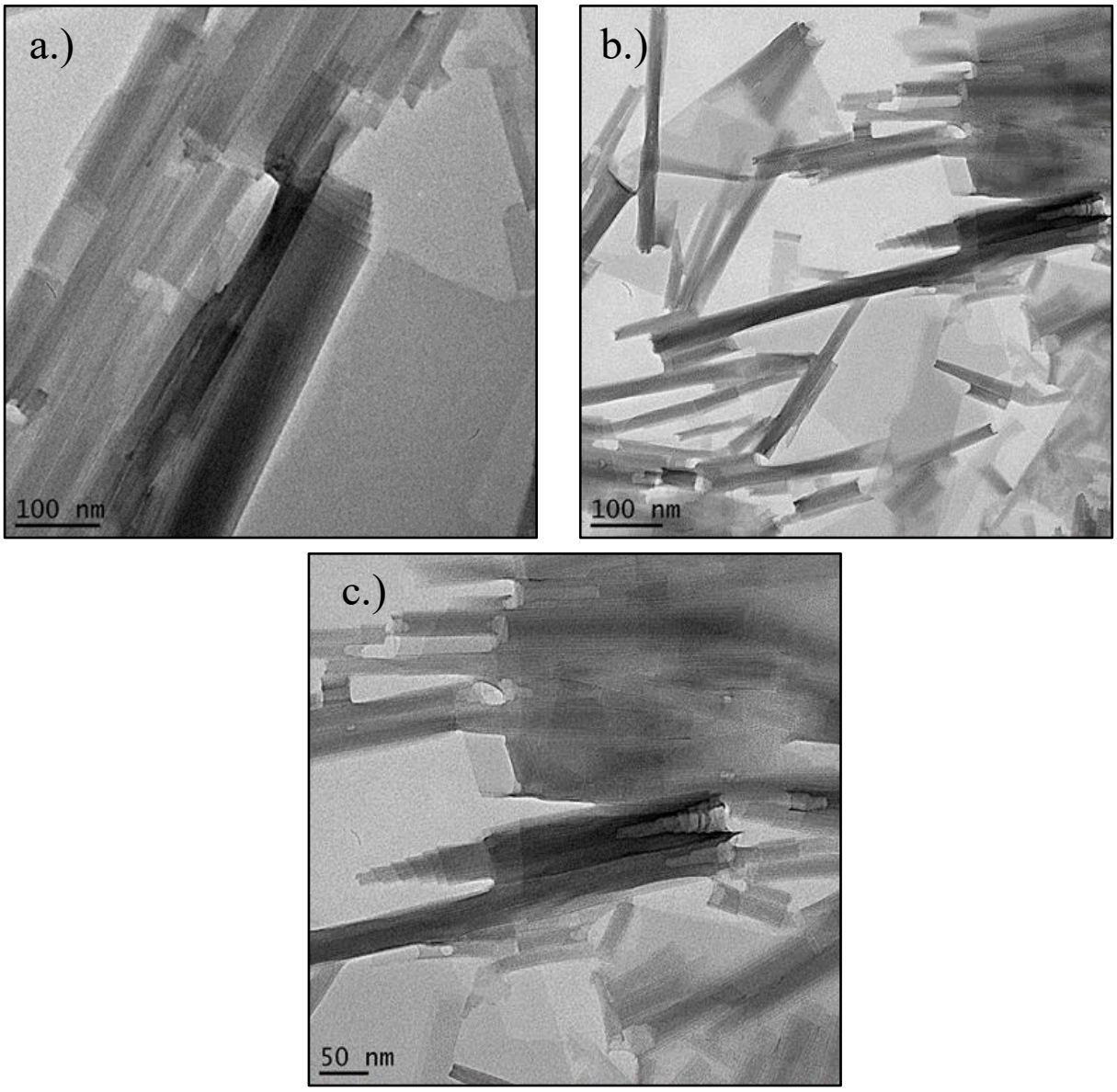

Figure 2.4. (a,b,c) TEM images of intercalated hexaniobate nanoscrolls synthesized via microwave protonation and scrolling methods from solid-state reaction #1 (SSR1). Telescoping of scrolled hexaniobate is notably observed.

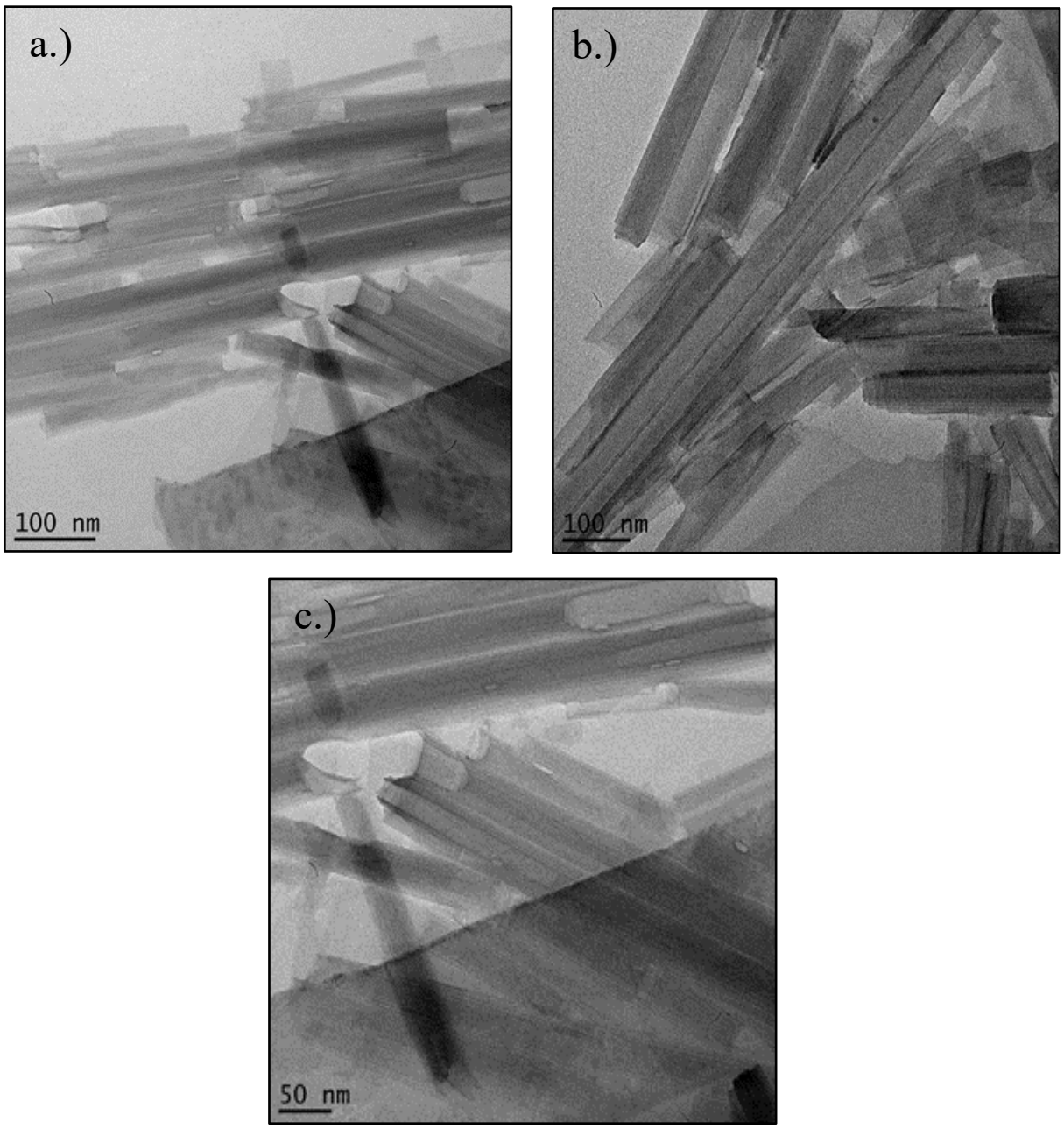

Figure 2.5. (a,b,c) TEM images of intercalated hexaniobate nanoscrolls synthesized via microwave protonation and scrolling methods from solid-state reaction #2 (SSR 2). Telescoping of some nanoscrolls are observed in Figure 2.5b.

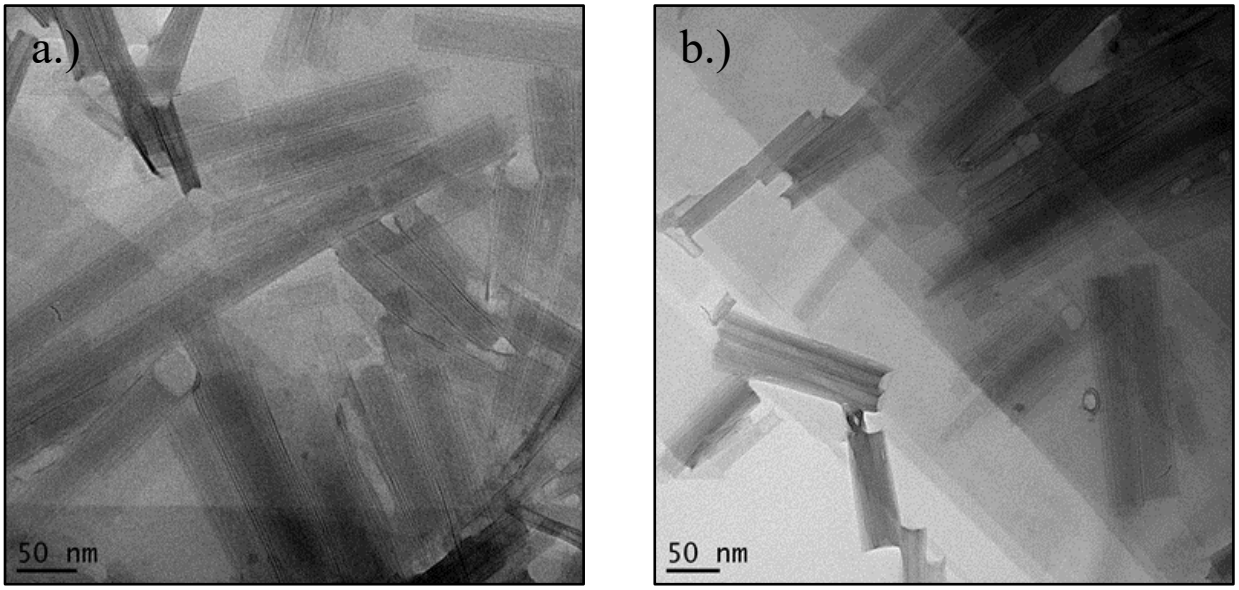

Figure 2.7. (a) TEM image of intercalated hexaniobate nanoscrolls synthesized via solvothermal protonation and microwave scrolling methods from solid-state reaction #1. (b) TEM image of intercalated hexaniobate nanoscrolls synthesized via solvothermal protonation.

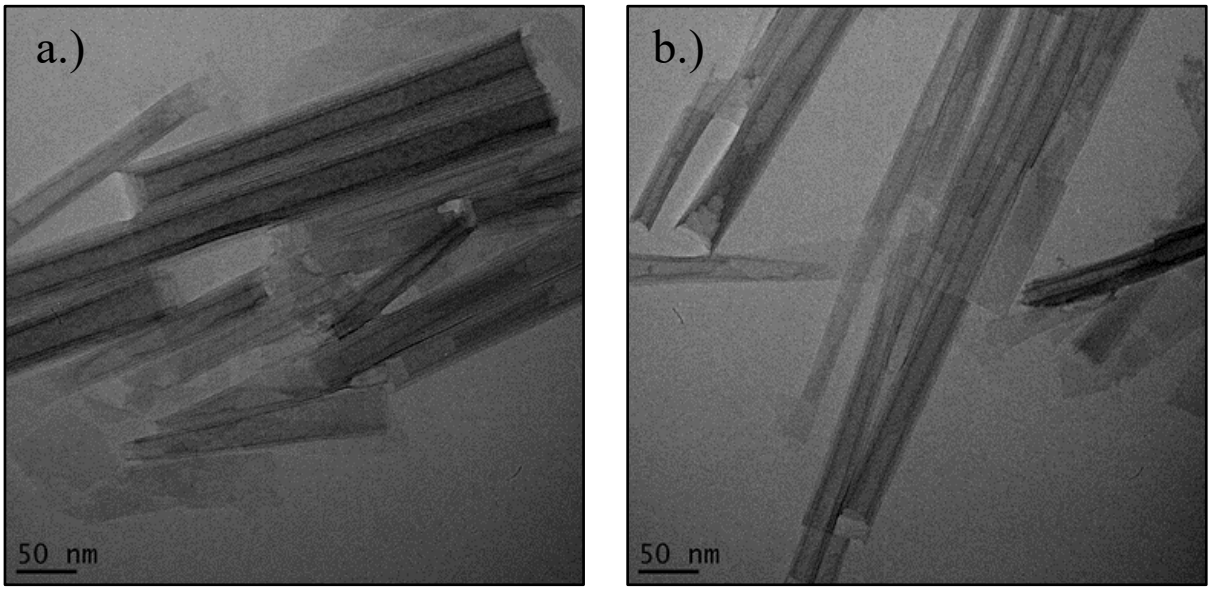

Figure 2.6. (a)TEM image of intercalated hexaniobate nanoscrolls synthesized via microwave protonation and solvothermal scrolling methods from solid-state reaction #1. (b) TEM image of intercalated hexaniobate nanoscrolls synthesized via microwave protonation and solvothermal srolling.

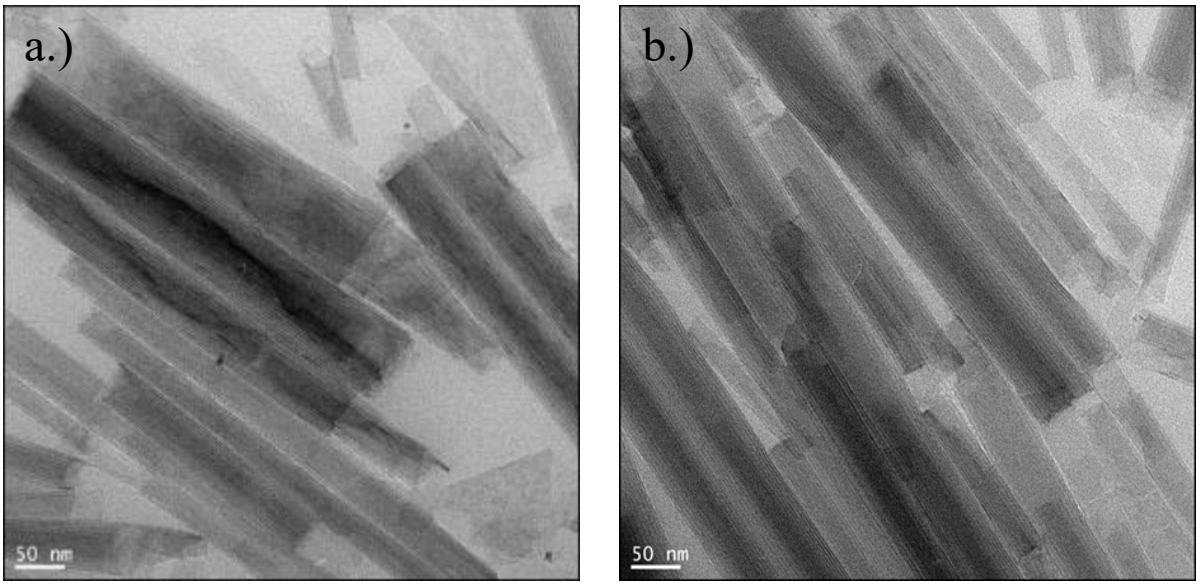

Figure 2.8. (a)TEM image of intercalated hexaniobate nanoscrolls synthesized via solvothermal protonation and solvothermal scrolling methods from solid-state reaction #1. (b) TEM image of intercalated hexaniobate nanoscrolls synthesized via solvothermal protonation.

Combining benchtop protonation with solvothermal and microwave scrolling. The combination of benchtop protonation with solvothermal scrolling methods yielded nanoscrolls of good quality (Figure 2.9a), however, the benchtop protonation with microwave scrolling yielded nanoscrolls that possessed defects on the surface (Figure 2.9b). It is unclear as to what may have caused these defects on the surface, however it is speculated that the increased exposure time to heating (4 days at 50 °C for protonation) and excess wattage from microwave synthesis (130 °C for 1 h at 700 W) may have some influence on the structural integrity of the nanosheets.

This series of studies has shown that microwave methods produce high yields of high-quality nanoscrolls in less time than in previously reported methods. K^+ ions in $K_4Nb_6O_{17}$ is readily exchanged with H^+ ions via acid exchange in only 3 h, compared to previous protonation of 2 to 4 days. Due to the proton exchange, the interlayer becomes more susceptible to exfoliation via the exchange of H^+ ions with TBA^+ ions, and thus, nanoscrolls can be formed from these exfoliated

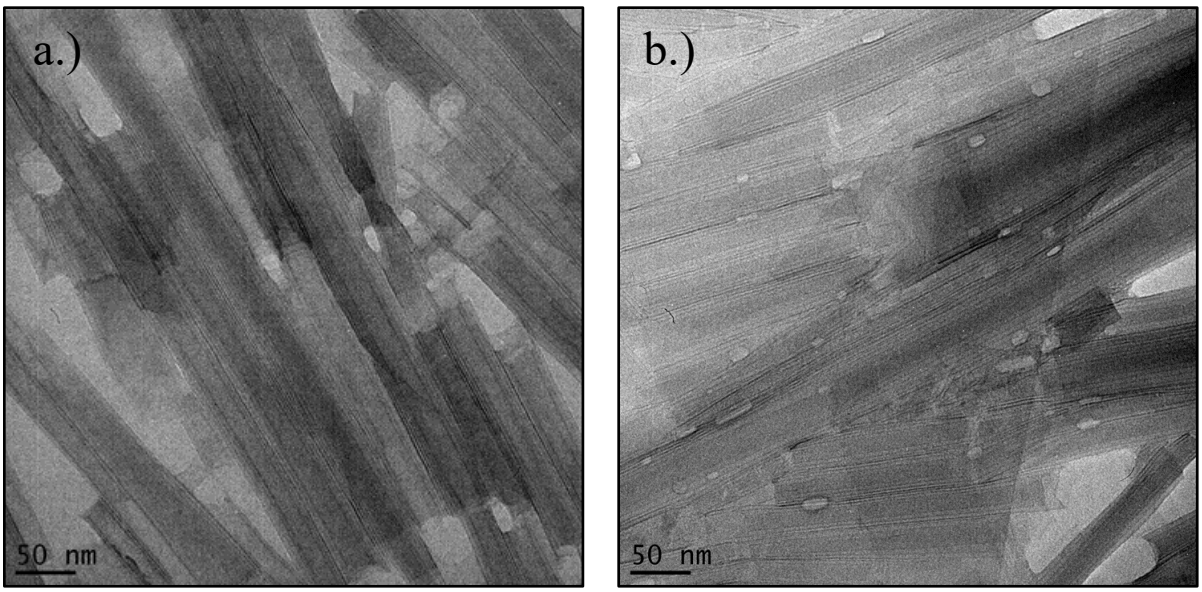

Figure 2.9. (a)TEM image of intercalated hexaniobate nanoscrolls synthesized via benchtop protonation and solvothermal scrolling methods from solid-state reaction #1. (b) TEM image of intercalated hexaniobate nanoscrolls synthesized via benchtop protonation and microwave scrolling.

sheets in an hour using microwave methods. Previously, conversion of hexaniobate nanosheets into nanoscrolls has taken 6 or more hours.[2,5,13,14,17] Figure 2.10 shows TEM images of microwave protonated, microwave nanoscrolls that have interlayer spacings of 9.5 – 12.5 nm, which are consistent with values previously reported for solvothermally synthesized nanomaterials.[2] To further verify our findings, we chose to make the microwave scrolling the common variable between syntheses, and observed the other two methods of solvothermal and benchtop protonation. As a result of these syntheses, we further see that microwave synthesis proves to be effective and faster synthetic route. Figure 2.11 shows solvothermal protonation with microwave scrolling and Figure 2.12 shows benchtop protonation with microwave scrolling. Measurement of the interlayer spacing confirms consistency in the interlayer spacings ranging from 11.7 – 15.5 nm and are within the range of values previously reported.[2]

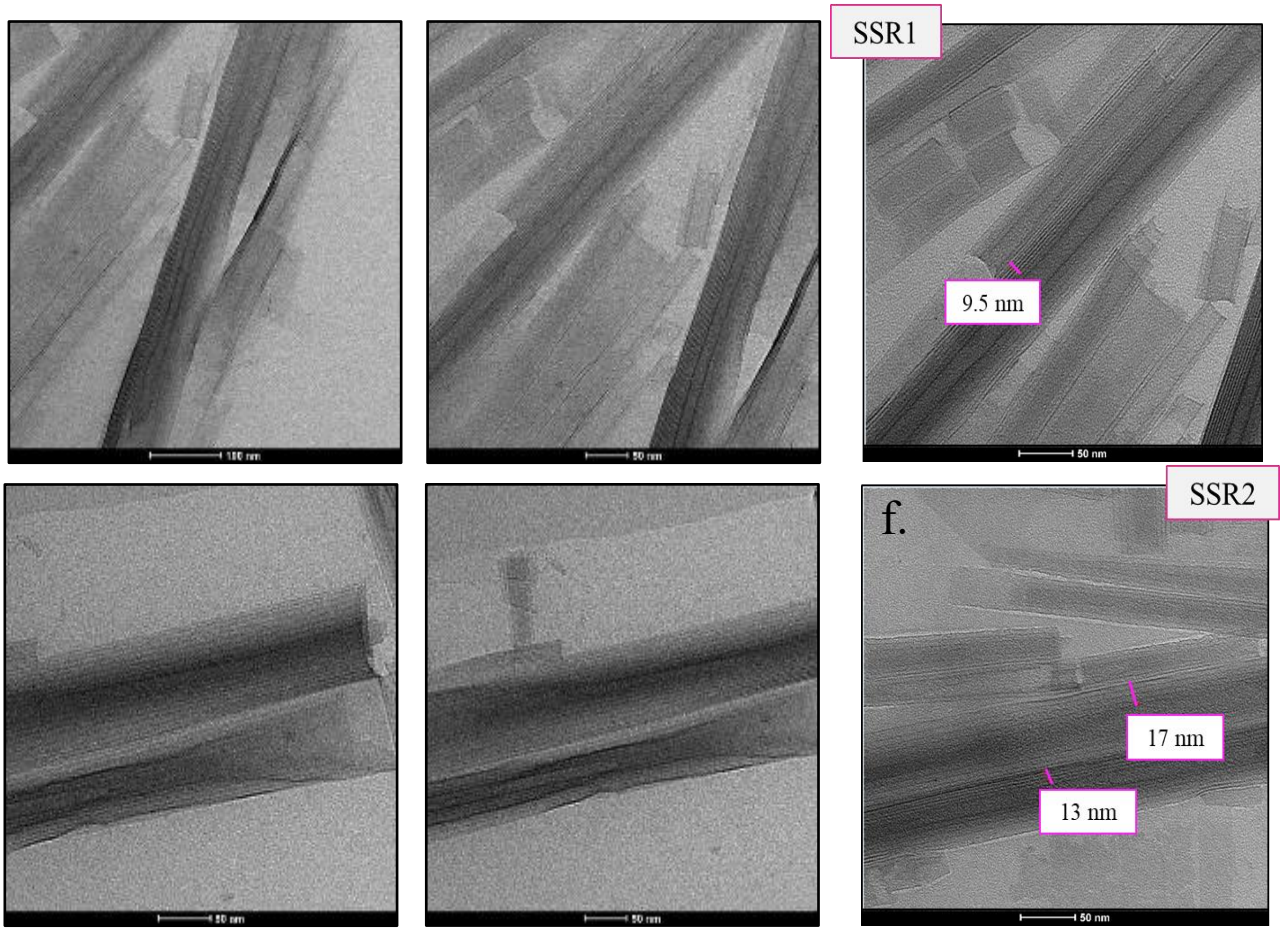

Figure 2.10. (a-c) TEM images of intercalated hexaniobate nanoscrolls synthesized via microwave protonation and scrolling methods from solid-state reaction #1 (SSR1). (d-f) TEM images of intercalated hexaniobate nanoscrolls synthesized via microwave protonation and scrolling for SSR 2.

2.4 Conclusions

A new, faster, and effective synthetic route for the fabrication of intercalated nanoscrolls could be achieved via microwave irradiation. This method proves to produce the same quality and quantity of nanoscrolls as previously reported in literature. The interlayer spacings and XRD diffraction patterns were easily reproducible via this method as well. This rapid synthetic approach can lead to the rapid synthesis of nanocomposites for various applications at the nanoscale.[3,5,21] Further applications of the microwave synthetic method for fabricating nanocomposites are highlighted in Chapter 4.

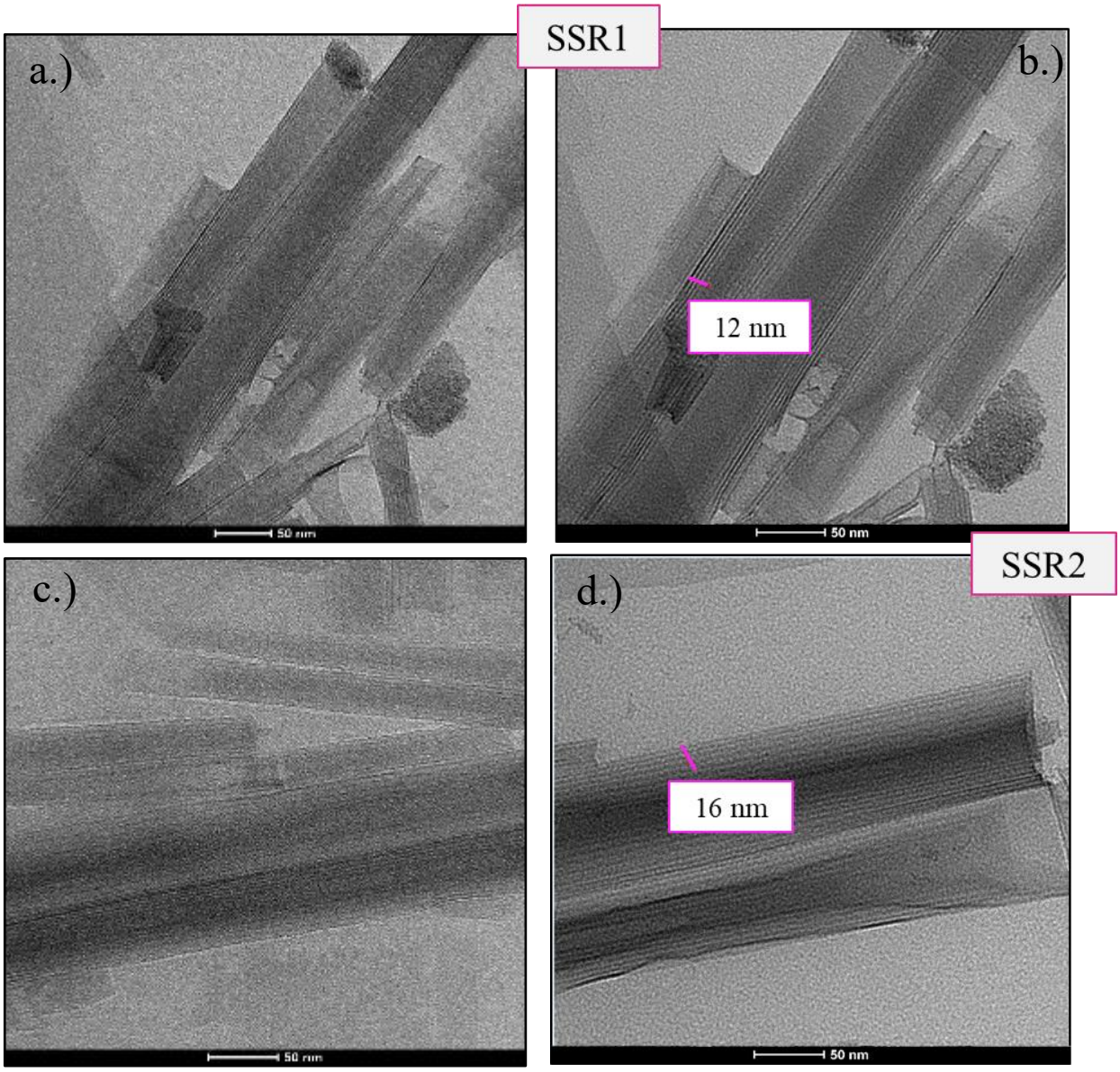

Figure 2.11. (a,b) TEM images of intercalated hexaniobate nanoscrolls synthesized via solvothermal protonation and microwave scrolling methods from solid-state reaction #1 (SSR1). (c,d) TEM images of intercalated hexaniobate nanoscrolls synthesized via solvothermal protonation and microwave scrolling (SSR2).

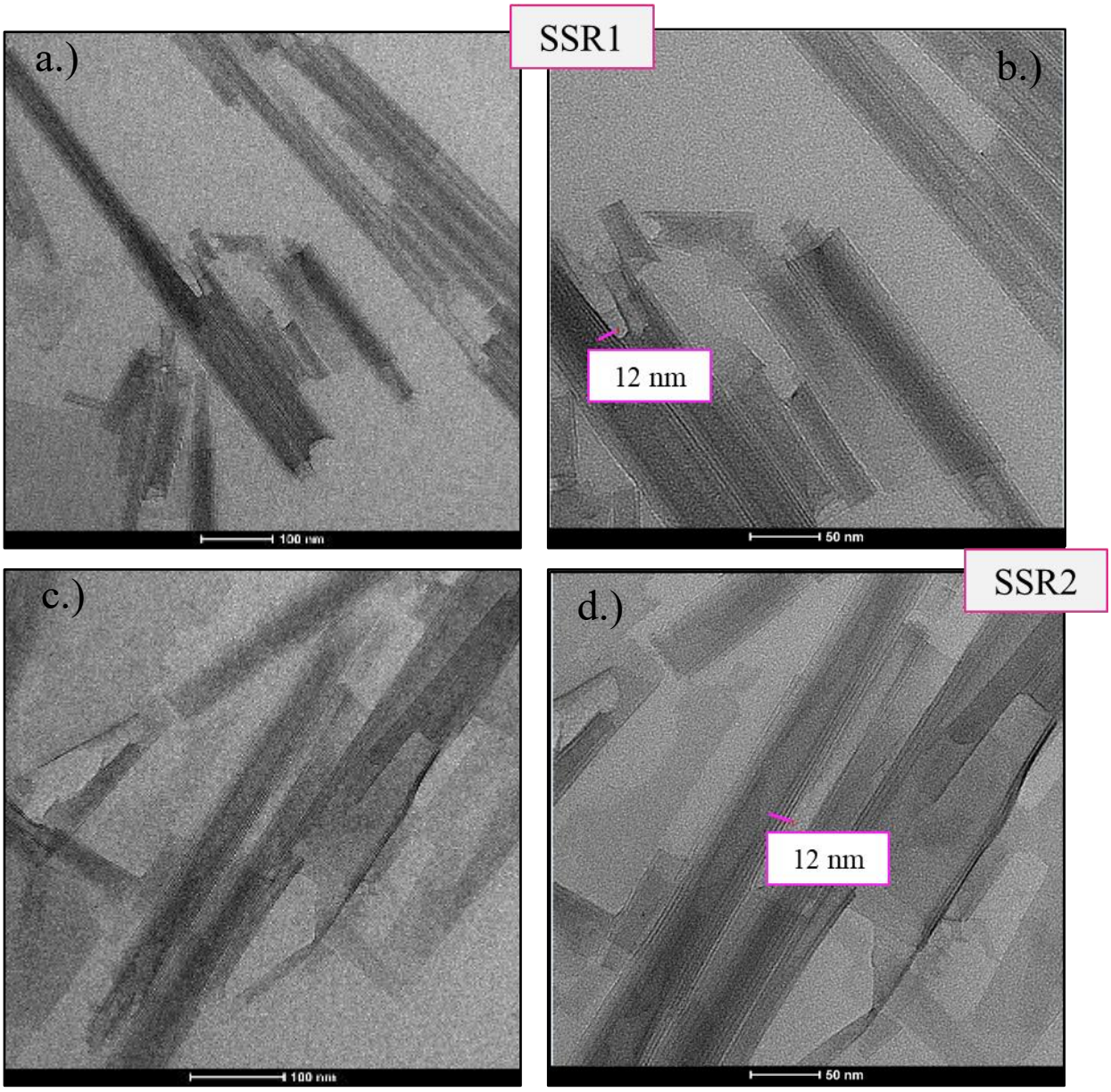

Figure 2.12. (a,b) TEM images of intercalated hexaniobate nanoscrolls synthesized via benchtop protonation and microwave scrolling methods from solid-state reaction #1 (SSR1). (c,d) TEM images of intercalated hexaniobate nanoscrolls synthesized via benchtop protonation (SSR2).

2.5 References

(1) Eguchi, M.; Angelone, M. S.; Yennawar, H. P.; Mallouk, T. E. Anisotropic Alignment of Lamellar Potassium Hexaniobate Microcrystals and Nanoscrolls in a Static Magnetic Field. *J. Phys. Chem. C* **2008**, *112* (30), 11280–11285 DOI: 10.1021/jp802702m.

(2) Adireddy, S.; Yao, Y.; He, J.; Wiley, J. B. Rapid solvothermal fabrication of hexaniobate nanoscrolls. *Mater. Res. Bull.* **2013**, *48* (9), 3236–3241 DOI: 10.1016/j.materresbull.2013.04.090.
(3) Viculis, L. M.; Mack, J. J.; Kaner, R. B. A Chemical Route to Carbon Nanoscrolls. *Science* **2003**, *299* (5611), 1361 DOI: 10.1126/science.1078842.
(4) Cao, J.; Musfeldt, J. L.; Mazumdar, S.; Chernova, N. A.; Whittingham, M. S. Pinned Low-Energy Electronic Excitation in Metal-Exchanged Vanadium Oxide Nanoscrolls. *Nano Lett.* **2007**, *7* (8), 2351–2355 DOI: 10.1021/nl071002l.
(5) Maeda, K.; Eguchi, M.; Youngblood, W. J.; Mallouk, T. E. Niobium Oxide Nanoscrolls as Building Blocks for Dye-Sensitized Hydrogen Production from Water under Visible Light Irradiation. *Chem. Mater.* **2008**, *20* (21), 6770–6778 DOI: 10.1021/cm801807b.
(6) Yao, Y.; Chaubey, G. S.; Wiley, J. B. Fabrication of Nanopeapods: Scrolling of Niobate Nanosheets for Magnetic Nanoparticle Chain Encapsulation. *J. Am. Chem. Soc.* **2012**, *134* (5), 2450–2452 DOI: 10.1021/ja206237v.
(7) Xiaobin Liu and Wenxiu Que and Peng Chen and Yapeng Tian and Jie Liu and Zuoli He and Huanfu Zhou and Ling Bing Kong. Facile preparation of protonated hexaniobate nanosheets and its enhanced photocatalytic activity. *Nanotechnology* **2017**, *28* (23), 235702.
(8) Lieber, C. M. One-dimensional nanostructures: Chemistry, physics & applications. *Solid State Commun.* **1998**, *107* (11), 607–616 DOI: 10.1016/S0038-1098(98)00209-9.
(9) Shiguihara, A. L.; Bizeto, M. A.; Constantino, V. R. L. Exfoliation of layered hexaniobate in tetra(n-butyl)ammonium hydroxide aqueous solution. *Colloids Surf. Physicochem. Eng. Asp.* **2007**, *295* (1), 123–129 DOI: 10.1016/j.colsurfa.2006.08.040.
(10) Saupe, G. B.; Waraksa, C. C.; Kim, H.-N.; Han, Y. J.; Kaschak, D. M.; Skinner, D. M.; Mallouk, T. E. Nanoscale Tubules Formed by Exfoliation of Potassium Hexaniobate. *Chem. Mater.* **2000**, *12* (6), 1556–1562 DOI: 10.1021/cm981136n.
(11) Bizeto, M. A.; Shiguihara, A. L.; Constantino, V. R. L. Layered niobate nanosheets: building blocks for advanced materials assembly. *J. Mater. Chem.* **2009**, *19* (17), 2512–2525 DOI: 10.1039/B821435B.
(12) Du, G. H.; Peng, L.-M.; Chen, Q.; Zhang, S.; Zhou, W. Z. Imaging helical potassium hexaniobate nanotubes. *Appl. Phys. Lett.* **2003**, *83* (8), 1638–1640 DOI: 10.1063/1.1605235.
(13) Sarahan, M. C.; Carroll, E. C.; Allen, M.; Larsen, D. S.; Browning, N. D.; Osterloh, F. E. K4Nb6O17-derived photocatalysts for hydrogen evolution from water: Nanoscrolls versus nanosheets. *Solid State Chem. Nanoscale Achiev. Chall. Oppor.* **2008**, *181* (7), 1678–1683 DOI: 10.1016/j.jssc.2008.06.021.
(14) Bizeto, M. A.; Constantino, V. R. L. Porphyrin inclusion into hexaniobate nanoscrolls. *Microporous Mesoporous Mater.* **2005**, *83* (1), 212–218 DOI: 10.1016/j.micromeso.2005.04.013.
(15) S. Akbarian-Tefaghi, T. Rostamzadeh, T. T. Brown, C. Davis-Wheeler, J. B. Wiley, ChemNanoMat 2017, 3, 538.
(16) Miyamoto, N.; Nakato, T. Liquid Crystalline Nanosheet Colloids with Controlled Particle Size Obtained by Exfoliating Single Crystal of Layered Niobate K4Nb6O17. *J. Phys. Chem. B* **2004**, *108* (20), 6152–6159 DOI: 10.1021/jp0363545.

(17) Maeda, K.; Eguchi, M.; Lee, S.-H. A.; Youngblood, W. J.; Hata, H.; Mallouk, T. E. Photocatalytic Hydrogen Evolution from Hexaniobate Nanoscrolls and Calcium Niobate Nanosheets Sensitized by Ruthenium(II) Bipyridyl Complexes. *J. Phys. Chem. C* **2009**, *113* (18), 7962–7969 DOI: 10.1021/jp900842e.
(18) Kobayashi, Y.; Hata, H.; Salama, M.; Mallouk, T. E. Scrolled Sheet Precursor Route to Niobium and Tantalum Oxide Nanotubes. *Nano Lett.* **2007**, *7* (7), 2142–2145 DOI: 10.1021/nl0708260.
(19) Brown, T.T., Akbarian-Tefaghi, S., Mitton, B., Moore, K., Veiga,E., Wiley, J.B., "Rapid Preparation of Hexaniobate Nanoscrolls and Nanopeapods via Microwave Assisted Reactions. Manuscript in Preparation.
(20) Du, G.; Yu, Y.; Peng, L.-M. Hexaniobate nanotubes with variable interlayer spacings. *Chem. Phys. Lett.* **2004**, *400* (4), 536–540 DOI: 10.1016/j.cplett.2004.11.011.
(21) Nicolosi, V.; Chhowalla, M.; Kanatzidis, M. G.; Strano, M. S.; Coleman, J. N. Liquid Exfoliation of Layered Materials. *Science* **2013**, *340* (6139) DOI: 10.1126/science.1226419.

Chapter 3 Solvothermal Synthesis of Cadmium Sulfide Peapod Nanocomposites

3.1 Introduction

Hollow one-dimensional nanostructures have been of great interest in recent years because they show significant promise in various scientific applications due to their inherent properties, one of which is their potential to encapsulate various nanomaterials.[1] One such structure that has been of recent research focus is a nanopeapod (NPP). NPPs are 1-dimensional nanoarchitectures that consist of a linear array of nanoparticles, the "peas", encapsulated within the hollow space of a nanotube or nanoscroll, the "pod". The first peapod structure, C_{60}@Carbon Nanotube (CNT), was discovered in 1998 by B. W. Smith.[2] Soon after, a host of other peapod structures were introduced by various research groups such as Au@MgO,[3] gold nanoparticle silica nanotube peapod (Au@SiO_2),[4] Au@Al_2O_3,[5] Cu@TiO_2,[6] Au@TiO_2,[6] and Ag@SiO_2.[7] The emergence of these peapod structures has shown how assembled enclosed nanoparticles exhibit intrinsic behavior that show great promise for the advancement of nanotechnology.[4,8]

Recently, much focus has been directed towards layered inorganic materials for use in various scientific applications. Because these materials have unique lamellar structures, there have been various approaches developed for the exfoliation of the sheets. Layered oxides, such as hexaniobate, can easily be exfoliated with the addition of acid and can readily form nanoscrolls along the [100] axis in an attempt to relieve structural stress and strain. [9–11] Moreover, one of the more interesting properties of layered hexaniobate is the fact that it is a wide band gap semiconductor material and exhibits photocatalytic activity under UV light, though the photocatalytic activity can be restricted due to its large band gap.[12] Therefore, because

of the scrolling capabilities of hexaniobate, encapsulating nanoparticles with light harvesting potential within hexaniobate nanoscrolls can lead to new nanoarchitectures for various scientific applications.

Cadmium sulfide is a known quantum dot material that has vast applications in optoelectronics.[13,14] It is also an important semiconductor that has been explored as a contender in solar cell fabrication, photoelectric devices and photocatalysts.[15,16] In this study, we have captured cadmium sulfide nanoparticles to form nanopeapods. In this report, preliminary results are shown, and further studies will be conducted on the UV and optical properties of these nanostructures.

3.2 Experimental

Starting Materials. K_2CO_3 (Alfa Aesar, 99%) and Nb_2O_5 (Alfa Aesar, 99%), tetrabutylammonium hydroxide 30-hydrate (TBAOH, Sigma Aldrich), oleylamine (Sigma Aldrich, 70%), toluene (Sigma Aldrich, anhydrous, 99.8%), hexanes (anhydrous, 95%), cadmium chloride (J.T. Baker Chemical Co.), sulfur (EM Science), distilled water, and ethanol (200 Proof, absolute).

3.2.1 Preparation of $K_4Nb_6O_{17}$ Nanosheets

$K_4Nb_6O_{17}$ Starting Material

K_2CO_3 and Nb_2O_5 (molar ratio of 1.1:1.5) were thoroughly mixed with grinding. The sample was then placed in an alumina crucible and heated at 900 ºC for 1 h and 1050 ºC for 48 h with one intermediate grinding. A 10 % excess of K_2CO_3 was used due to the volatilization of potassium oxide during the heating process.[11,17] The resulting white solid was then washed with distilled water to remove any excess reagents and centrifuged twice for 10 minutes, followed by

one 5-minute centrifugation with 15 mL of acetone. The products were then dried overnight at 70 ºC.

Acid exchange of $K_4Nb_6O_{17}$

Solvothermally, 1.0 g of $K_4Nb_6O_{17}$ was combined with 8 mL of 6M HNO_3 and placed into a Teflon-lined stainless-steel autoclave (Parr, model 4749, 1800 psi, 23 mL). The autoclave was heated to 90 ºC and held at that temperature for 48 h before cooling to room temperature. The product was then washed with 45 mL of distilled water before drying overnight at 70 °C.

3.2.2 Cadmium Sulfide Nanoparticle Synthesis

Cadmium sulfide (CdS) nanoparticles (NPs) of different shapes and sizes were synthesized according to previously published work.[18,19] Three different sets of CdS NPs were successfully synthesized, quasi-spherical, rod-shaped, and pseudo-cubic. All CdS NP syntheses were synthesized in a three-neck flask attached to a heating mantle, thermocouple, and aided by a magnetic stir bar.

Synthesis of quasi-spherical NPs.[18] Quasi-spherical nanoparticles were synthesized from 0.75 mmol (0.024g) of sulfur that was dissolved in 5 mL of oleylamine by heating at 50 °C. Separately, 1.5 mmol (0.275g) of cadmium chloride ($CdCl_2$) was dissolved in 10 mL of OAm at 160 °C and aged for 30 minutes under steady argon flow to form a cadmium-oleylamine (Cd-Oam) complex. Once dissolved, the sulfur-oleylamine (S-OAm) solution was injected into the Cd-OAm complex and the resulting mixture was aged for 6 h at 160 °C. The yellow cadmium sulfide NPs were precipitated out of solution with the addition of 50 mL of ethanol (EtOH), centrifuged, then dispersed in toluene. The resulting color was yellow.

Synthesis of rod-shaped NPs.[19] For the synthesis of rod-shaped NPs, 6 mmol (0.1926 g) of sulfur was added to 5 mL of oleylamine and heated to 50 °C. Separately, 1 mmol (0.183 g) of $CdCl_2$ was added to 10 mL of OAm and heated to 100 °C under a steady flow of argon for 30 minutes to completely dissolve the cadmium chloride. Once dissolved, the sulfur-oleylamine solution was injected into the hot cadmium-oleylamine solution, and the resulting reaction mixture was then aged at 100 °C with stirring for 19 hours. The reaction was quenched by the addition of excess ethanol. The resulting NPs were centrifuged in 50 mL of ethanol three times and re-dispersed in hexanes. The resulting color was yellow.

Synthesis of pseudo-cubic NPs.[19] Irregular shaped CdS NPs were synthesized by adding 30 mmol (0.962 g) of sulfur to 10 mL of oleylamine and heating under argon flow for 35 minutes at 70 ºC to fully dissolve the sulfur. In a separate flask, 10 mmol (1.832g) of cadmium chloride was dissolved in 15 mL oleylamine by heating at 100 ºC for 30 minutes. The resulting Cd-oleylamine complex was then injected into the hot sulfur-oleylamine solution, and the resulting mixture was aged for 19 hours with stirring. The NPs were then precipitated out of solution by the addition of ethanol with centrifugation and re-dispersed in toluene. The resulting color was yellow.

3.2.3 Cadmium Sulfide Nanopeapod Synthesis

To prepare CdS nanopeapods, 1 mL of as-synthesized CdS nanoparticle solution was added to a reaction mixture of 0.05 g of $H_xK_{4-x}Nb_6O_{17}$, 0.15 g (0.19 mmol) TBAOH, 5 mL (15 mmol) OAm, and 8 mL of toluene. The reaction mixture was then stirred at room temperature for 1h before being transferred to a 23 mL Teflon-lined stainless-steel autoclave (Parr, model 4749, 1800 psig). The autoclave was heated at 220 °C for 6h before being cooled to room temperature. The light-yellow precipitate was then washed with a combination of 10 mL ethanol and 5 mL toluene, then

centrifuged to isolate the solid. The washed product was then re-dispersed in toluene. The resulting color was light yellow.

3.2.4 Characterization

Transmission electron microscopy (TEM) images were acquired by a JEOL 2010 high-resolution microscope powered by an operating voltage of 200 keV and equipped with a Gatan slow scan charge-coupled device (CCD) camera. TEM sample preparation was carried out by drop-casting a dilute dispersion of nanoscrolls onto a 200-mesh copper grid.

3.3 Results

3.3.1 Cadmium Sulfide Nanoparticles

Three types of CdS NPs were successfully synthesized, but only two types were successfully encapsulated: rod-shaped and pseudo-cubic shaped. Quasi-spherical CdS NPs were encapsulated only when combined with pseudo-cubic CdS NPs and were synthesized using methods developed by Joo et al.[18] rod and pseudo-cubic-shaped CdS NPs were synthesized via procedures developed by Yong et al.[19] Figure 3.1 shows TEM images of the resulting synthesis of quasi-spherical CdS NPs with NP size ranging to be ~5-6 nm. It is known from previous reports of encapsulated nanomaterials that the ideal size of nanoparticles for this process is ~6-11nm.[9,20,21] It was evident from the lack of encapsulation within hexaniobate nanoscrolls that these nanoparticles were not ideal for fabricating nanopeapods.

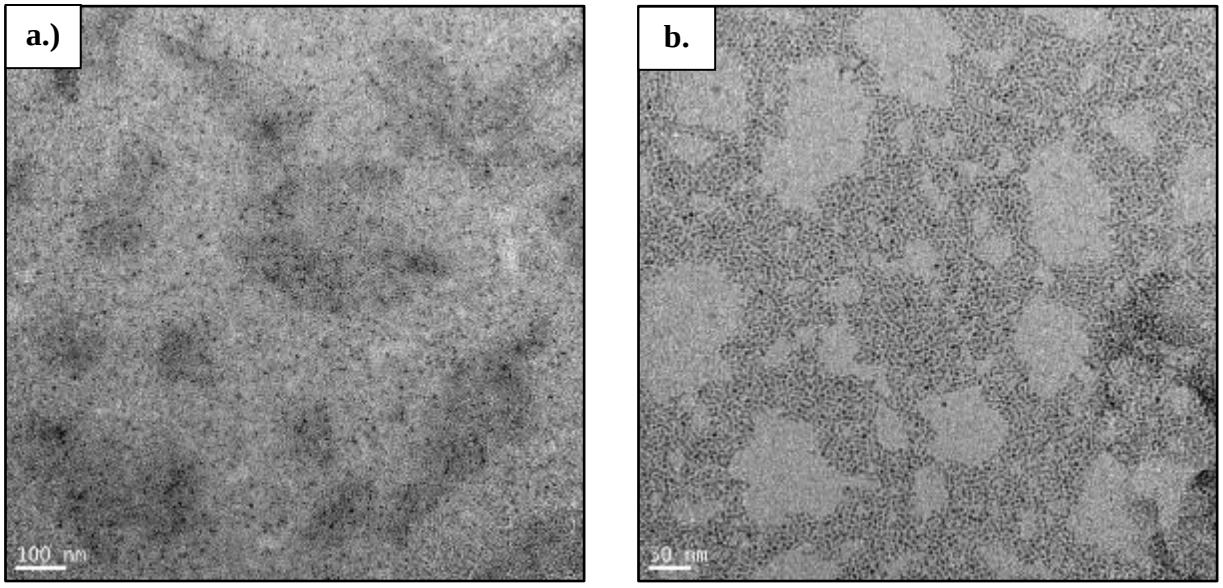

Figure 3.1. (a,b) TEM images of quasi-spherical CdS nanoparticles.

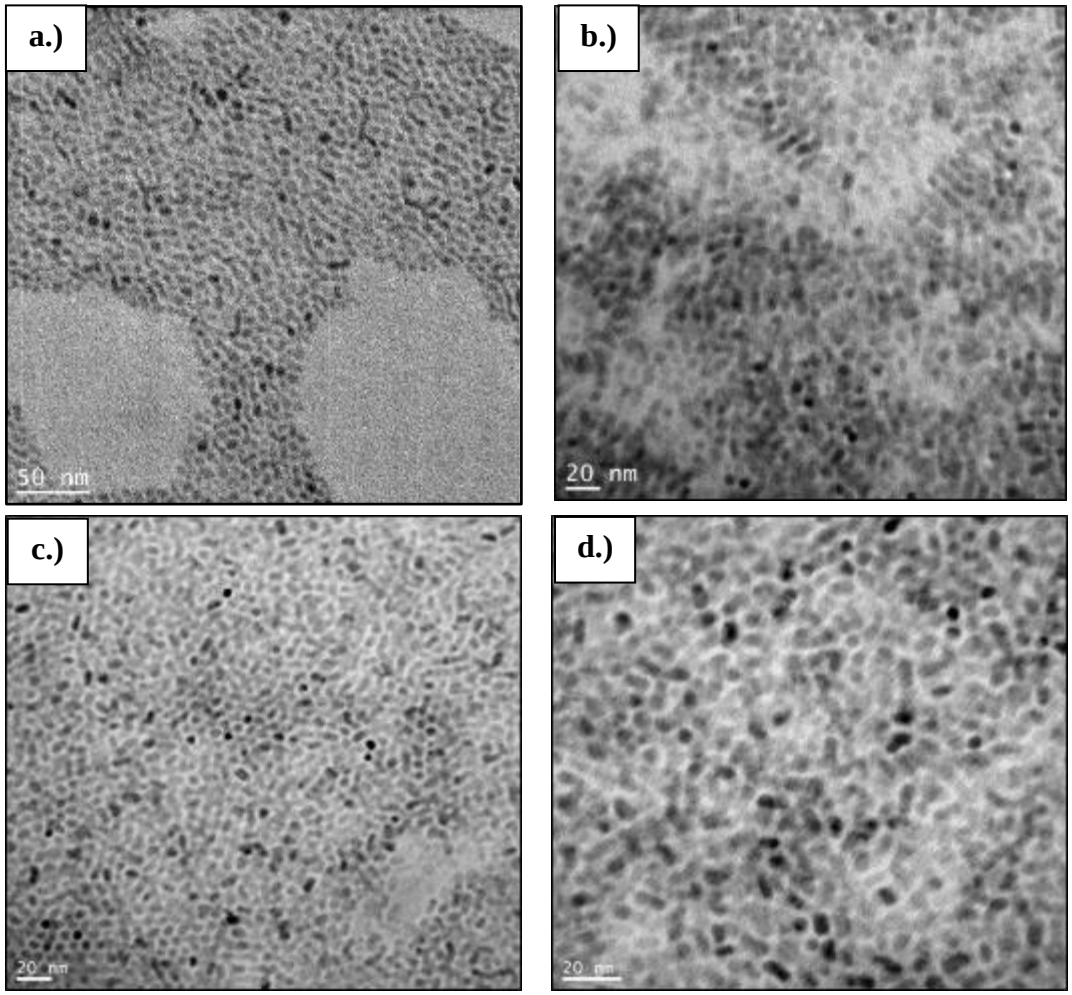

Figure 3.2. (a,b) TEM images of rod-shaped CdS nanoparticles. (c,d) TEM images of irregular-shaped CdS nanoparticles.

However, rod shaped (Figure 3.2) and pseudo-cubic shaped CdS NPs (~9-10 nm),

exhibited great loading behavior into hexaniobate nanoscrolls. Figure 3.3 shows the TEM images for the rod and pseudo-cubic – shaped cadmium sulfide nanopeapod (NPP) systems. As seen in Figure 3.3 a and 3.3b, rod-shaped NPs were successfully encapsulated within hexaniobate nanoscrolls, but there is also a high number of free nanoparticles in the system. The presence of excess free nanoparticles can be easily resolved by extra centrifugation of the sample. In Figure 3.3c and 3.3d, pseudo-cubic NPs were successfully encapsulated within hexaniobate nanoscrolls. It is interesting to note that with the pseudo-cubic CdS nanopeapod system, encapsulation of nanoparticles does not seem to be dependent upon shape of the nanoparticles. Furthermore, as observed previously,[20] the nanoparticles dictate the size of the inner diameter of the hexaniobate nanoscroll.

Mixed nanopeapod structures are shown in Figure 3.4. Figures 3.4a and 3.4b show as-synthesized nanoparticles of pseudo-cubic and quasi-spherical shaped NPs that were used for NPP preparation. Figure 3.4c shows the encapsulation of both NP shapes with an average size of ~9-10nm. From these observations, there may be some significance in the alignment of similarly sized and shaped nanoparticles. Highlighted in yellow, Figure 3.4c also shows both pseudo-cubic and quasi-spherical shaped NPs encapsulated within one NPP. It is obvious that the nanoparticles are separated in a way that hints at the segregation of the NPs with like-sized particle shapes and sizes.

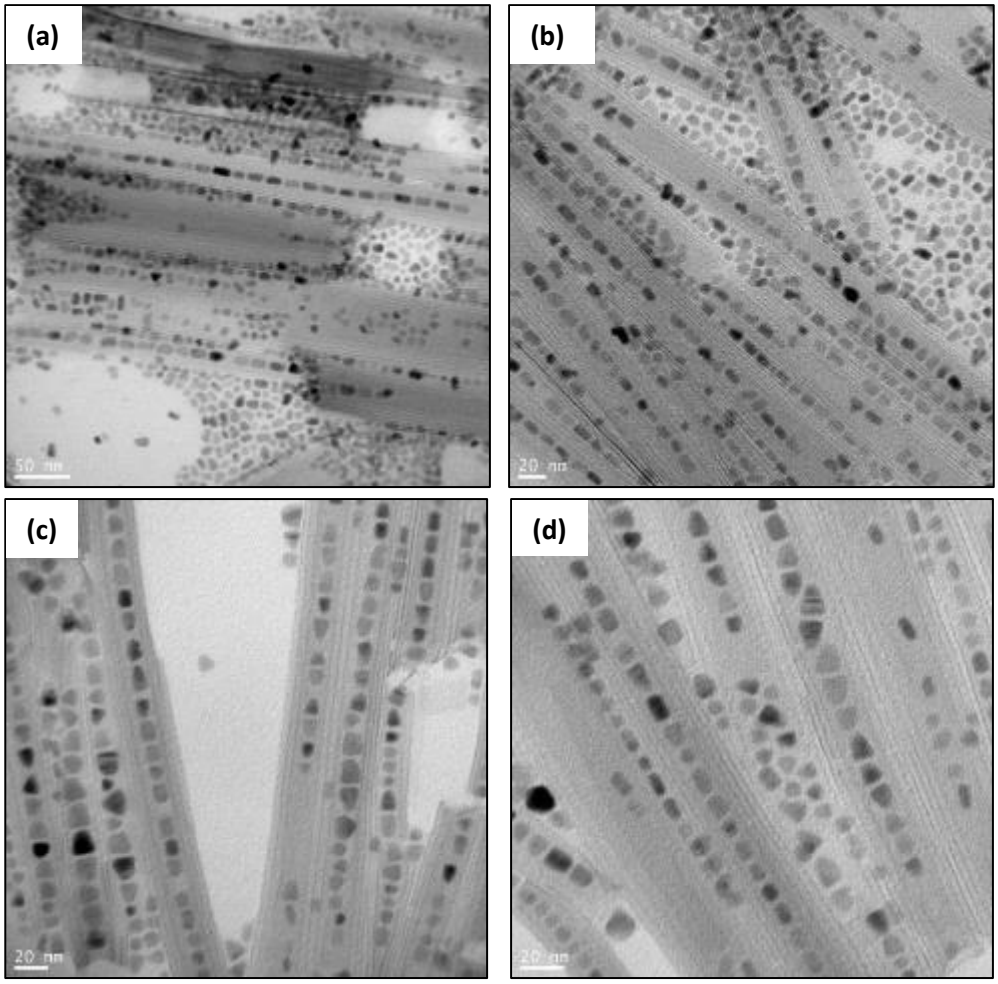

Figure 3.1. (a-b) TEM images of rod-shaped CdS NP@hexaniobate nanopeapods (c-d) TEM images of pseudo-cubic CdS NP@hexaniobate.

3.4 Discussion

Cadmium sulfide nanoparticles have been successfully encapsulated within hexaniobate nanoscrolls by the solvothermal method as outlined in Chapter 1, adding to the library of hexaniobate encapsulated nanocomposites.[9,20–22] The various CdS NPs were chosen based on the reproducibility of the procedures, the expected size and shapes that were to be produced, and the encapsulation observations seen with these NPs within the hexaniobate nanoscrolls. We observed that regardless of shape and size (≤ 11 nm), nanoparticles of various shapes could be successfully encapsulated within hexaniobate nanoscrolls.

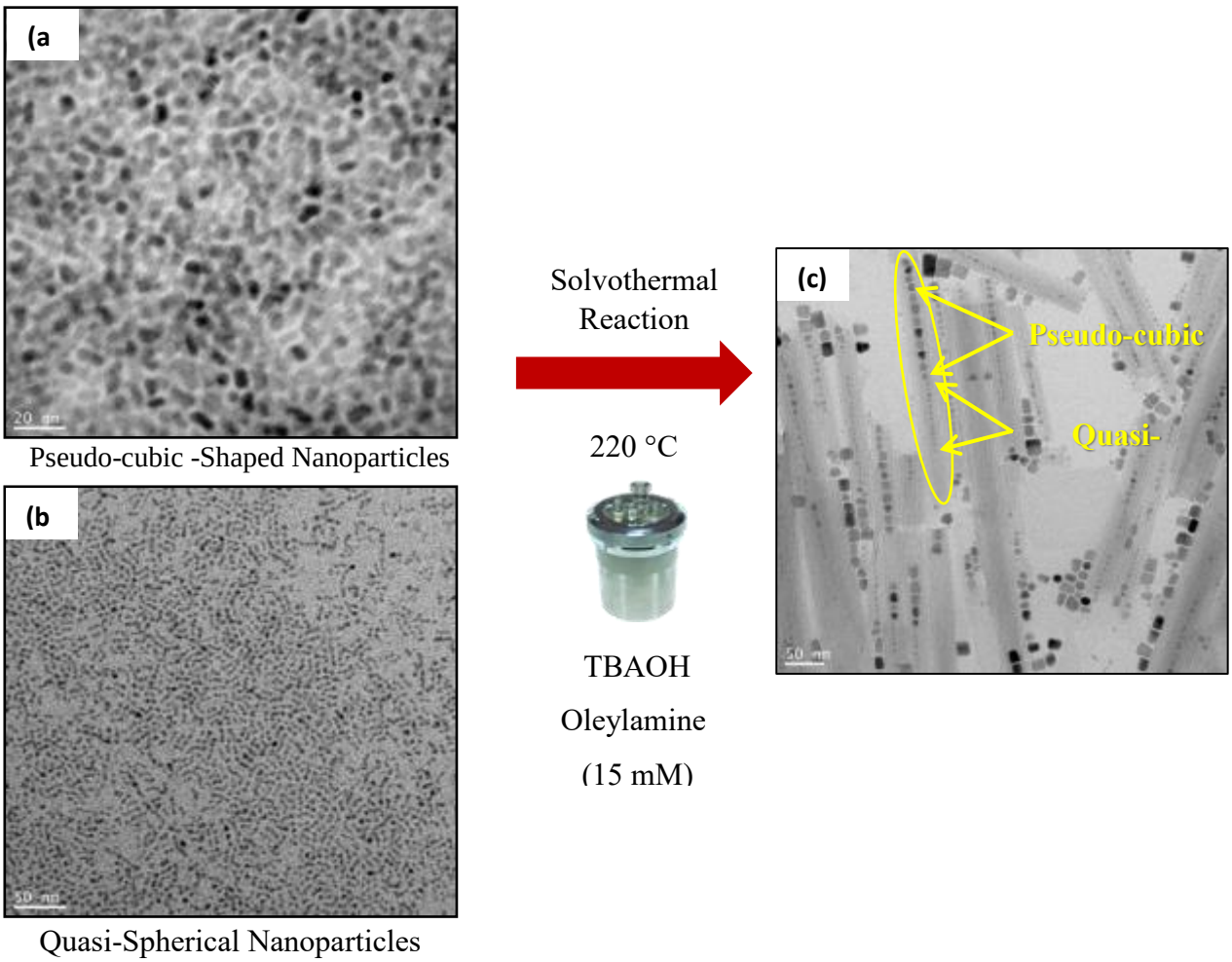

Figure 3.2. TEM images of (a) pseudo-cubic CdS QDs (b) quasi-spherical QDs and (c) the resulting CdS@hexaniobate nanopeapod structures combining the differently shaped CdS quantum dots.

It is important to note the role of TBAOH and oleylamine (OAm) in the synthesis of these nanopeapod formations. TBAOH is used to aide in the exfoliation of the nanosheets, whereas OAm is used to make sure the particles and peapods remain suitable for the environment they are in. Temperature is also an important factor in nanopeapod formation because higher temperatures have been proven to produce higher nanopeapod yields. [11] Moreover, in considering scroll formation, it is important to note the various factors which influence nanopeapod formation such as mechanical stress on the nanosheet during the

delamination and scrolling processes, structural defects of the nanosheets, and the pressure evolving from the use of the autoclave during the solvothermal process. [11,17]

One question that continues to arise concerns the mechanism for nanoscroll and nanopeapod formation. From this experiment, it can be determined that the scrolling and capture of pre-formed nanoparticles is not a random occurrence due to the amount of structures that are able to be formed. As seen in Figure 3.4c, there is some sort of organization that happens with the capture of nanoparticles once introduced to the surface of the hexaniobate nanosheets. Due to this phenomenon, it has been theorized that nanoparticles organize along the perimeter of the nanosheets due to interactions of surface groups before scrolling begins to occur.[22] Figure 3.4c also shows size segregation in different areas of the same NPP, again, confirming size selectivity of the NPs in the scrolling process. On the other hand, it has also been suggested that the nanoparticles aide in the scrolling and capture processes since the inner diameters of the nanoscroll match closely with the size of the nanoparticle encapsulated. [11,21]

3.5 Conclusions

Encapsulating nanoparticles is a significant feature of the scrolling of hexaniobate nanosheets. Being able to encapsulate nanoparticles allows for the enhancement of various properties exhibited by different types of nanoparticles such as CdS NPs. From this study, CdS NPs were captured in rod and irregular shapes, along with providing insight on the size and shape selectivity in terms of observing the encapsulation of the same size and shape of nanoparticles within the same nanopeapod. Applications for nanopeapods could encompass areas focused on catalysis,[23] hydrogen production,[24–26] and even in solar cell development. [27]

3.6 References

(1) Adireddy, S.; Carbo, C. E.; Yao, Y.; Vargas, J. M.; Spinu, L.; Wiley, J. B. High-Yield Solvothermal Synthesis of Magnetic Peapod Nanocomposites via the Capture of Preformed

Nanoparticles in Scrolled Nanosheets. *Chem. Mater.* **2013**, *25* (19), 3902–3909 DOI: 10.1021/cm402352k.

(2) Smith, B. W.; Monthioux, M.; Luzzi, D. E. Encapsulated C60 in carbon nanotubes. *Nature* **1998**, *396* (6709), 323–324 DOI: 10.1038/24521.

(3) (a) Sun, Y. Q.; Wu, Q. O.; Shi, G. Q., Graphene based new energy materials. Energy & Environmental Science 2011, 4 (4), 1113-1132; (b) Cui, X.; Zhang, C. Z.; Hao, R.; Hou, Y. L., Liquid-phase exfoliation, functionalization and applications of graphene. Nanoscale 2011, 3 (5), 2118-2126; (c) Chen, D.; Tang, L. H.; Li, J. H., Graphene-based materials in electrochemistry. Chemical Society Reviews 2010, 39 (8), 3157-3180; (d) Dias, A. S.; Lima, S.; Carriazo, D.; Rives, V.; Pillinger, M.; Valente, A. A., Exfoliated titanate, niobate and titanoniobate nanosheets as solid acid catalysts for the liquid-phase dehydration of D-xylose into furfural. Journal of Catalysis 2006, 244 (2), 230-237.

(4) Cong, V. T.; Ganbold, E.-O.; Saha, J. K.; Jang, J.; Min, J.; Choo, J.; Kim, S.; Song, N. W.; Son, S. J.; Lee, S. B.; et al. Gold Nanoparticle Silica Nanopeapods. *J. Am. Chem. Soc.* **2014**, *136* (10), 3833–3841 DOI: 10.1021/ja411034q.

(5) TY - JOUR AU - Qin, Yong AU - Vogelgesang, Ralf AU - Eßlinger, Moritz AU - Sigle, Wilfried AU - van Aken, Peter AU - Moutanabbir, Oussama AU - Knez, Mato TI - Waveguides: Bottom-Up Tailoring of Plasmonic Nanopeapods Making Use of the Periodical Topography of Carbon Nanocoil Templates (Adv. Funct. Mater. 24/2012) JO - Advanced Functional Materials JA - Adv. Funct. Mater. VL - 22 IS - 24 PB - WILEY-VCH Verlag SN - 1616-3028 UR - http://dx.doi.org/10.1002/adfm.201290149 DO - 10.1002/adfm.201290149 SP - 5284 EP - 5284 KW - atomic layer deposition KW - carbon nanocoils KW - nanopeapods KW - plasmon resonance KW - waveguides PY - 2012 ER -.

(6) Kasuga, T.; Hiramatsu, M.; Hoson, A.; Sekino, T.; Niihara, K., Formation of titanium oxide nanotube. Langmuir 1998, 14 (12), 3160-3163.

(7) (a) Takagi, S.; Eguchi, M.; Tryk, D. A.; Inoue, H., Porphyrin photochemistry in inorganic/organic hybrid materials: Clays, layered semiconductors, nanotubes, and mesoporous materials. Journal of Photochemistry and Photobiology C-Photochemistry Reviews 2006, 7 (2-3), 104-126; (b) Mao, J. G.; Wang, Z. K.; Clearfield, A., New lead inorganic-organic hybrid microporous and layered materials: Synthesis, properties, and crystal structures. Inorganic Chemistry 2002, 41 (23), 6106-6111; (c) Shimojima, A.; Sugahara, Y.; Kuroda, K., Inorganic-organic layered materials derived via the hydrolysis and polycondensation of trialkoxy (alkyl) silanes. Bulletin of the Chemical Society of Japan 1997, 70 (11), 2847-2853.

(8) Hunyadi, S. E.; Murphy, C. J. The Journal of Physical Chemistry B 2006, 110, 7226.

(9) Yao, Y.; Chaubey, G. S.; Wiley, J. B. Fabrication of Nanopeapods: Scrolling of Niobate Nanosheets for Magnetic Nanoparticle Chain Encapsulation. *J. Am. Chem. Soc.* **2012**, *134* (5), 2450–2452 DOI: 10.1021/ja206237v.

(10) Kong, X.; Hu, D.; Wen, P.; Ishii, T.; Tanaka, Y.; Feng, Q. Transformation of potassium Lindquist hexaniobate to various potassium niobates: solvothermal synthesis and structural evolution mechanism. *Dalton Trans.* **2013**, *42* (21), 7699–7709 DOI: 10.1039/C3DT00062A.

(11) Adireddy, S.; Yao, Y.; He, J.; Wiley, J. B. Rapid solvothermal fabrication of hexaniobate nanoscrolls. *Mater. Res. Bull.* **2013**, *48* (9), 3236–3241 DOI: 10.1016/j.materresbull.2013.04.090.

(12) Smith, R. J.; King, P. J.; Lotya, M.; Wirtz, C.; Khan, U.; De, S.; O'Neill, A.; Duesberg, G. S.; Grunlan, J. C.; Moriarty, G. Advanced materials 2011, 23, 3944.

(13) Kar, S.; Chaudhuri, S. Cadmium sulfide one-dimensional nanostructures: synthesis, characterization and application. *Synth. React. Inorg. Met.-Org. Nano-Met. Chem.* **2006**, *36* (3), 289–312.

(14) Chang, S.; Liu, L.; Asher, S. A. Preparation and properties of tailored morphology, monodisperse colloidal silica-cadmium sulfide nanocomposites. *J. Am. Chem. Soc.* **1994**, *116* (15), 6739–6744.

(15) Yang, H.; Huang, C.; Li, X.; Shi, R.; Zhang, K. Luminescent and photocatalytic properties of cadmium sulfide nanoparticles synthesized via microwave irradiation. *Mater. Chem. Phys.* **2005**, *90* (1), 155–158.

(16) Olea, A.; Sebastian, P. (Zn, Cd) S porous layers for dye-sensitized solar cell application. *Sol. Energy Mater. Sol. Cells* **1998**, *55* (1), 149–156.

(17) Saupe, G. B.; Waraksa, C. C.; Kim, H.-N.; Han, Y. J.; Kaschak, D. M.; Skinner, D. M.; Mallouk, T. E. Nanoscale Tubules Formed by Exfoliation of Potassium Hexaniobate. *Chem. Mater.* **2000**, *12* (6), 1556–1562 DOI: 10.1021/cm981136n.

(18) Joo, J.; Na, H. B.; Yu, T.; Yu, J. H.; Kim, Y. W.; Wu, F.; Zhang, J. Z.; Hyeon, T. Generalized and Facile Synthesis of Semiconducting Metal Sulfide Nanocrystals. *J. Am. Chem. Soc.* **2003**, *125* (36), 11100–11105 DOI: 10.1021/ja0357902.

(19) Yong, K.-T.; Sahoo, Y.; Swihart, M. T.; Prasad, P. N. Shape Control of CdS Nanocrystals in One-Pot Synthesis. *J. Phys. Chem. C* **2007**, *111* (6), 2447–2458 DOI: 10.1021/jp066392z.

(20) High-Yield Solvothermal Synthesis of Magnetic Peapod Nanocomposites via the Capture of Preformed Nanoparticles in Scrolled Nanosheets. *Chem. Mater.* **2013**, 130917074751007.

(21) Peapod-Type Nanocomposites through the In Situ Growth of Gold Nanoparticles within Preformed Hexaniobate Nanoscrolls. *Angew. Chem. Int. Ed.* **2014**, *53* (18), 4614.

(22) Adireddy, S.; Rostamzadeh, T.; Carbo, C. E.; Wiley, J. B. Particle Placement and Sheet Topological Control in the Fabrication of Ag–Hexaniobate Nanocomposites. *Langmuir* **2015**, *31* (1), 480–485 DOI: 10.1021/la503775f.

(23) Chapleski, R. C.; Musaev, D. G.; Hill, C. L.; Troya, D. Reaction Mechanism of Nerve-Agent Hydrolysis with the Cs8Nb6O19 Lindqvist Hexaniobate Catalyst. *J. Phys. Chem. C* **2016**, *120* (30), 16822–16830 DOI: 10.1021/acs.jpcc.6b05528.

(24) Maeda, K.; Eguchi, M.; Lee, S.-H. A.; Youngblood, W. J.; Hata, H.; Mallouk, T. E. Photocatalytic Hydrogen Evolution from Hexaniobate Nanoscrolls and Calcium Niobate Nanosheets Sensitized by Ruthenium(II) Bipyridyl Complexes. *J. Phys. Chem. C* **2009**, *113* (18), 7962–7969 DOI: 10.1021/jp900842e.

(25) Maeda, K.; Eguchi, M.; Youngblood, W. J.; Mallouk, T. E. Niobium Oxide Nanoscrolls as Building Blocks for Dye-Sensitized Hydrogen Production from Water under Visible Light Irradiation. *Chem. Mater.* **2008**, *20* (21), 6770–6778 DOI: 10.1021/cm801807b.

(26) Nakato, T.; Fujita, T.; Mouri, E. Synergistic photocatalytic hydrogen evolution over oxide nanosheets combined with photochemically inert additives. *Phys. Chem. Chem. Phys.* **2015**, *17* (8), 5547–5550 DOI: 10.1039/C4CP06083K.

(27) Li, X.; Zhang, T.; Gu, S.; Kang, S.-Z.; Li, G.; Mu, J. Reduced graphene oxide/potassium niobate composite nanoscrolls with enhanced photocatalytic activity for dye degradation. *Sep. Purif. Technol.* **2013**, *108* (Supplement C), 139–142 DOI: 10.1016/j.seppur.2013.02.018.

Chapter 4 Microwave-Assisted Synthesis of Metal and Metal Oxide Nanoparticles and Nanopeapods

4.1 Introduction

Advances in the technological capability to advance the synthesis of nanomaterials has become of great interest in a variety of fields. More specifically, the ability to synthesize nanomaterials via solvothermal methods has gained much popularity in the area of synthesizing various nanocomposites such as nanopeapod (NPP) structures.[1–5] However, these methods can be time-consuming and produce unnecessary waste products. As a result, microwave-assisted reactions have become a great compromise for synthesizing such products.[6–10]

In this chapter, microwave synthetic approaches have been used to synthesize protonated hexaniobate, hexaniobate nanoscrolls, hexaniobate nanopeapods, and cadmium sulfide (CdS) nanoparticles. Microwave assisted (MA) methods were found to be successful in creating nanopeapod architectures in three hours or less with minimal waste product. These peapod-like nanostructures can provide a means for applications in areas such as photonics,[11] magnetic devices,[12] and catalysis[2,13,14] with the advantage of being fabricated in less time than previously reported methods. [1, 3]

4.2 Experimental

Starting Materials. K_2CO_3 (Alfa Aesar, 99%) and Nb_2O_5 (Alfa Aesar, 99%), tetrabutylammonium hydroxide 30-hydrate (TBAOH, Sigma Aldrich), oleylamine (Sigma Aldrich, 70%), iron(III) acetylacetonate (97%, Sigma Aldrich), cadmium chloride (J.T. Baker Chemical Co.), sulfur (EM Science), toluene (Sigma Aldrich, anhydrous, 99.8%), distilled water, and ethanol (Pharmco-Aaper, 200 Proof, absolute).

4.2.1 Preparation of $K_4Nb_6O_{17}$ Nanosheets

$K_4Nb_6O_{17}$ Starting Material. K_2CO_3 and Nb_2O_5 (molar ratio of 1.1:1.5) was completed in an alumina crucible at 900º C for 1 h with intermediate grinding before further heating at 1050 º C for 48h. Ten percent excess of K_2CO_3 was present due to the volatilization of potassium oxide during the heating process.[15, 16] The resulting white solid was then washed via centrifugation twice for 10 minutes with distilled water to remove any excess reagents, followed by one 5-minute centrifugation with 15 mL of acetone. The products were then dried overnight at 70 ºC.

Acid exchange of $K_4Nb_6O_{17}$. Microwave protonation of $K_4Nb_6O_{17}$ was achieved by treating 0.5 g hexaniobate with 5 mL of 6M HNO_3 solution in a StartSYNTH Microwave Synthesis Labstation in which the reaction itself was kept inside a of a quartz pressure reaction vessel (<15 bar) and placed in a rotor within the instrument for 3 h at 60 ºC, 10 minute warmup, with constant stirring and power maintained at 300W.[17] The resulting products was washed via centrifugation twice with distilled water to remove any excess reagents followed by centrifugation with 15 mL of acetone then dried overnight at 70 ºC.

4.2.2 Nanoparticle Synthesis

Synthesis of Fe_3O_4 NPs. $Fe(acac)_2$ (1.1g) with 11 mL of oleylamine and 1.5 mL of oleic acid was placed in a three-neck flask attached to a heating mantle, thermocouple, and aided by a magnetic stir bar and stirred for 30 minutes at 70 °C. The solution was then sonicated for 1 min before being transferred into a Teflon-lined stainless-steel autoclave (Parr, model 4749, 1800 psi, 23 mL) and heated at 240°C for 24 h.

Synthesis of Rod-Shaped CdS NPs.[18] For the synthesis of rod-shaped NPs, 6 mmol (0.2g) of sulfur was added to 5 mL of oleylamine and heated to 50 °C. Separately, 1 mmol (0.2 g) of $CdCl_2$ was added to 10 mL of OAm and heated to 100 °C under a steady flow of argon for 30

minutes to completely dissolve the cadmium chloride. Once dissolved, the sulfur-oleylamine solution was injected into the hot cadmium-oleylmine solution, and the resulting reaction mixture was then aged at 100 °C with stirring for 19 hours. The reaction was quenched by the addition of excess ethanol. The resulting NPs were centrifuged in 50 mL of ethanol three times and re-dispersed in hexanes.

Microwave-Assisted Synthesis of CdS NPs. A modified synthesis of rod-shaped CdS NPs derived from the synthesis stated above was used for microwave synthesis. 3 mmol (0.1 g) of sulfur was added to 5 mL of oleylamine and heated to 50 °C. Separately, 0.5 mmol (0.1 g) of CdCl2 was added to 10 mL of OAm inside a of a quartz pressure reaction vessel (<15 bar) and placed in a rotor within a StartSYNTH Microwave Synthesis Labstation for 1.5 h at 135 ºC, 15-minute warmup, with constant stirring and power maintained at 700W. The resulting product was washed via centrifugation with ethanol followed by centrifugation with toluene and re-dispersed in toluene.

4.2.3 Preparation of Microwave Synthesized Nanopeapods

Nanopeapod formation was achieved by microwave-irradiated synthesis by adding 0.05 g $H_xK_{4-x}Nb_6O_{17}$, TBAOH (9.5 mmol), and olelylamine (7.5 mmol), 0.5 mL of Fe_3O_4 or CdS nanoparticle solution in 4.5 mL toluene to a quartz pressure reaction vessel (<15 bar) and placed in a rotor within a StartSYNTH Microwave Synthesis Labstation at 135 C for 1.5 h with a 15-minute warmup and max power maintained at 700W. The products were centrifuged in 30 mL of ethanol and intermittently sonicated to remove any excess nanoparticles. The nanopeapods were then re-dispersed in toluene.

4.2.4 Characterization

Transmission electron microscopy (TEM) images were acquired by a JEOL 2010 high-resolution microscope powered by an operating voltage of 200 keV and equipped with a Gatan

slow scan charge-coupled device (CCD) camera. TEM sample preparation was carried out by drop-casting a dilute dispersion of nanoparticles or nanopeapods onto a 200 mesh copper grid.

4.3 Results

Microwave irradiation is a rapidly growing technique in which nanomaterials can be produced quickly and with tunable parameters. Figure 4.1 shows TEM images of Fe_3O_4 nanoparticles that were synthesized solvothermally and used in microwave reaction to form the Fe_3O_4@hexaniobate nanocomposites shown in Figure 4.2. In a reaction that took less than 2 hours, we observed the capture of Fe_3O_4 nanoparticles via microwave synthesis for the very first time in our group. The nanoparticles are uniformly aligned within the hexaniobate. To confirm the reproducibility of this synthetic approach to form nanopeapods, the experiment was tried repeatedly, and results are shown in Figure 4.3. This method proves to be effective in successfully

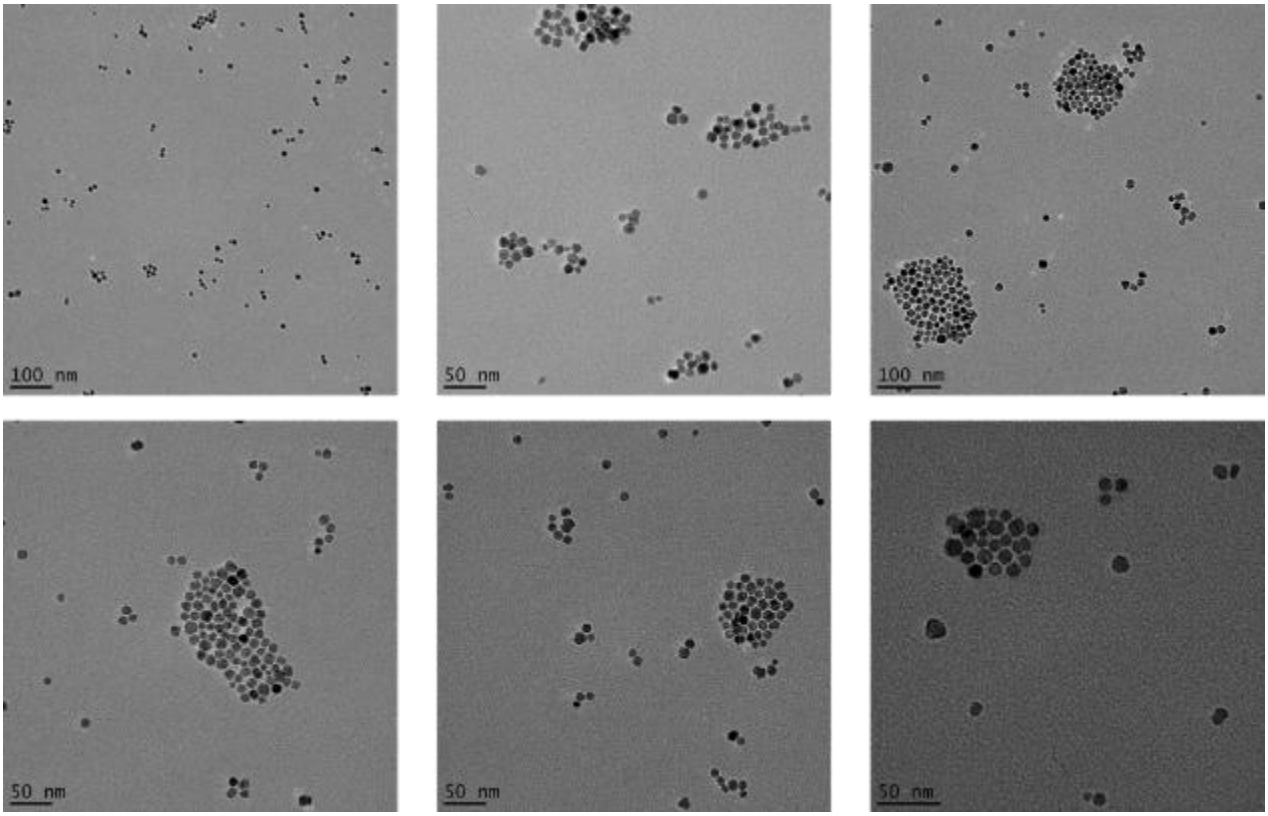

Figure 4.1. TEM images of solvothermally prepared Fe3O4 nanoparticles measuring ~11-12nm.

capturing Fe_3O_4 nanoparticles with uniform alignment of the nanoparticles within the hexaniobate nanoscrolls.

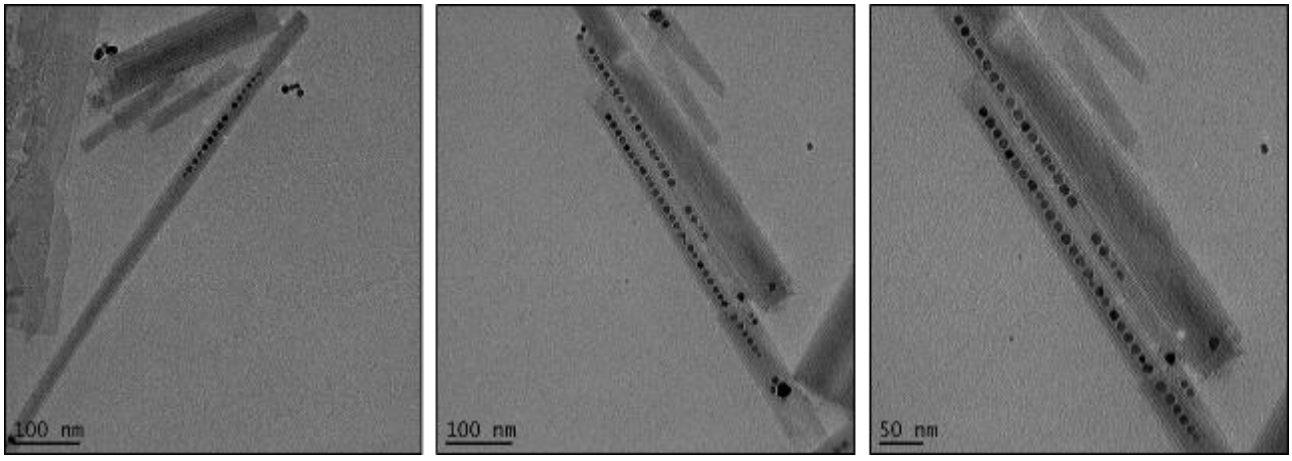

Figure 4.2. TEM images of the first attempt at microwave synthesized Fe3O4@hexaniobate nanopeapods.

Another system studied via microwave synthesis for the formation of nanopeapods was CdS nanoparticles. Rod-shaped CdS nanoparticles, originally synthesized by the bottom-up approach as outlined in Chapter 3, was used in the microwave method for the formation of CdS@hexaniobate nanopeapods shown in Figure 4.4. It is interesting to note the encapsulation of small rod shaped (~5nm) CdS nanoparticles which have been difficult to capture in previous studies. However, due to the small size of the nanoparticles, there are also a lot of free nanoparticles congregated outside of the nanopeapods as well. Another observation is of circular dark spots seen in Figure 4.4 which are gold nanoparticles that were a result of contamination from a previous reaction done in the same reaction vessel. Interestingly enough, these nanoparticles have successfully been encapsulated inside of the hexaniobate nanoscrolls as well along with the CdS nanoparticles.

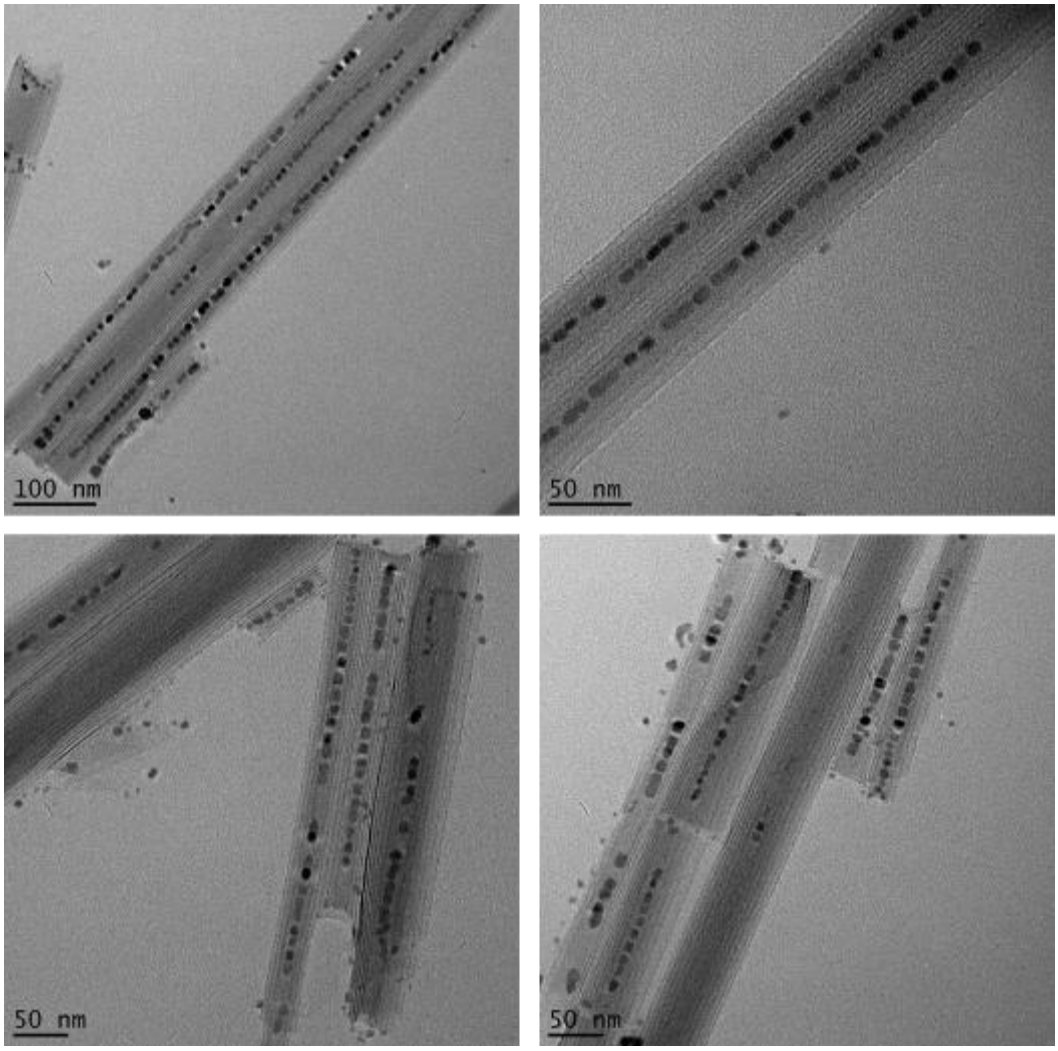

Figure 4.3. TEM images of microwave synthesized Fe3O4@hexaniobate nanopeapods showing uniform encapsulation.

After observations of successful encapsulation of solvothermally prepared nanoparticles, interest was turned to microwave synthesized nanoparticles for encapsulation. Following the same synthetic protocol for microwave synthesized nanopeapods, CdS nanoparticles (Figure 4.5) could be obtained. These nanoparticles were then used to form the CdS@hexaniobate nanopeapods shown in Figure 4.6. It is interesting to observe the phenomena of large CdS nanoparticles that seem to be setting the template for the inter diameter spacing of the hexaniobate nanopeapods. Normally, when we observe encapsulated nanoparticles within hexaniobate nanopeapods, distinctive interlayer spacings can be seen. However, in Figure 4.6, not only do we see much

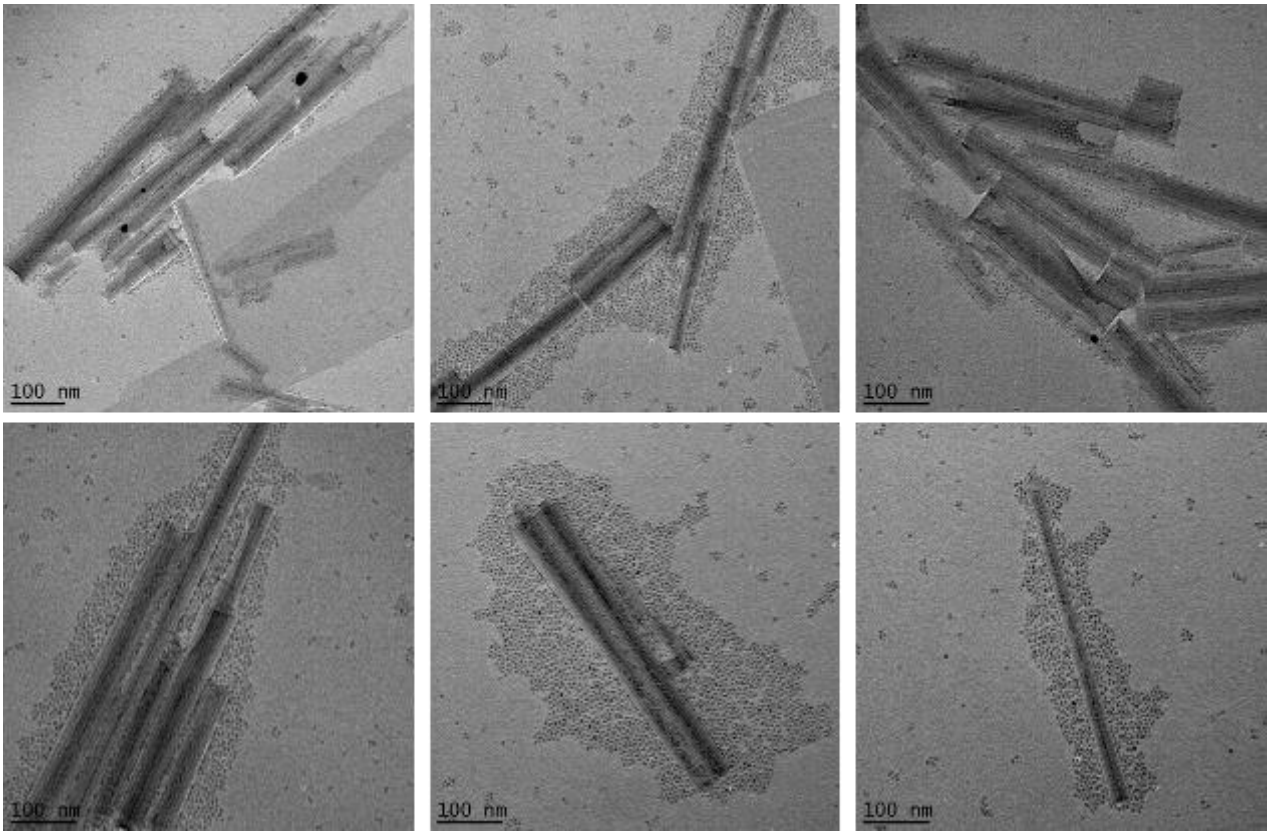

Figure 4.4. TEM images of microwave synthesized CdS@hexaniobate nanopeapods showing uniform encapsulation.

smaller interlayer spacings akin to characteristics of simple nanoscrolls (SNS), we also observe a non-uniform loading of nanoparticles into the nanoscroll. It is unclear as to how the formation of these nanocomposites occurred in this manner, but it is noteworthy that the size of majority of the nanoparticles encapsulated are larger (~20-25 nm) than what has been successfully encapsulated as documented in past literature.

4.4 Discussion

Microwave synthesis of nanopeapods has proved to be a more rapid and effective method in the formation of nanopeapods compared to that of previous studies presented by our group.[1,2,19] Nanocomposites formed via microwave synthesis show the same attributes as those formed

solvothermally, however, the size of nanoparticles introduced to the nanoscrolls in reaction seem to defy the size limitations we previously thought could not be encapsulated in these structures.

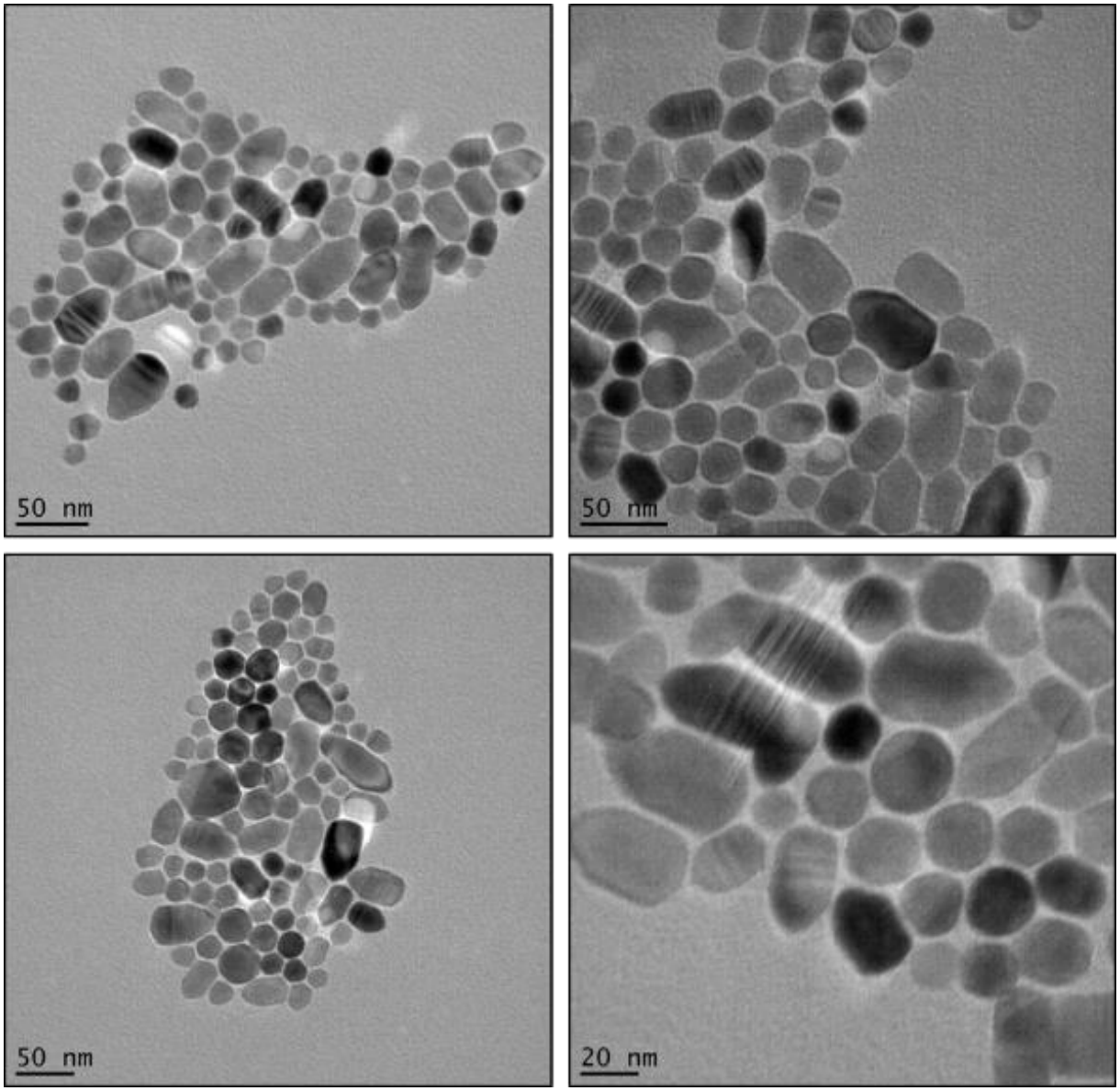

Figure 4.5. TEM images of irregular shaped CdS nanoparticles synthesized via microwave irradiation.

Moreover, not only are we able to fabricate these structures in rapid time, but we can also use less heat to still synthesize the same quality of nanopeapods. However, it can be observed that there is still a variation in length, inner and outer diameters of the nanopeapods, clearly made evident in Figure 4.6. The inner diameters of the nanoscroll seem to be dictated by the size

of the nanoparticles being encapsulated. In reference to a previous study[2] in our group, the nanoparticles seem to prearrange themselves on the nanosheet before capture which may give premise to the evidence of the non-uniformity in the alignment of the encapsulated CdS nanoparticles shown in Figure 4.6 compared to the alignment uniformity of the encapsulation of Fe_3O_4 nanoparticles shown in Figures 4.2 and 4.3. The difference is within the size of the nanoparticles. There are still further studies needed to determine if the size of the nanoparticles have a direct correlation to the non-uniformity seen in the nanopeapods that have encapsulated larger sized CdS nanoparticles.

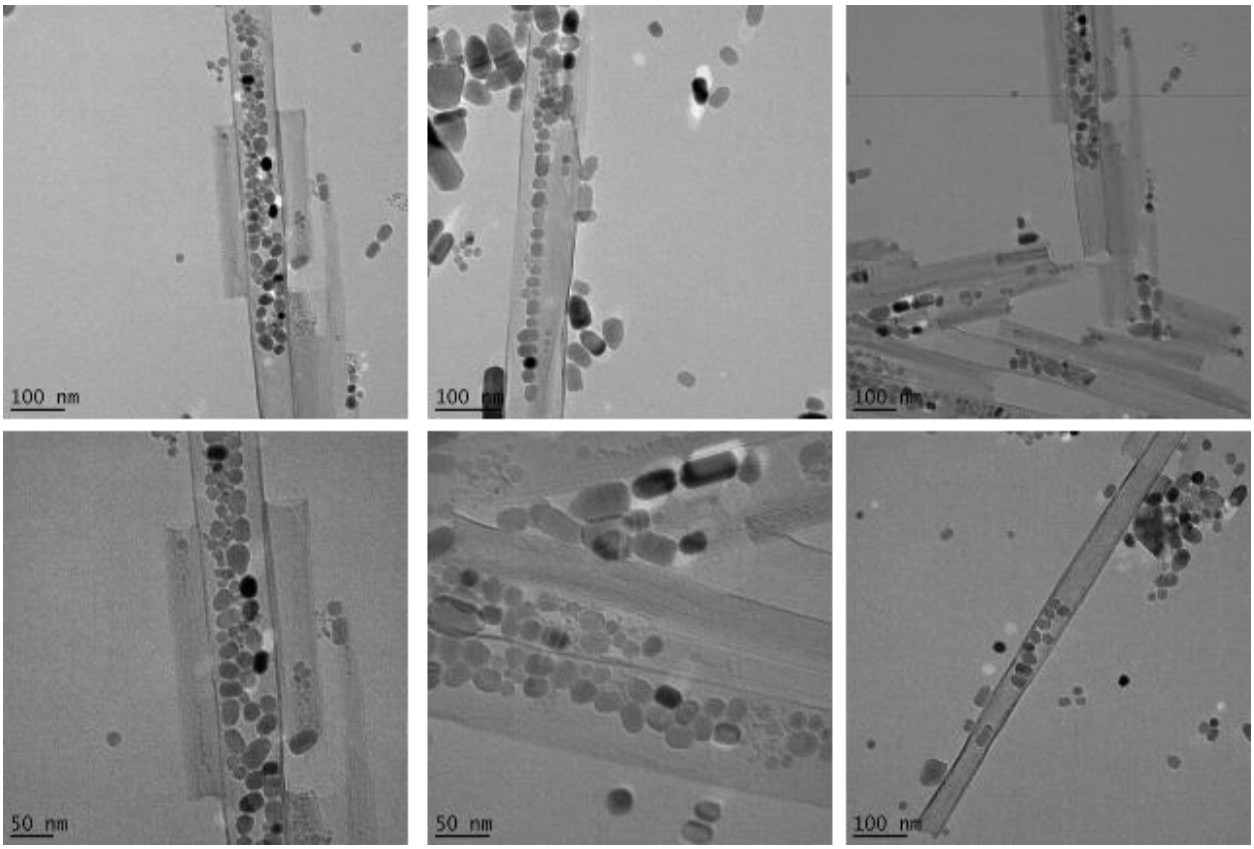

Figure 4.6. TEM images of encapsulated irregular shaped CdS nanoparticles within hexaniobate nanoscrolls via microwave irradiation.

4.5 Conclusions

Overall, the ability to produce nanocomposites at a much faster rate by using microwave irradiation synthesis continues to provide diversity amongst the hexaniobate studies the group has demonstrated to date. This method proved successful in the formation of iron oxide and cadmium sulfide nanopeapods, and can certainly be expanded and modified to create other nanopeapod systems. Being able to produce these nanostructures in half of the time originally reported (<3h) and in a much greener synthetic approach, gives rise to this technique becoming applicable in various applications of nanomaterial synthesis.

4.6 References

(1) Adireddy, S.; Carbo, C. E.; Yao, Y.; Vargas, J. M.; Spinu, L.; Wiley, J. B. High-yield solvothermal synthesis of magnetic peapod nanocomposites via the capture of preformed nanoparticles in scrolled nanosheets. *Chem. Mater.* **2013**, *25* (19), 3902–3909.

(2) Yao, Y.; Chaubey, G. S.; Wiley, J. B. Fabrication of nanopeapods: scrolling of niobate nanosheets for magnetic nanoparticle chain encapsulation. *J. Am. Chem. Soc.* **2011**, *134* (5), 2450–2452.

(3) Adireddy, S.; Carbo, C. E.; Rostamzadeh, T.; Vargas, J. M.; Spinu, L.; Wiley, J. B. Peapod-Type Nanocomposites through the In Situ Growth of Gold Nanoparticles within Preformed Hexaniobate Nanoscrolls. *Angew. Chem. Int. Ed.* **2014**, *53* (18), 4614–4617.

(4) Rostamzadeh, T.; Adireddy, S.; Wiley, J. B. Formation of scrolled silver vanadate nanopeapods by both capture and insertion strategies. *Chem. Mater.* **2015**, *27* (10), 3694–3699.

(5) Gao, C.; Li, W.; Morimoto, H.; Nagaoka, Y.; Maekawa, T. Magnetic carbon nanotubes: synthesis by electrostatic self-assembly approach and application in biomanipulations. *J. Phys. Chem. B* **2006**, *110* (14), 7213–7220.

(6) Hu, H.; Wang, X.; Liu, F.; Wang, J.; Xu, C. Rapid microwave-assisted synthesis of graphene nanosheets–zinc sulfide nanocomposites: optical and photocatalytic properties. *Synth. Met.* **2011**, *161* (5), 404–410.

(7) Murugan, A. V.; Muraliganth, T.; Manthiram, A. Rapid, facile microwave-solvothermal synthesis of graphene nanosheets and their polyaniline nanocomposites for energy strorage. *Chem. Mater.* **2009**, *21* (21), 5004–5006.

(8) Sanghi, R. Microwave Irradiation-A way to eco-friendly Green Chemistry. *Resonance* **2000**, *5* (3), 77–81.

(9) Sun, F.; Qiao, X.; Tan, F.; Wang, W.; Qiu, X. One-step microwave synthesis of Ag/ZnO nanocomposites with enhanced photocatalytic performance. *J. Mater. Sci.* **2012**, *47* (20), 7262–7268.

(10) Zhu, J.-F.; Zhu, Y.-J.; Ma, M.-G.; Yang, L.-X.; Gao, L. Simultaneous and Rapid Microwave Synthesis of Polyacrylamide− Metal Sulfide (Ag2S, Cu2S, HgS) Nanocomposites. *J. Phys. Chem. C* **2007**, *111* (10), 3920–3926.

(11) Kong, J.; Franklin, N. R.; Zhou, C.; Chapline, M. G.; Peng, S.; Cho, K.; Dai, H. Nanotube molecular wires as chemical sensors. *science* **2000**, *287* (5453), 622–625.
(12) Pian, X.-T.; Lin, B.-Z.; Chen, Y.-L.; Kuang, J.-D.; Zhang, K.-Z.; Fu, L.-M. Pillared nanocomposite TiO2/Bi-doped hexaniobate with visible-light photocatalytic activity. *J. Phys. Chem. C* **2011**, *115* (14), 6531–6539.
(13) Miyamoto, N.; Yamamoto, H.; Kaito, R.; Kuroda, K. Formation of extraordinarily large nanosheets from K 4 Nb 6 O 17 crystals. *Chem. Commun.* **2002**, No. 20, 2378–2379.
(14) Sayama, K.; Tanaka, A.; Domen, K.; Maruya, K.; Onishi, T. Photocatalytic decomposition of water over platinum-intercalated potassium niobate (K4Nb6O17). *J. Phys. Chem.* **1991**, *95* (3), 1345–1348.
(15) Adireddy, S.; Yao, Y.; He, J.; Wiley, J. B. Rapid solvothermal fabrication of hexaniobate nanoscrolls. *Mater. Res. Bull.* **2013**, *48* (9), 3236–3241 DOI: 10.1016/j.materresbull.2013.04.090.
(16) Saupe, G. B.; Waraksa, C. C.; Kim, H.-N.; Han, Y. J.; Kaschak, D. M.; Skinner, D. M.; Mallouk, T. E. Nanoscale Tubules Formed by Exfoliation of Potassium Hexaniobate. *Chem. Mater.* **2000**, *12* (6), 1556–1562 DOI: 10.1021/cm981136n.
(17) S. Akbarian-Tefaghi, T. Rostamzadeh, T. T. Brown, C. Davis-Wheeler, J. B. Wiley, ChemNanoMat 2017, 3, 538.
(18) Yong, K.-T.; Sahoo, Y.; Swihart, M. T.; Prasad, P. N. Shape Control of CdS Nanocrystals in One-Pot Synthesis. *J. Phys. Chem. C* **2007**, *111* (6), 2447–2458 DOI: 10.1021/jp066392z.
(19) Adireddy, S.; Rostamzadeh, T.; Carbo, C. E.; Wiley, J. B. Particle Placement and Sheet Topological Control in the Fabrication of Ag–Hexaniobate Nanocomposites. *Langmuir* **2014**, *31* (1), 480–485.

Chapter 5 Atomic Force Microscopy of Hexaniobate Nanostructures

5.1 Introduction

Recently, much focus has been directed towards layered inorganic materials for use in numerous scientific applications. Because these materials have unique lamellar structures, there have been many approaches developed for their fabrication - ion exchange,[1] atomic layer deposition (ALD),[2] chemical vapor deposition (CVD),[3] liquid oxidation,[4] and ion intercalation.[5] One definitive approach, however, is a simple solvothermal synthesis in which pre-formed nanoparticles are added to layered inorganic crystallites with exfoliating agents and surfactants to form nanopeapod structures of various types.[6] Layered oxides, such as hexaniobate, can easily be exfoliated with the addition of acid and can readily form nanoscrolls in attempt to relieve structural stress and strain.[1,6,7]Moreover, one of the more interesting properties of layered hexaniobate is the fact that it is a wide band gap semiconductor material and exhibits photocatalytic activity under UV light, though the photocatalytic activity can be restricted.[8] Therefore, because of the scrolling capabilities of hexaniobate, encapsulating nanoparticles with light harvesting potential within hexaniobate nanoscrolls can lead to new nanoarchitectures with applications in photonics and chemical and biological nanosensing devices.[9,10]

One particular nanoparticle of interest for encapsulating within hexaniobate nanoscrolls is cadmium sulfide nanoparticles which have been extensively studied for their inherent chemical and physical properties [11–13] which are characteristically related to their size, shape, and crystal structure. During solvothermal treatment, exfoliated hexaniobate nanosheets scroll around highly ordered chains of preformed QDs to produce nanopeapods (NPPs) in high yields, in addition to the potential for advanced functional device fabrication.

Typically, characterization of nanoscrolls and nanopeapods has been based on results from Transmission Electron Spectroscopy (TEM) and X-Ray Diffraction (XRD) analysis. Currently, there is very little research that focuses on Atomic Force Microscopy (AFM) as a characterization method for these nanomaterials. With the advancement of atomic force microscopes, there is much more information that can be extrapolated qualitatively and quantitatively. Furthermore, atomic force microscopes can aid in the advancement of knowledge surrounding the scrolling and potentially un-scrolling of these materials via nanomanipulation and nanolithography that can be achieved with the AFM tip.

5.2 Experimental

***Materials*.** K_2CO_3 (Alfa Aesar, 99%), Nb_2O_5 (Alfa Aesar, 99%), tetrabutylammonium hydroxide 30-hydrate (TBAOH, Sigma-Aldrich), oleylamine (Sigma-Aldrich), toluene (Aldrich, anhydrous, 99.8%), ethanol (200 Proof, absolute), cadmium chloride (J.T. Baker Chemical Co.), sulfur (EM Science), distilled water.

5.2.1 Synthesis of Niobate Nanosheets

Synthesis of $K_4Nb_6O_{17}$. Niobate nanosheets were synthesized using previously reported methods from the Wiley group. [19] Potassium carbonate (1.95 g) and niobium pentoxide (5.12 g) were first ground together by mortar and pestle before being placed into a high temperature oven at 900 °C for one hour. The solid-state reaction was then removed from the oven, re-ground, and placed back into the oven at 1050 °C for 24 h. The resulting product of potassium hexaniobate ($K_4Nb_6O_{17}$) was then washed three times with 50 mL of milli-Q water then dried for 24 hours at 70 °C.

Acid-exchange of niobate nanosheets. Potassium hexaniobate was then protonated by treating 1 g of $K_4Nb_6O_{17}$ with 8 mL of dilute HNO_3 in a Teflon lined Parr bomb and heated at 90

°C for 2 days. The product was then washed three times with 50 mL of milli-Q water and dried for 24 hours at 70 °C.

Intercalated Nanoscroll Synthesis. Nanoscroll formation was achieved by solvothermal synthesis akin to what has been previously reported by our group[7]. Solvothermally, a solution of $H_xK_{4-x}Nb_6O_{17}$ (0.1g), TBAOH (19 mmol), and 5 mL oleylamine (~15 mmol) in 9 mL toluene was prepared and magnetically stirred for 1hr before transferring into a Teflon-lined stainless-steel autoclave (Parr, model 4749, 1800 psi, 23 mL) for 6h at 220º C.

5.2.2 Cadmium Sulfide Nanoparticle Synthesis

Synthesis of pseudo-cubic NPs.[12] Pseudo-cubic cadmium sulfide nanoparticles (NPs), were synthesized by adding 30 mmol (0.962 g) of sulfur to 10 mL of oleylamine and heated under argon flow for 35 minutes at 70 ºC to fully dissolve the sulfur. In a separate flask, 10 mmol (1.832g) of cadmium chloride was dissolved in 15 mL oleylamine by heating at 100 ºC s for 30 minutes. The resulting Cd-oleylamine complex was then injected into the hot sulfur-oleyamine solution, and the resulting mixture was aged for 19 hours with stirring. The nanocrystals were then precipitated out of solution by the addition of ethanol with centrifugation and re-dispersed in toluene. The resulting color was a bright yellow with NPs ranging in size from 9-11nm.

5.2.3 Synthesis of Cadmium Sulfide @ Hexaniobate Nanopeapods

To fabricate these peapod systems, 1 mL of as-synthesized cadmium sulfide nanocrystals was added to a reaction mixture of 0.05 g of $H_xK_{4-x}Nb_6O_{17}$, 0.15 g TBAOH, 5 mL OAm, and 7 mL of toluene and stirred at room temperature for 1h. The reaction mixture was then transferred into a Teflon lined Parr bomb and heated at 220 °C for 6h. The precipitate was

then washed with a combination of 10 mL ethanol and 5 mL toluene, then centrifuged to isolate the solid. The resulting color was a dull yellow.

5.2.4 Preparation of samples for Atomic Force Microscopy Studies

Since AFM strongly relies on the force of the tip as it is raster scanned across the surface, a 3:1 molar ratio solution of sulfuric acid and hydrogen peroxide, known as piranha solution, was used to "roughen" or etch the surface of the silicon substrates. The roughening of the surface would allow for the adhering of the nanoscrolls on the substrate as the tip is raster scanned across the sample.

Piranha Etching. In a 50-mL glass jar, eight substrates, initially cleaned with ethanol and milli-Q water, were placed at the bottom of the jar equally spaced apart. Then, 6 mL of H_2SO_4 was added followed by 2 mL of H_2O_2. **(CAUTION! Reaction must be done under fume hood.)** The substrates were left in this solution for 2 hours before being removed and washed with excessive EtOH and deionized water. The substrates were then dried with a slow and study flow of nitrogen. Samples were then drop cast onto the freshly etched silicon substrates and allowed to dry in an oven for 24 hours at 70º C.

5.2.5 Characterization

Transmission electron microscopy. TEM images were acquired on a JEOL 2010 microscope equipped with a Gatan charge-coupled device camera at an operating voltage of 200 keV. Sample preparation involved drop casting a toluene diluted suspension of sample onto a carbon coated 200 mesh copper grid.

Atomic force microscopy. AFM observations were carried out with intermittent "tapping" mode (Figure 2) in ambient on a Keysight 5500 SPM/AFM system equipped with PicoView v1.20 software (Keysight Technologies, Inc., Santa Rosa, CA) at Louisiana State

University. The surface was investigated using commercially available silicon nitride (Si_3N_4) AFM tips (SSS-NCH50, resonance frequency of 330 kHz) purchased from NanoSensors (Tempe, AZ). Raw images were collected in situ and processed with Gwyddion[14] software (version 2.47, 64-bit).

5.3 Results and Discussion

5.3.1 Tapping Mode AFM

Initial AFM results of hexaniobate nanoscrolls are shown in the following images with a scan size 4 µm by 4 µm and obtained simultaneously. The topography image (Figure 5.1a) is constructed by showing the difference of heights as a variation of colors, with the darker areas showing lower topographic details opposed to the brighter areas showing higher topographical details of the surface. The color scale bar to the right of the images are arbitrarily produced by the software to give a perspective of the height variation of the surface of the sample. The phase image, as shown in Figure 5.1b, can be thought of as an enhanced image that shows viscoelasticity, [15] but more so, the phase image allows us to clearly see defined features that are unable to be seen in topography images. Furthermore, the phase image can show variants of composition, adhesion, friction, chemical composition.[16,17] The 3-D topography image (Figure 5.1) is a three-dimensional representation of the topography image, and its difference in color is attributed to the lighting representation that the software uses to enhance the features of these types of images.

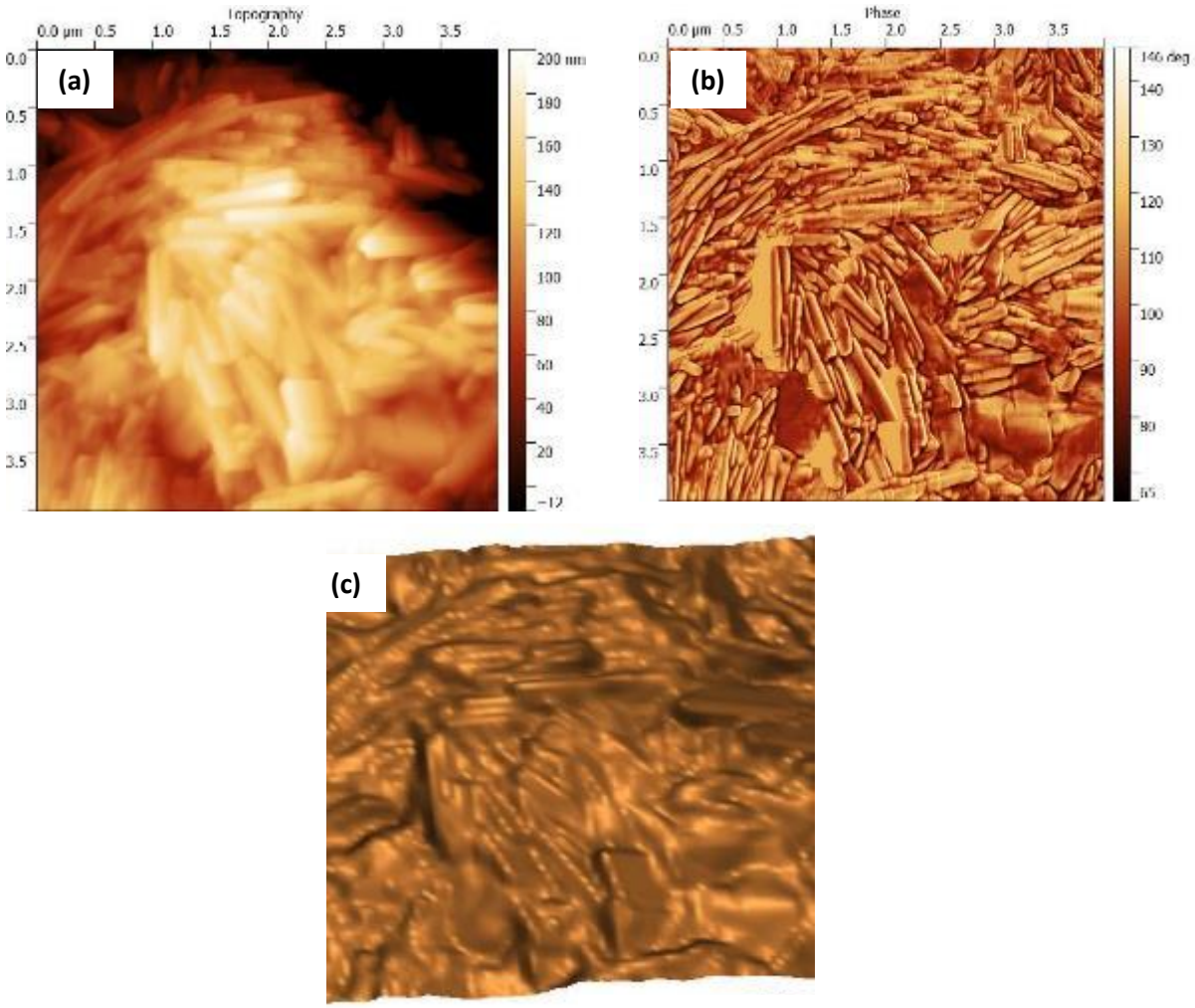

Figure 5.1. 4x4 µm^2 scan image of hexaniobate nanoscrolls showing (a) topography, (b) phase and (c) 3-D rendering of topography image with lighting color variant applied.

It is also possible to look at features on the surface and successively zoom in on objects of interest in AFM. Figure 5.2 shows a zoomed in image from Figure 5.1, which shows how it is possible to see the layers of scrolled sheets which make up the nanoscroll. The phase and phase 3-D images give good representation of the scrolling of hexaniobate layers which can further be explored via various AFM techniques. Furthermore, information about the sample can be extrapolated by drawing a cursor line across the feature(s) of interest, and thus a cursor profile is

formed which can give information on height, length, width, changes in layer height, etc. (Figure 5.3).

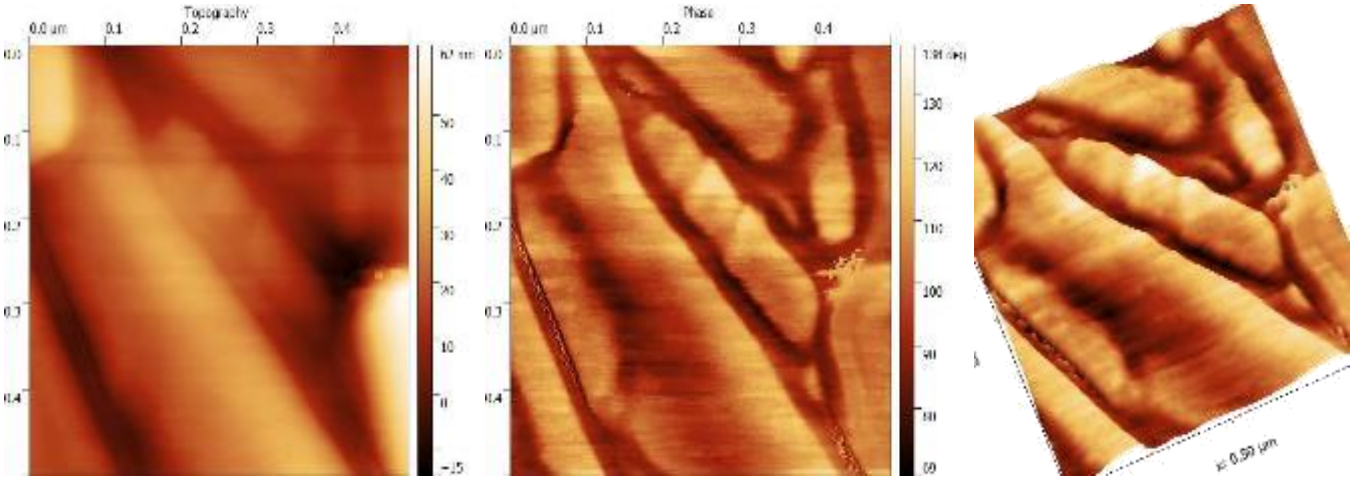

Figure 5.2. 500 x 500 nm^2 scan image of hexaniobate nanoscrolls showing topography, phase and a 3-D rendering of phase image.

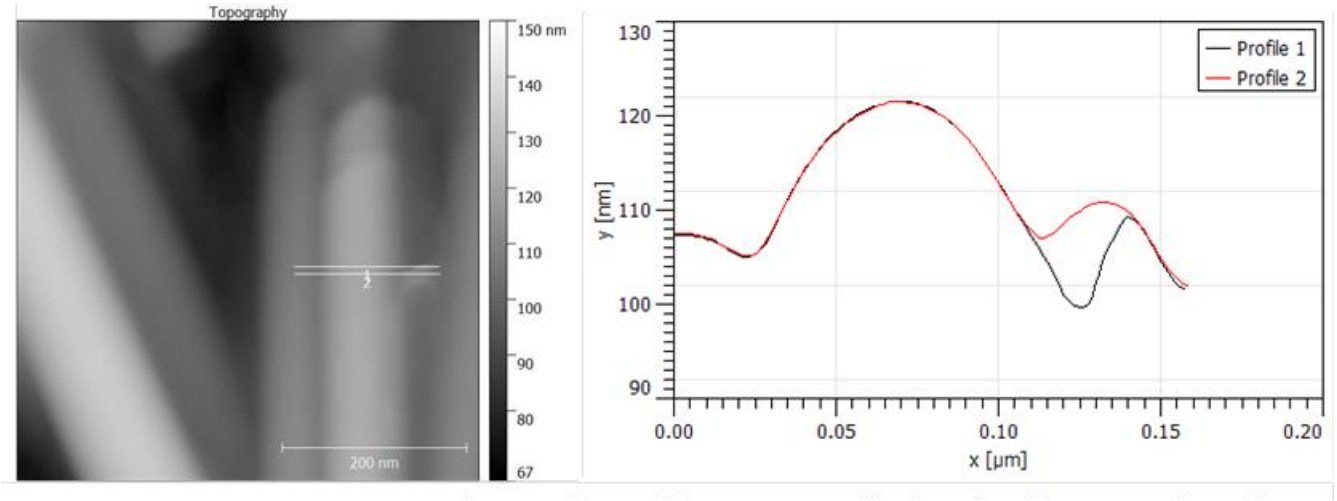

Figure 5.3. 300 x 300 nm^2 scan image of hexaniobate nanoscrolls showing topography with cursor line and cursor profile of one nanoscroll depicting a height ~17 nm and a width of ~ 60 nm.

The following images are observed with tapping mode AFM imaging. Figure 5.4 displays AFM images of intercalated nanoscrolls with successive zoomed in images of the same area. It is interesting the see the surface topology and features of these scrolls that were not easily

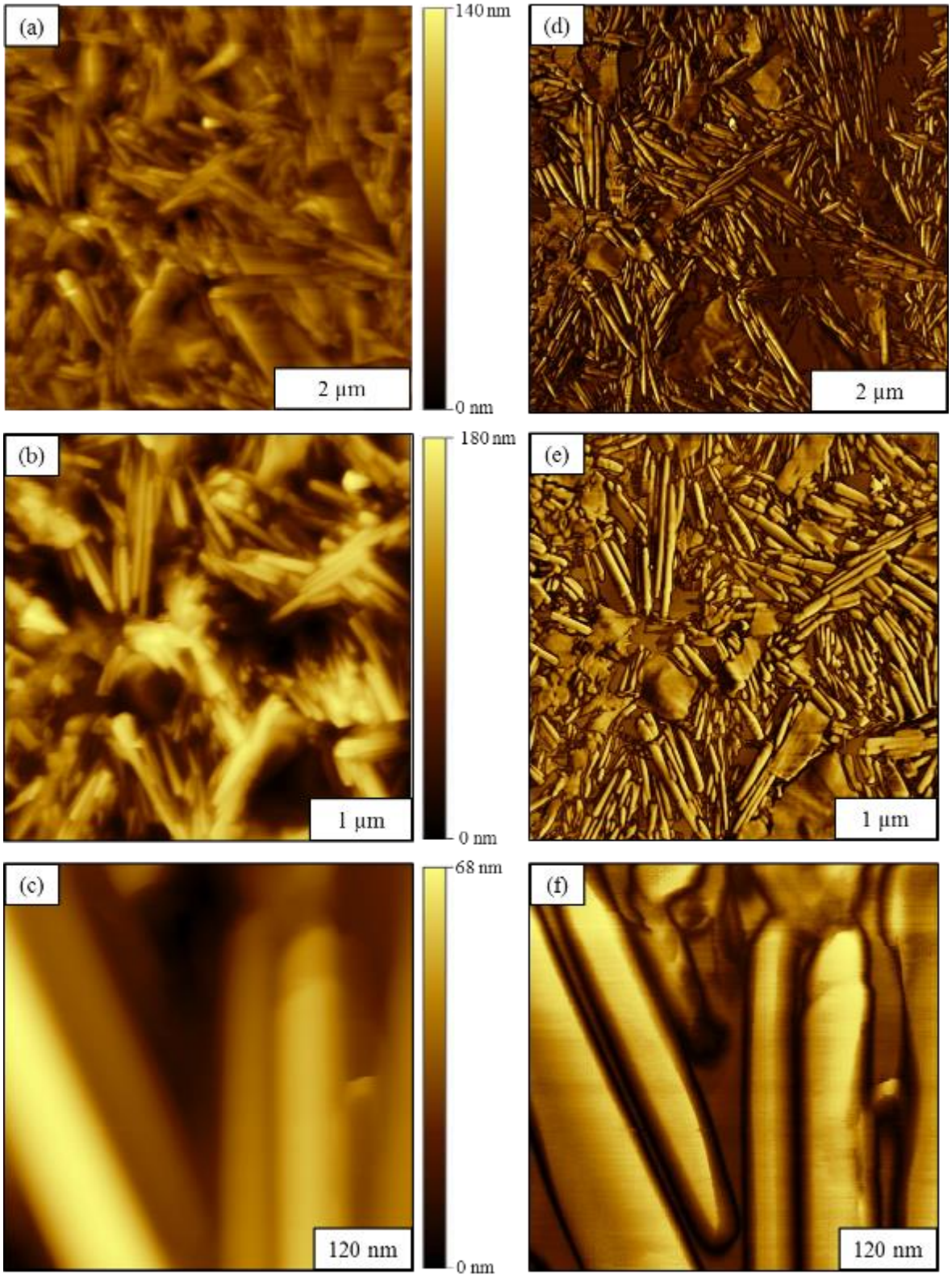

Figure 5.2. Nanoscrolls imaged with tapping mode AFM. (a)6 x 6 µm^2 topography, (b) 4 x 4 µm^2 topography (c) 500 x 500 nm^2 topography (d) corresponding phase image for (a). (e) corresponding phase image for (b). (f) corresponding phase image for (c).

seen by other forms of microscopy. Figures 5.5 and 5.6 show tapping mode AFM images of nanoscrolls synthesized by microwave assisted (MA) methods that were further discussed in Chapter 4. The topography, amplitude, and phase images are shown in Figures 5.5 and 5.6 at various magnifications. The topography shows what the tip "feels" as it as raster scanned along the surface of the sample, the amplitude shows the feedback from the resulting z-direction piezo movements from which height information is used to generate the surface topography,[16,18] and the phase shows inhomogeneity in sample composition. These studies indicate that even under

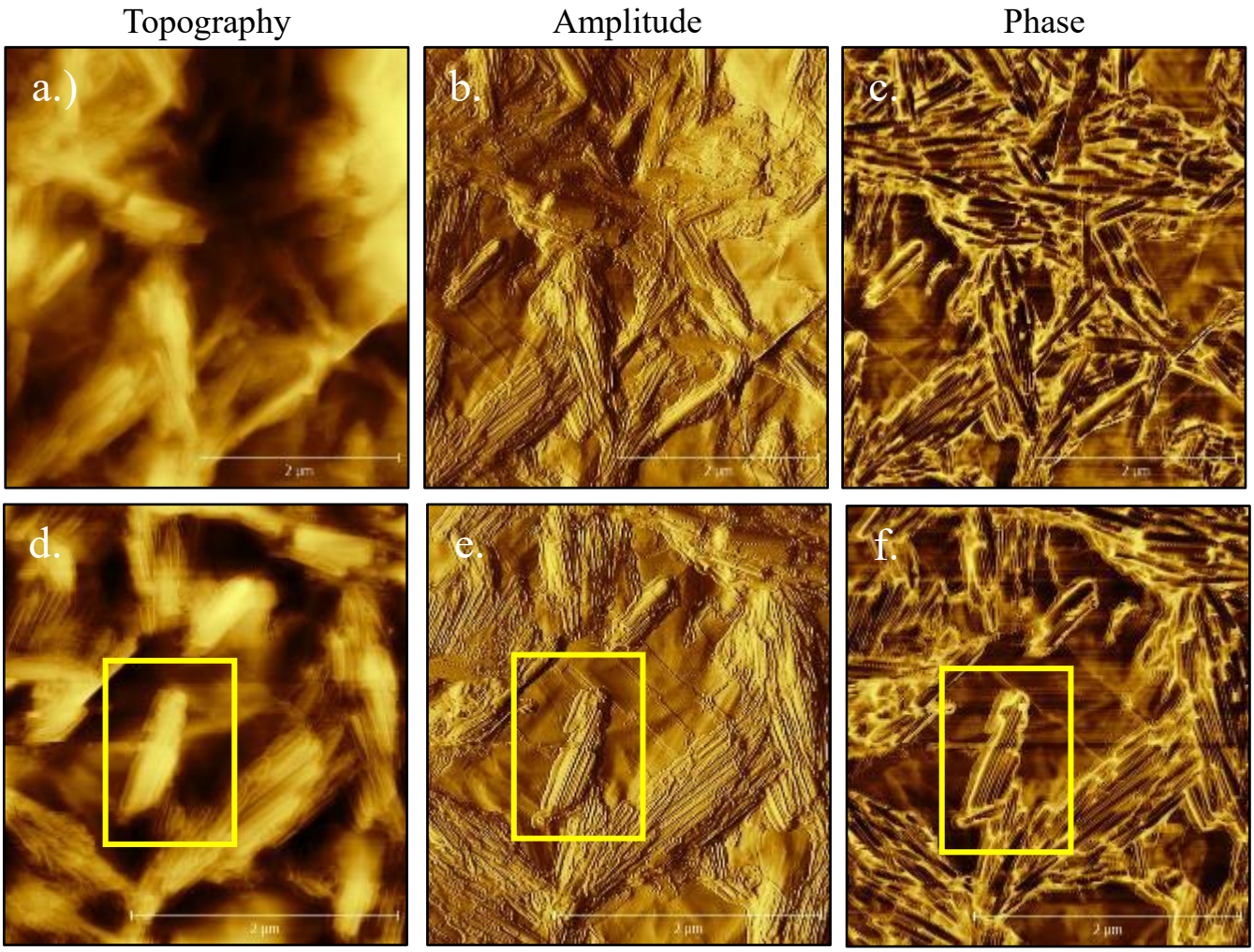

Figure 5.3. Tapping mode AFM images of intercalated hexaniobate nanoscrolls synthesized via microwave protonation and scrolling methods. Showing topography, amplitude, and phase (a-c) 6x6μm^2 images, (d-f) 3x3 μm^2 images.

the force of an AFM tip, these structures are still rigid, cylindrical, and exhibit known surface characteristics such as the presence of scrolled hexaniobate nanosheets nanoscrolls forming atop of nanosheets indicated by the yellow boxes (Figure 5.5, d-f). Further topographical studies were extended to the CdS@hexaniobate nanopeapod systems shown in Figure 5.7. Scrolled morphologies are again evident on the surface, however, there is also evidence of surface decoration of some kind. It is unclear if these are free nanoparticles or islands of TBA^+ on the surface (indicated by yellow boxes). Lastly, Figure 5.8 shows how cursor profiles were extrapolated to map the topology of the sample surfaces shown in Figure 5.4. These cursor profiles give quantitative measurements of height, length and width.

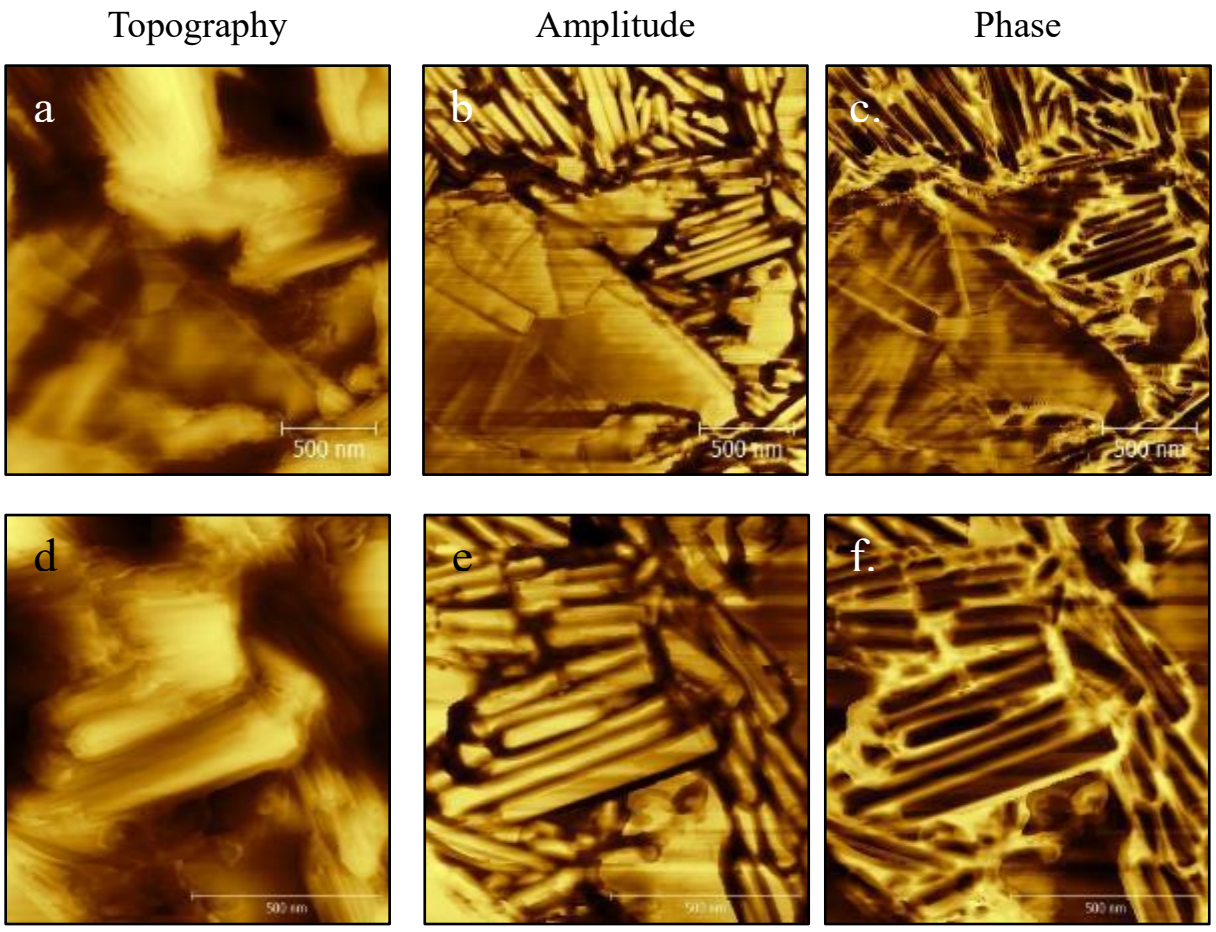

Figure 5.4. Tapping mode AFM images of intercalated hexaniobate nanoscrolls synthesized via microwave protonation and scrolling methods. Showing topography, amplitude, and phase (a-c) 2x2µm^2 images, (d-f) 1x1 µm^2 images.

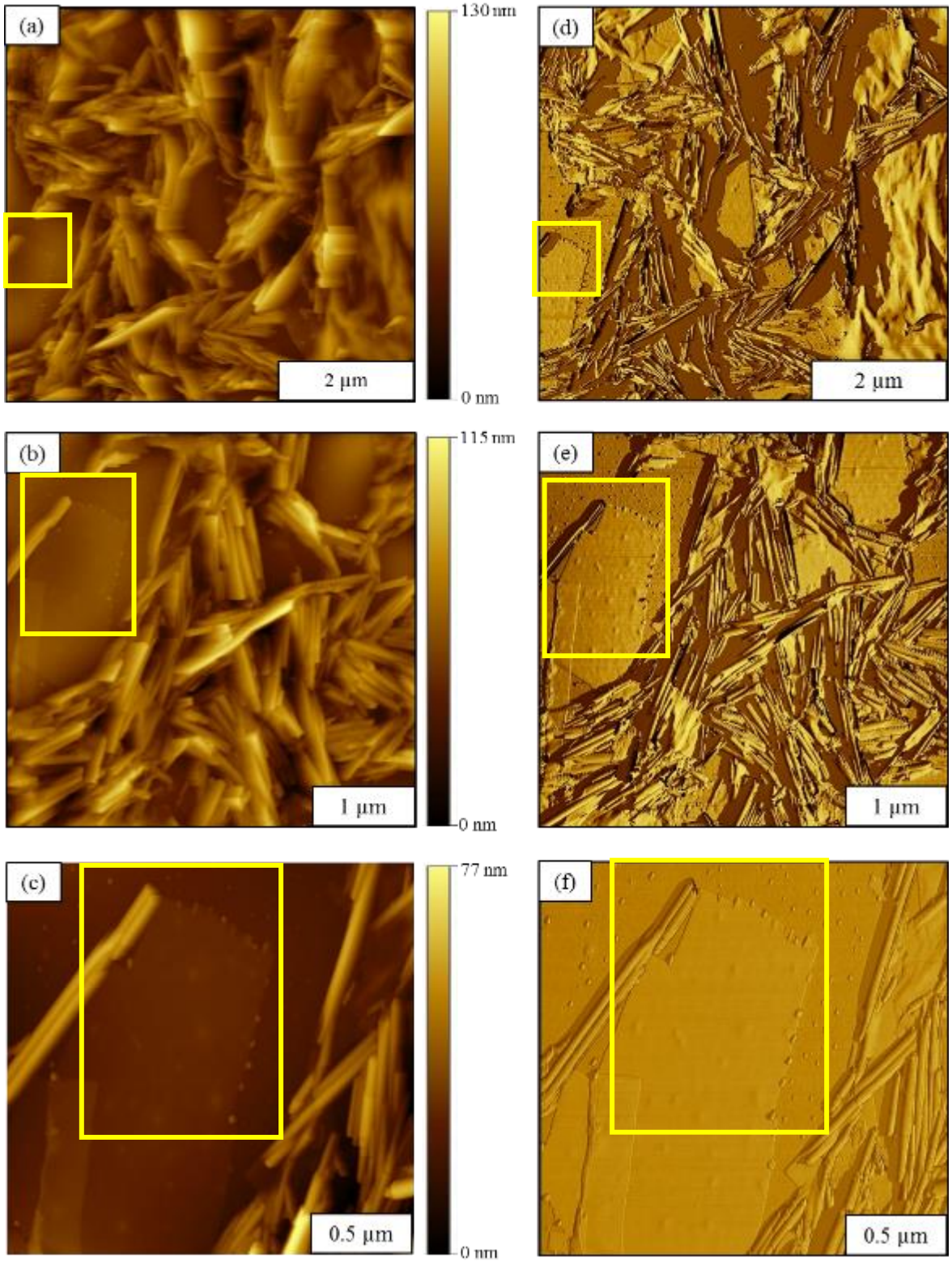

Figure 5.5. CdS@hexaniobate nanoaeapods imaged with tapping mode AFM. (a)6 x 6 µm^2 topography, (b) 4 x 4 µm^2 topography (c) 500 x 500 nm^2 topography (d) corresponding phase image for (a). (e) corresponding phase image for (b). (f) corresponding phase image for (c).

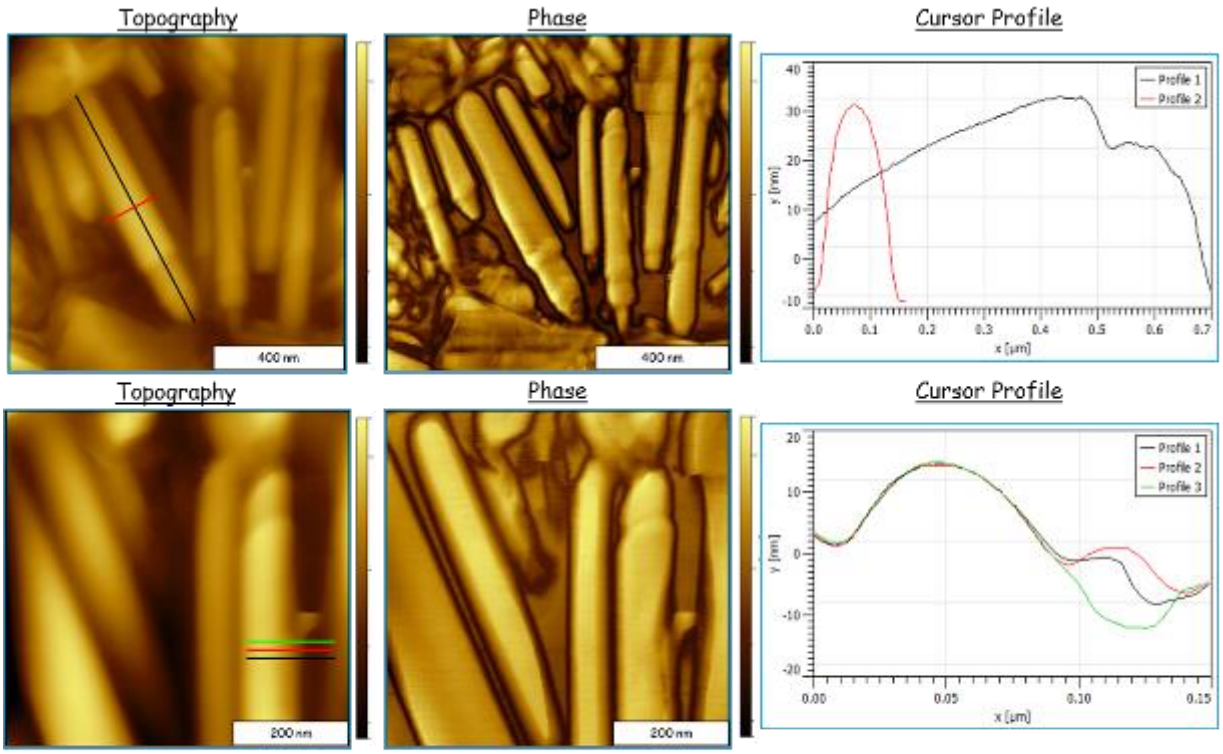

Figure 5.6. AFM images of intercalated nanoscrolls. Cursor plots map topology of sample surfaces which can be used to find lengths, widths, and heights of samples being studied.

5.4 Conclusions

Atomic force microscopy has allowed for a new type of characterization method to use in conjunction with already existing characterization methods. With promising results found through AFM, further work will be continued to characterize hexaniobate nanocomposites quantitatively by investigating mechanical properties such as Young's Modulus and frictional coefficients (Chapter 7). These studies will aide in creating a library of characteristics geared towards better understanding the surface morphologies of hexaniobate nanocomposites for further nanoscale applications.

5.5 References

1.Liang, J. *et al.* Topochemical Synthesis, Anion Exchange, and Exfoliation of Co−Ni Layered Double Hydroxides: A Route to Positively Charged Co−Ni Hydroxide Nanosheets with Tunable Composition. *Chem. Mater.* **22,** 371–378 (2010).

2.Song, J.-G. *et al.* Layer-Controlled, Wafer-Scale, and Conformal Synthesis of Tungsten Disulfide Nanosheets Using Atomic Layer Deposition. *ACS Nano* **7,** 11333–11340 (2013).

3.Reina, A. *et al.* Large Area, Few-Layer Graphene Films on Arbitrary Substrates by Chemical Vapor Deposition. *Nano Lett.* **9,** 30–35 (2009).

4.Nicolosi, V., Chhowalla, M., Kanatzidis, M. G., Strano, M. S. & Coleman, J. N. Liquid Exfoliation of Layered Materials. *Science* **340,** (2013).

5.Huang, X., Zeng, Z. & Zhang, H. Metal dichalcogenide nanosheets: preparation, properties and applications. *Chem. Soc. Rev.* **42,** 1934–1946 (2013).

6.Adireddy, S. *et al.* High-Yield Solvothermal Synthesis of Magnetic Peapod Nanocomposites via the Capture of Preformed Nanoparticles in Scrolled Nanosheets. *Chem. Mater.* **25,** 3902–3909 (2013).

7.Smith, B. W., Monthioux, M. & Luzzi, D. E. Encapsulated C60 in carbon nanotubes. *Nature* **396,** 323–324 (1998).

8.*Institute of Electrical and Electronics Engineers, 'The IEEE standard dictionary of electrical and electronics terms'; 6th ed. New York, N.Y., Institute of Electrical and Electronics Engineers, c1997. IEEE Std 100-1996. ISBN 1-55937-833-6 [ed. Standards Coordinating Committee 10, Terms and Definitions; Jane Radatz, (chair).*

9.http://www.lightourfuture.org/about/what_is_photonics.

10.Willets, K. A.; Van Duyne, R. P. Annu. Rev. Phys. Chem. 2007, 58, 267.

11.Joo, J. *et al.* Generalized and Facile Synthesis of Semiconducting Metal Sulfide Nanocrystals. *J. Am. Chem. Soc.* **125,** 11100–11105 (2003).

12.Yong, K.-T., Sahoo, Y., Swihart, M. T. & Prasad, P. N. Shape Control of CdS Nanocrystals in One-Pot Synthesis. *J. Phys. Chem. C* **111,** 2447–2458 (2007).

13.Peng, Z. A. & Peng, X. Formation of High-Quality CdTe, CdSe, and CdS Nanocrystals Using CdO as Precursor. *J. Am. Chem. Soc.* **123,** 183–184 (2001).

14.Klapetek, P.; Necas, D. Gwyddion, Czech Metrology Institute: Czech Republic, 2007.

15.Tamayo, J. & García, R. Deformation, Contact Time, and Phase Contrast in Tapping Mode Scanning Force Microscopy. *Langmuir* **12,** 4430–4435 (1996).

16.Brown, T. T., et al. Journal of Laboratory Automation. April 2011 16: 112-125.

17.'Atomic Force Microscopy' by Eaton and West, OUP, 2010.

18.Binnig, G., Quate, C. F. & Gerber, C. Atomic Force Microscope. *Phys. Rev. Lett.* **56,** 930–933 (1986).

Chapter 6 Magnetic Sampling Modulation of Functionalized Metal Oxide Nanosheets

6.1 Introduction

Magnetic properties of nanomaterials have been of recent interest due to the technological advances of various characterization techniques. When considering a nanomaterial's intrinsic properties, it has been well studied that these properties change dramatically from their bulk properties.[1,2] Recently, our group has reported on rapid microwave assisted methods for the bulk modification of layered perovskites containing metal cations in the innerlayers.[3] By introducing a magnetic component to the structures, these materials could have applications in data storage, catalysis, and coatings.[1,2,4,5] In this chapter, the use of a new magnetic imaging mode known as Magnetic Sampling Modulation (MSM) on functionalized metal-oxide nanosheets will be described.

Magnetic sampling modulation is an atomic force microscopy (AFM) technique which allows for the mapping of unique magnetic phenomena on nanomaterials.[6] Unlike its counterpart, magnetic force modulation (MFM),[6–9] MSM relies on the mapping of a magnetic surface that is vibrated in the presence of an electromagnetic field by a soft, non-magnetic AFM tip (usually silicon nitride). Because the tip stays in constant contact with the sample, high resolution images of nanoscale magnetic samples can be acquired. MSM amplitude and phase images are possible to be acquired due to the changes in the phase angle and amplitude from the interaction of the vibrating sample remaining in constant contact with the AFM tip.[6,9,10] Also, by placing the tip in contact with the vibrating sample, a frequency sweep of the field frequency can also be extracted.[6] The working principle of MSM can be found in Chapter 1, Section 1.5.4.

This chapter will be adapted for poster presentation: Treva T. Brown, Sara Akbarian-Tefaghi, Alexis A. Blanco, Zachary L. Highland, Neepa M. Kuruppu, Ashley M. Taylor, Jayne C. Garno, John B. Wiley, * "Nano-Mechanical and Physical Investigations of Novel Oxide Nanocomposites Using Atomic Force Microscopy" *2018 American Chemical Society Spring National Meeting and Exhibition, New Orleans, LA,* March 2018.

6.2 Experimental

6.2.1 Materials and Synthesis

TBA^+-$Ca_2Nb_2FeO_9$ and TBA^+-$PrNb_2O_7$ nanosheet samples for this study were acquired from Dr. Sara Akbarian-Tefaghi. Proton exchanged intermediates of $HLnNb_2O_7$ were exfoliated in an aqueous solution of TBAOH by typical microwave-assisted exfoliation reactions by previously reported methods found in *ChemNanoMat*, **2017**, *3*, 538.[3] All products were sonicated in water and ethanol, centrifuged while maintaining the precipitate rather than the supernatant, and finally dried at 70 °C for several hours. Dried flakes of TBA-functionalized nanosheets were used for MSM analysis.

6.2.2 Preparation of Substrates

Piranha Etching. In a 50-mL glass jar, eight silicon substrates, initially cleaned with ethanol and milli-Q water, were placed at the bottom of the jar equally spaced apart. Then, 6 mL of H_2SO_4 was added followed by 2 mL of H_2O_2. **(CAUTION! This process should be carried out in a fume hood.)** The substrates were left in this solution for 2 hours before being removed and washed with excessive ethanol and deionized water. The substrates were then dried with a slow and study flow of nitrogen gas. Samples were then drop cast onto the freshly etched silicon substrates and allowed to dry in an oven for 24 hours at 70º C.

6.2.3 Atomic Force Microscopy Characterization

A Keysight 5500 SPM system equipped with a multipurpose AFM scanner (Keysight Technologies, Inc., Santa Rosa, CA) was used for surface characterizations at Louisiana State University in Baton Rouge, LA. Picoscan v1.20 software was used for data acquisition. Magnetic Sample Modulation (MSM)-AFM studies required a MAC-mode sample plate to generate an alternating electromagnetic field to induce vibration of the magnetic components of the

nanosheets.[9] The nosecone required to successfully image in MSM mode contained metal-free components so that no interference would be occur in evaluating the magnetic portions of the sample. Silicon nitride cantilevers (SSS-NCH50, resonance frequency of 330 kHz) purchased from NanoSensors (Tempe, AZ), were used for MSM imaging. In-situ images were processed with Gwyddion[11] open-source software (Czech Metrology Institute, http://gwyddion.net/) version 2.47, 64-bit.

6.3 Results

6.3.1 TBA^+-$Ca_2Nb_2FeO_9$ Nanosheets

An arbitrary region of TBA^+-$Ca_2Nb_2FeO_9$ nanosheets was initially scanned in conventional contact mode to find an area of interest. Figure 6.1 shows a 4x4 micron image of the selected area. Figure 6.1a shows the topology of TBA^+-$Ca_2Nb_2FeO_9$ nanosheets, revealing correct nanosheet morphologies as to be expected from previously evaluated TEM and AFM studies reported by Akbarian-Tefaghi.[3] It can be noted from figures 6.1b and 6.1c that without the magnetic field turned on, the nanosheets are featureless in the amplitude and phase channels. However, when the electromagnetic field is applied with the AFM tip kept in constant contact with the surface, clear features can be observed in the MSM Amplitude and MSM Phase Channels (Figure 6.2). The magnitude of the electromagnetic field was measured to be 0.2 T by a portable magnetometer.[10] Figure 6.2 shows a zoomed-out area of the nanosheets from the 4x4 micron image shown in Figure 6.1 with the electromagnetic field turned on. Because the samples contain magnetically active iron cations (Fe^{3+}) within the structure, the actuation of the nanosheets present brightly colored features now evident in the MSM-Amplitude and MSM Phase channels (Figure 6.2b and Figure 6.2c). It can further be noted in Figure 6.2 how much more defined the nanosheets are in comparison to Figure 6.1 in which the electromagnetic field

is turned off. Based on the observations in the MSM channels, it is clearly that the magnetic component of the nanosheets allows for successful surface mapping of the sample when it is modulated within an electromagnetic field.

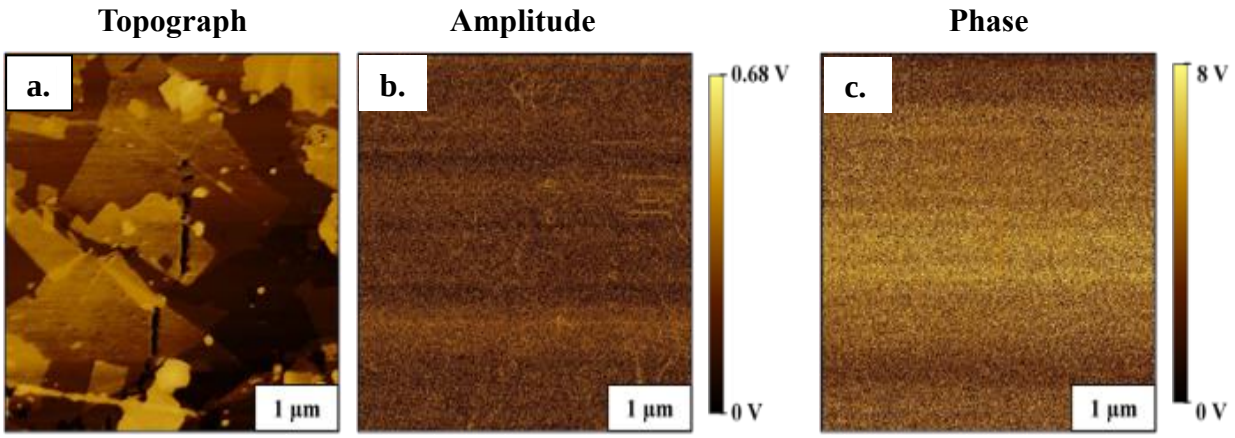

Figure 6.1. AFM images of TBA+-$Ca_2Nb_2FeO_9$ nanosheets captured in contact mode with magnetic field off. (a.) Topography image (4x4 µm^2) (b.) amplitude (c.) phase.

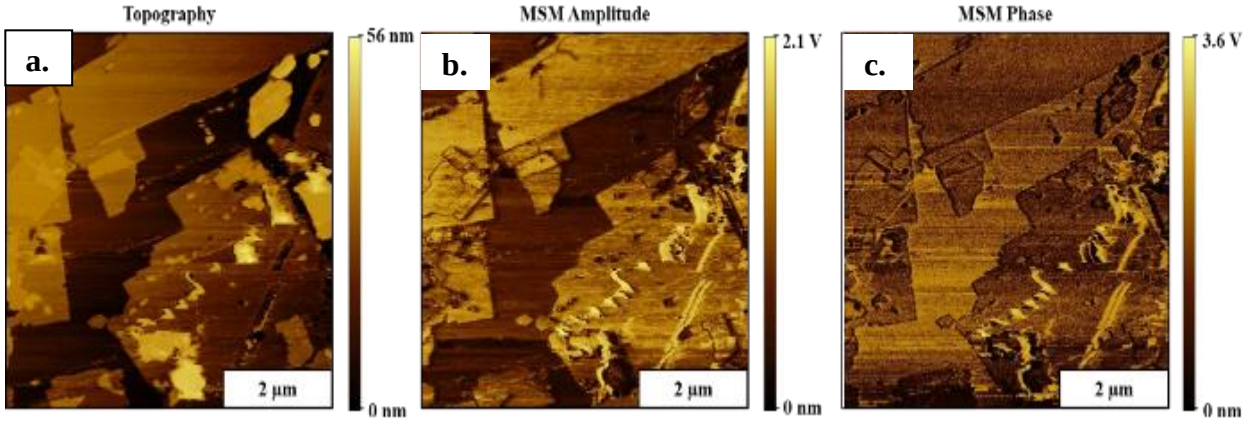

Figure 6.2. AFM images of TBA+-$Ca_2Nb_2FeO_9$ nanosheets captured with MSM-AFM. Electromagnetic Field on, 0.2 T at 240 kHz. (a.) MSM Topography image (6x6 µm^2) (b.) MSM-amplitude (c.) MSM-phase images.

To make a direct comparison of contact mode with MSM imaging within a single frame, the same area was scanned from Figure 6.1 to acquire the images displayed in Figures 6.3 and 6.4. In the top half of the images in Figure 6.3 a-d, the field was switched off. The scan was then stopped, the electromagnetic field was switched on, then the bottom half of the images were

scanned via MSM. Figure 6.3 a-d shows the corresponding change from contact mode to MSM. With the electromagnetic field turned on, nanosheets can be characterized in the MSM amplitude and phase channels as seen in Figure 6.3 b-c. This comparison from contact mode to MSM is further studied in Figure 6.4, in which the electromagnetic field is turned on and off more than

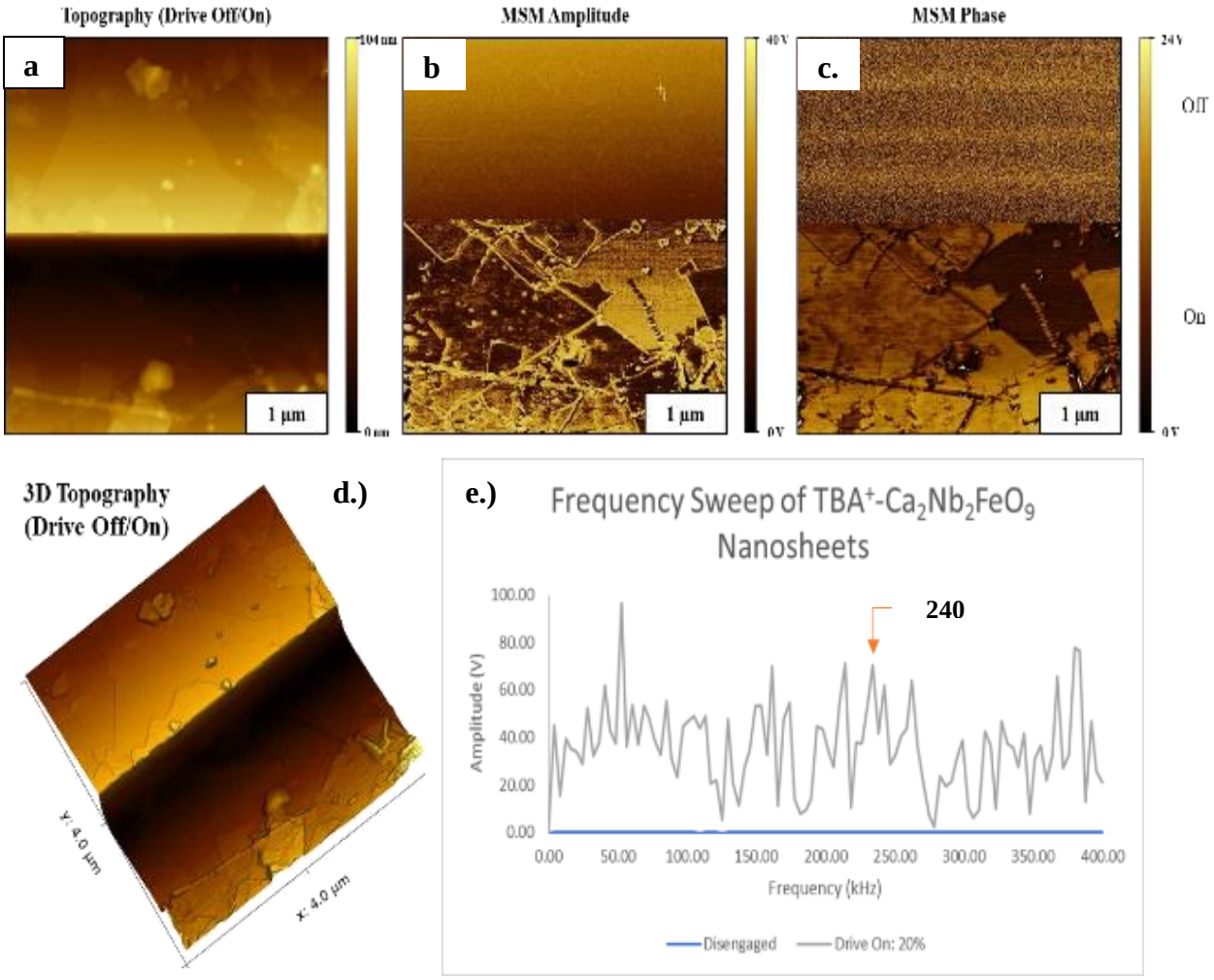

Figure 6.1. AFM images of TBA+-$Ca_2Nb_2FeO_9$ nanosheets captured by MSM-AFM with field switched on then off. Electromagnetic Field on, 0.2 T at 240 kHz. (a.) MSM Topography image (4x4 µm^2) (b.) MSM-amplitude (c.) MSM-phase images (d) 3D Topography (e)Example frequency sweep.

once. Again, it can be determined that the correlation of turning the electromagnetic field on and off can be directly mapped in the corresponding MSM amplitude and phase images.

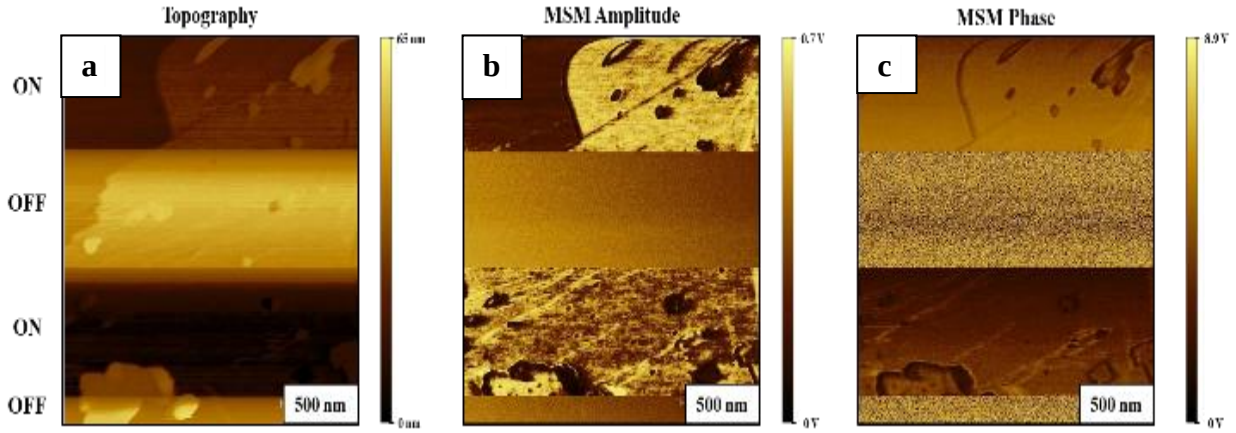

Figure 6.2. AFM images of TBA+-$Ca_2Nb_2FeO_9$ nanosheets captured by MSM-AFM with field switched on then off. Electromagnetic Field on, 0.2 T at 240 kHz. (a.) MSM Topography image (2x2 μm^2) (b.) MSM-amplitude (c.) MSM-phase images.

Furthermore, a frequency sweep of the sample can be obtained by placing the tip in direct contact with a vibrating area of the sample when the electromagnetic field is turned on. Figure 6.3e shows an example of a frequency sweep obtained from TBA^+-$Ca_2Nb_2FeO_9$ nanosheets. The frequency sweep shows how the z-deflection of the AFM tip changes as the AC frequency is increased. When the tip is disengaged from contact with the sample, a flat baseline (blue line) is rightfully observed since there is no modulation of sample to be detected out of sample contact. However, once the tip does come in contact with the sample, several distinguishable peaks can be observed (grey line) as the frequency increases from 0-400 kHz. For this set of MSM characterization studies, the peak at 240 kHz was selected to obtain the images shown in the MSM channels.

6.3.2 TBA^{+}-$PrNb_2O_7$ Nanosheets

Magnetic Force Modulation characterization was also used to characterize TBA^{+}-$PrNb_2O_7$. As previously mentioned, an arbitrary area was initially scanned in conventional contact mode to find an area of interest. Figure 6.5 shows an 8x8 micron image of the selected area of interest. Figure 6.5a shows the topology of TBA^{+}-$PrNb_2O_7$ nanosheets, revealing the morphologies as to be expected from previously evaluated TEM and AFM studies reported by Akbarian-Tefaghi.[3] Without the magnetic field turned on, it can be noted from figure 6.5c that there is no evidence of any features in the phase channel. However, Figure 6.5b shows some sort of response in the amplitude channel, but it is unconfirmed as to what is causing the response without the presence of the electromagnetic field.

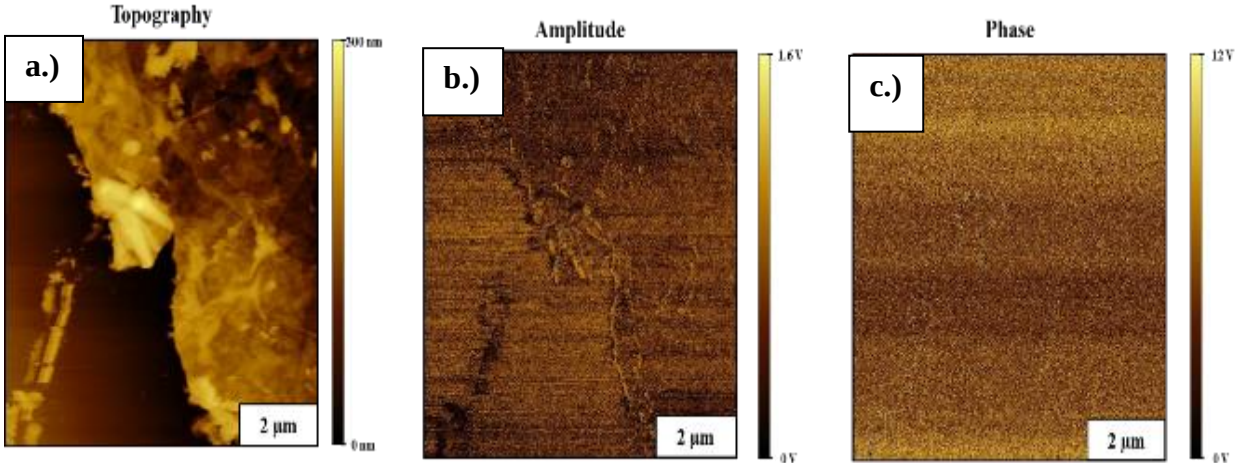

Figure 6.3. AFM images of TBA+-$PrNb_2O_7$ nanosheets captured in contact mode with magnetic field off. (a.) Topography image (8x8 µm^2) (b.) amplitude (c.) phase.

On the other hand, when the electromagnetic field is turned on with the AFM tip kept in constant contact with the surface, features can be observed in the MSM Amplitude and MSM Phase Channels as shown in Figure 6.6. The magnitude of the electromagnetic field was measured by portable magnetometer at 0.2T.[10] Figure 6.6 shows a zoomed-in area of the nanosheets from the 8x8 micron image shown in Figure 6.5. The samples consist of the

praseodymium (Pr^{3+}) as the magnetic component within the structure, and the actuation of these nanosheets present brightly colored features in the 3D topography image (Figure 6.6b) as well as well-defined features now evident in the MSM-Amplitude and MSM Phase channels (Figure 6.6c and Figure 6.6d). Also, Figure 6.6b suggests that these particular sheets are not as rigid as

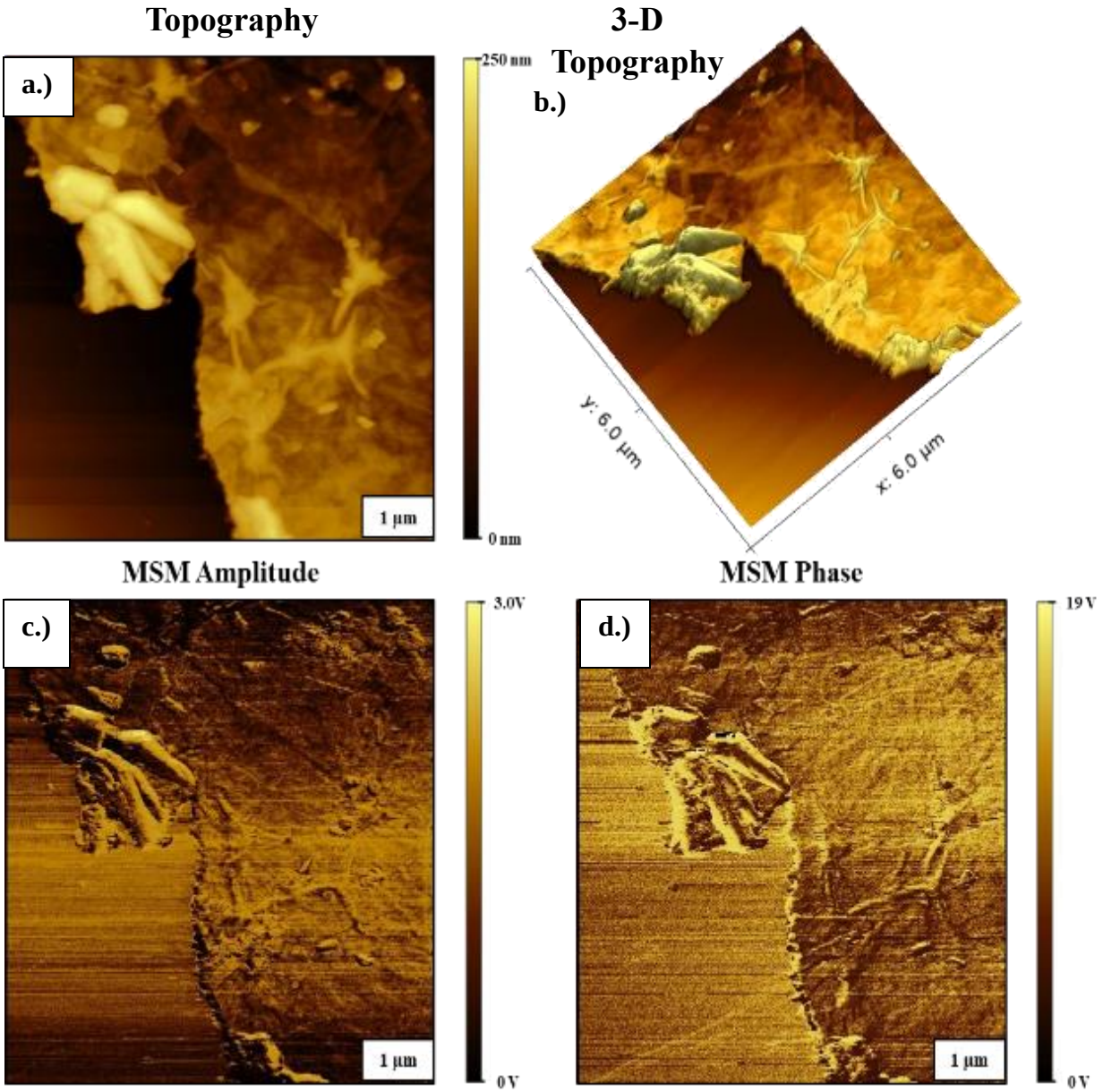

Figure 6.4. AFM images of TBA+-$PrNb_2O_7$ nanosheets captured with MSM-AFM. Electromagnetic Field on, 0.2 T at 240 kHz. (a.) MSM Topography image (6x6 µm^2), (b) 3-D topography images (c.) MSM-amplitude (d.) MSM-phase.

the iron nanosheets due to evidence of slight surface undulations of the sheets. However, as mentioned before, based on the observations in the MSM channels, it is clearly distinguished that the magnetic component of the nanosheets allows for successful surface mapping of the sample when it is modulated within an electromagnetic field.

6.4 Discussion

Novel MSM-AFM approaches have been utilized to image functionalized metal-oxide nanosheets in the presence of an applied electromagnetic field. Imaging is carried out by a soft, non-magnetic silicon nitride AFM tip in contact mode to probe the sample surface in response to the movement of the magnetic material by the electromagnetic field.[9] This technique is ideal for mapping magnetic samples, especially at the nanoscale, because of its high sensitivity for magnetic areas embedded within a sample.

Typical magnetic imaging in atomic force microsocpy is usually carried out by magnetic force microscopy (MFM), however, there are quite a few drawbacks in using this approach for these types of materials. One of the main disadvantages of MFM concerns the tip-sample interaction. The tip for MFM imaging must be magnetic in order to successfully probe the surface of magnetic materials, and the field must be strong enough for z-deflection of the tip to map the surface.[6,9,10] What this means is that detection of the magnetic areas of the sample strongly depend on the size and spring constant of the AFM tip itself. With MSM, this is not the case. In MSM, the magnetic field is applied externally which induces vibration of the magnetic areas of a sample which is then mapped in contact by a non-magnetic tip.[9] Because the tip is in constant contact with the sample, the level of resolution is much higher than that in MFM where the topography resolution is poor on nanomeer sized samples. Therefore, MSM proves to be the best scanning probe technique for mapping the surface of metal-oxide nanosheets.

6.5 Conclusions

Magnetic sample modulation on functionalized metal oxide nanosheets provided interesting insight on the magnetic response of TBA^+-$Ca_2Nb_2FeO_9$ and TBA^+-$PrNb_2O_7$ nanosheets in the presence of an external vibrating magnetic field. Surface characteristics of the nanosheets were also nicely resolved when observing the MSM amplitude and phase images. This scanning probe technique will further add to the library of existing AFM techniques by providing a means for imaging hybrid magnetic samples that exhibit behaviors different from their bulk magnetic counterparts.

6.6 References

(1) Gupta, A.; Sakthivel, T.; Seal, S. Recent development in 2D materials beyond graphene. *Prog. Mater. Sci.* **2015**, *73*, 44–126 DOI: 10.1016/j.pmatsci.2015.02.002.

(2) Tiwari, J. N.; Tiwari, R. N.; Kim, K. S. Zero-dimensional, one-dimensional, two-dimensional and three-dimensional nanostructured materials for advanced electrochemical energy devices. *Prog. Mater. Sci.* **2012**, *57* (4), 724–803.

(3) Akbarian-Tefaghi, S.; Rostamzadeh, T.; Brown, T. T.; Davis-Wheeler, C.; Wiley, J. B. Rapid Exfoliation and Surface Tailoring of Perovskite Nanosheets via Microwave-Assisted Reactions. *ChemNanoMat* **2017**, *3* (8), 538–550 DOI: 10.1002/cnma.201700124.

(4) Liao, J.-W.; Zhang, H.-W.; Lai, C.-H. Magnetic Nanomaterials for Data Storage. *Magn. Nanomater. Fundmental Appl.* **2017**.

(5) Osada, M.; Sasaki, T. Two-Dimensional Dielectric Nanosheets: Novel Nanoelectronics From Nanocrystal Building Blocks. *Adv. Mater.* **2012**, *24* (2), 210–228.

(6) Li, J.-R.; Lewandowski, B. R.; Xu, S.; Garno, J. C. Detecting the Magnetic Response of Iron Oxide Capped Organosilane Nanostructures Using Magnetic Sample Modulation and Atomic Force Microscopy. *Anal. Chem.* **2009**, *81* (12), 4792–4802 DOI: 10.1021/ac900369v.

(7) Grütter, P.; Mamin, H.; Rugar, D. Magnetic force microscopy (MFM). In *Scanning Tunneling Microscopy II*; Springer, 1992; pp 151–207.

(8) Deng, Z.; Yenilmez, E.; Leu, J.; Hoffman, J.; Straver, E. W.; Dai, H.; Moler, K. A. Metal-coated carbon nanotube tips for magnetic force microscopy. *Appl. Phys. Lett.* **2004**, *85* (25), 6263–6265.

(9) Daniels, S. L.; Ngunjiri, J. N.; Garno, J. C. Investigation of the magnetic properties of ferritin by AFM imaging with magnetic sample modulation. *Anal. Bioanal. Chem.* **2009**, *394* (1), 215 DOI: 10.1007/s00216-009-2618-y.

(10) Serem, Wilson K., “Dynamic Measurements with Scanning Probe Microscopy: Surface Studies Using Nanostructured Test Platforms of Metalloporphyrins, Nanoparticles and Amyloid Fibrils” (2011). LSU Doctoral Dissertations. 1417.

(11) Akbarian-Tefaghi, Sara, “Microwave-Assisted Topochemical Manipulation of Layered Oxide Perovskites: From Inorganic Layered Oxides to Inorganic-Organic Hybrid Perovskites and Functionalized Metal-Oxide Nanosheets” (2017). University of New Orleans Theses and Dissertations. 2287.

(12) Klapetek, P.; Necas, D. Gwyddion, Czech Metrology Institute: Czech Republic, 2007.

Chapter 7 Dynamic Lateral Force Modulation Studies of Layered Oxide Nanocomposites

7.1 Introduction

Atomic force microscopy (AFM) is an ever-evolving scanning probe technique which analyzes materials at sub-nanometer levels. Much interest has been drawn to such techniques to study materials at the nanoscale due to AFM's ability to produce high-resolution images along with varying imaging modes to study many kinds of samples. When attempting to utilize regular optical microscopy techniques to study nanomaterials, the resolution is not pristine enough to provide topological enhancements such as that found by AFM techniques.[1] Conversely, when considering electron and X-Ray microscopy techniques, imaging and resolution can be hindered by the property of the material itself.[2] With the evolution of various AFM techniques that focused on obtaining various types of information from samples, it was possible to begin quantifying various parameters of samples at the nanoscale.[3–5]

Nanoscience is an increasing area of curiosity, and finding materials to quantify their strength and durability are of critical interest.[1] Much research to date has been centered around quantifying the bulk counterparts of nanoscale materials, however, little work has been done to quantify materials at the nanoscale. As a response to this limitation, the advancement of the dynamic lateral force modulation (DLFM) technique using AFM began to take shape.[6–8] Research has been done on the elastic modulus of various nanomaterials such as graphene/self-assembled monolayer interfaces,[9] thin films,[7,10] and carbon nanotubes,[11] just to name a few. And, because of investigative studies using these various types of nanomaterials, this was the motivation for quantifying layered oxide nanocomposites utilizing this specific AFM technique.

This chapter was adapted from poster presentation: Treva T. Brown,[1] Sara Akbarian-Tefaghi,[1] Taha Rostamzadeh,[1] Alexis A. Blanco,[1] Zachary L. Highland,[2] Jayne C. Garno,[2] John B. Wiley[1,*] "Nano-Mechanical Properties of Novel Oxide Nanocomposites Using Atomic Force Microscopy". Best Poster Award Nominee. *2017 Materials Research Spring Exhibition, Phoenix, AZ,* April 2017.

7.1.1 Dynamic Lateral Force Microscopy

In dynamic operation modes of scanning probe microscopy, the cantilever is mounted onto a piezoceramic scanning tube, to allow an external excitation of an oscillation, and is deliberately vibrated.[12] When the tip approaches the sample, elastic and inelastic interactions cause a change in both the amplitude and the phase of the cantilever, and are interpreted by the feedback signal.[12] Using force-distance curves taken at the time of scanning, elastic and frictional properties (adhesion) can be measured.[13]

7.2 Experimental

Starting Materials. K_2CO_3 (Alfa Aesar, 99%) and Nb_2O_5 (Alfa Aesar, 99%), tetrabutylammonium hydroxide 30-hydrate (TBAOH, Sigma Aldrich), oleylamine (Sigma Aldrich, 70%), toluene (Sigma Aldrich, anhydrous, 99.8%), hexanes (anhydrous, 95%), cadmium chloride (J.T. Baker Chemical Co.), sulfur (EM Science), silver nitrate (J.T. Baker Chemical Co.), distilled water, and ethanol (Pharmco-Aaper, 200 Proof, absolute).

7.2.1 Hexaniobate Nanocomposites

$K_4Nb_6O_{17}$ Starting Material

$K_4Nb_6O_{17}$ was synthesized by the solid-state reaction of K_2CO_3 and Nb_2O_5 (molar ratio of both syntheses was 1.1:1.5) completed in air at 900 ºC for 1 h with intermediate grinding before further heating at 1050 ºC for 48h. A 10% excess of K_2CO_3 was added to compensate for the volatilization of potassium oxide during the heating process.[14,15] The resulting product was washed twice with distilled water to remove any excess reagents, centrifuging the sample for 10 minutes each time, followed by one 5-minute centrifugation with 15 mL of acetone. Finally, the sample was dried overnight at 70 ºC.

Acid exchange of $K_4Nb_6O_{17}$

The proton-exchange form of $K_4Nb_6O_{17}$ to form $H_xK_{4-x}Nb_6O_{17}$ was obtained by the solvothermal method in which 0.5 g of hexaniobate was treated with 5 mL of 6 M HNO_3 and placed into a Teflon-lined stainless-steel autoclave (Parr, model 4749, 1800 psi, 23 mL). The autoclave was heated to 90 ºC, held at that temperature for 48 h, and then cooled to room temperature. The resulting product was washed twice with distilled water to remove any excess reagents, centrifuging the sample for 10 minutes each time, followed by one 5-minute centrifugation with 15 mL of acetone. The product was then dried overnight at 70 ºC.

Preparation of Intercalated Multi-Walled Nanoscrolls (INS)

Nanoscroll formation was achieved by solvothermal synthesis in a method similar to what has been previously reported by our group.[14] Solvothermally, a solution of $H_xK_{4-x}Nb_6O_{17}$ (0.1 g), TBAOH (19 mmol), and 5 mL oleylamine (~15 mmol) in 9 mL toluene was prepared and magnetically stirred for 1hr before transferring into a Teflon-lined stainless-steel autoclave (Parr, model 4749, 1800 psi, 23 mL). The autoclave was then kept at 220 ºC for 6 h and cooled to room temperature thereafter. The product was centrifuged to remove the supernatant, then purified by centrifugation in 30 mL of ethanol for 20 minutes with intermediate cycles of ultrasonic treatment. The nanoscrolls were then re-dispersed in toluene.

Amine-functionalized Nanosheet Synthesis

Amine-functionalized nanosheet samples for this study were acquired from Dr. Sara Akbarian-Tefaghi. Experimental details can be found referenced in Chapter 4 and Chapter 6 of "Microwave-Assisted Topochemical Manipulation of Layered Oxide Perovskites: From Inorganic Layered Oxides to Inorganic-Organic Hybrid Perovskites and Functionalized Metal-

Oxide Nanosheets" [16]. The experimental details have also been documented in publications by Akbarian-Tefaghi et al.[17,18]

Silver Nanocomposite Synthesis

Nanopeapods containing Ag nanoparticles (NPs) were synthesized in a one-pot synthesis (three neck flask outfitted with a thermocouple and heating mantle) outlined by Dr. Shiva Adireddy.[19] The NPs were combined with hexaniobate nanosheets under two different reaction conditions. Ag NPs either attached to the surfaces of nanosheets at a reaction temperature of 180 °C for 6 h or Ag NPs produced NPP structures at 220 °C for 6 h with the addition of oleylamine, toluene, and oleic acid (same amounts outlined in Chapter 1). The resulting products were washed with ethanol and re-dispersed in toluene.

7.2.2 Preparation of Substrates

Piranha Etching. In a 50-mL glass jar, eight substrates, initially cleaned with ethanol and milli-Q water, were placed at the bottom of the jar equally spaced apart. Then, 6 mL of H_2SO_4 was added followed by 2 mL of H_2O_2. **(CAUTION! Reaction must be completed under the hood).** The substrates were left in this solution for 2 hours before being removed and washed with excessive ethanol and deionized water. The substrates were then dried with a slow and study flow of nitrogen. Samples were then drop cast onto the freshly etched silicon substrates and allowed to dry in an oven for 24 hours at 70º C.

7.2.3 Characterization

A Keysight 5500 SPM system equipped with a multipurpose AFM scanner (Keysight Technologies, Inc., Santa Rosa, CA) was used for surface characterizations at Louisiana State University in Baton Rouge, LA. Picoscan v1.20 software was used for data acquisition. Dynamic

Lateral Force Modulation (DLFM)-AFM was performed by measuring the deflection of the AFM tip in the x-direction instead of the standard z-direction as done in conventional modes of AFM. Silicon nitride cantilevers (SSS-NCH50, resonance frequency of 330 kHz) purchased from NanoSensors (Tempe, AZ), were used for DLFM imaging. In-situ images were processed with Gwyddion[20] open-source software (Czech Metrology Institute, http://gwyddion.net/) version 2.47, 64-bit. Transmission electron microscopy (TEM) images were acquired by a JEOL 2010 high-resolution microscope powered by an operating voltage of 200 keV and equipped with a Gatan slow scan charge-coupled device (CCD) camera.

7.3 Results and Discussion

Various interactions such as amplitude, phase shift and cantilever deflection allow for atomic resolution imaging due to tip-sample interaction. Shown in Figure 7.1 are stacked layers of hexaniobate nanosheets which are not easily seen in conventional imaging modes of AFM. The island observed in the AFM images (denoted by the blue boxes) are indicative of stacked hexaniobate nanosheets as one would observe under field-emission scanning electron

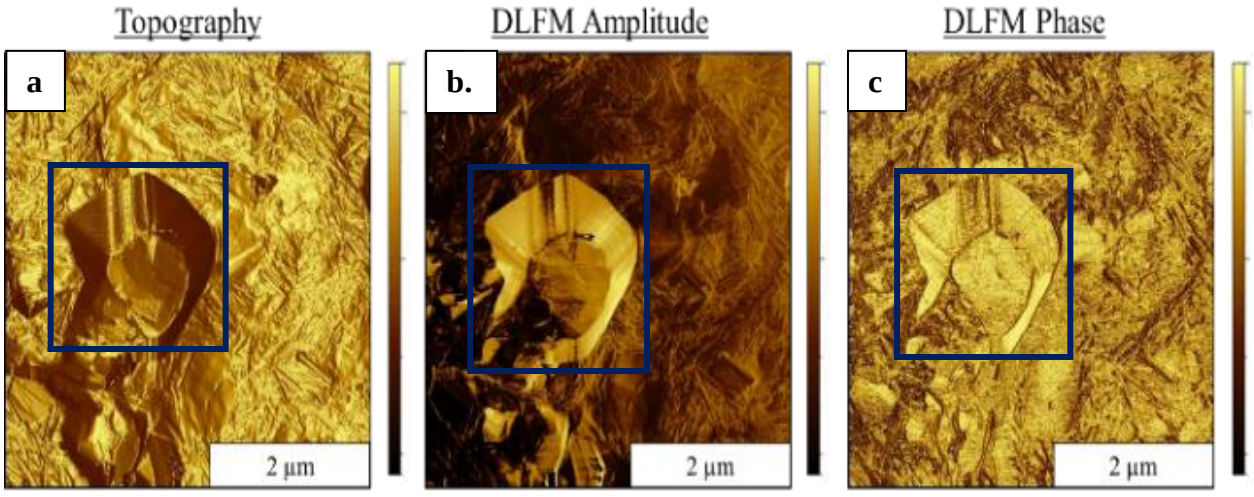

Figure 7.1. AFM images in DLFM mode of stacked layers of hexaniobate nanosheets not easily seen in conventional imaging modes of AFM. (a) 10 x10µm^2 topography image (b) corresponding DLFM amplitude image (c) corresponding DLFM phase image.

microscopy (FE-SEM) as shown in Figure 7.2. Moreover, DLFM phase imaging provides for complementary information to the topography channel. For example, in the DLFM phase image in Figure 7.3, it is easy to observe a nanoscroll atop of a clearly defined nanosheet which is not easily observed in the topography image (denoted by blue boxes).

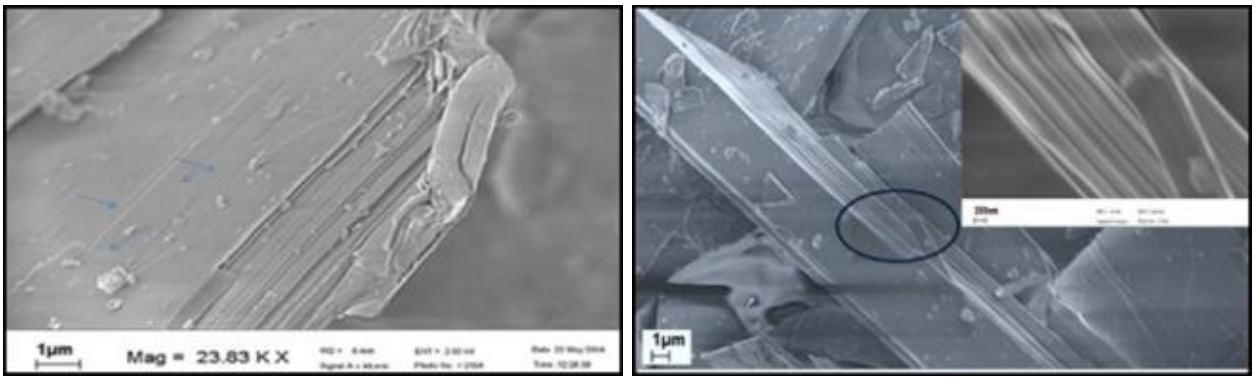

Figure 7.3. FE-SEM images of multi-lamellar hexaniobate nanosheets.

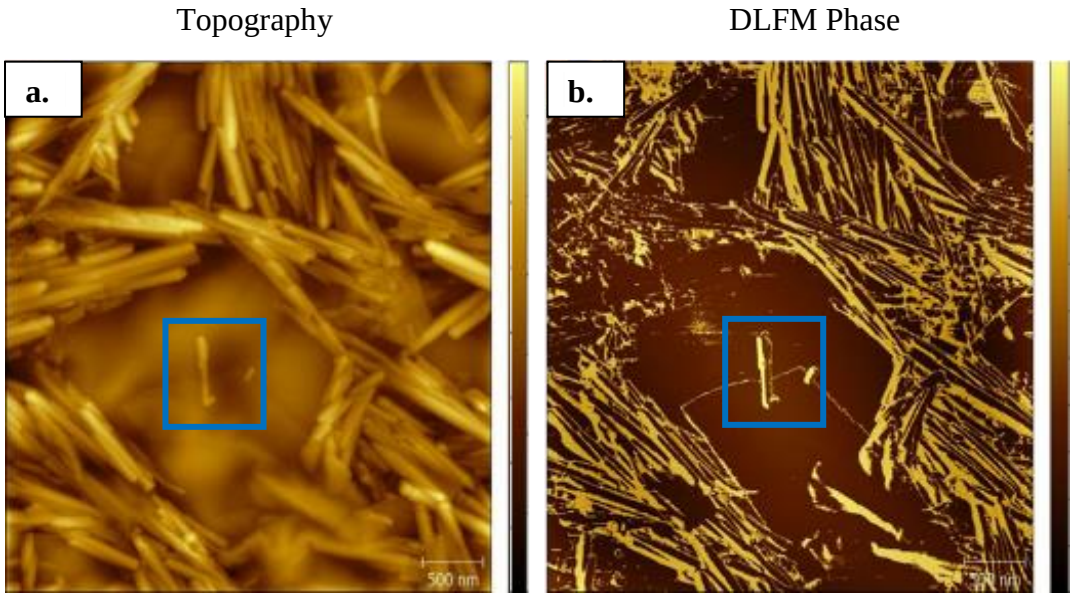

Figure 7.2. 4 x 4 µm^2 DLFM images of intercalated nanoscrolls. DLFM phase imaging provides complementary information to the topography imaging. Pictured here is a nanoscroll atop of a nanosheet easily observed in the DLFM phase image. (a) DLFM Topography image. (b)DLFM phase image.

Information can also be gained from the differences in contrast in the DLFM amplitude and phase images. Changes in contrast for the DLFM amplitude image shows differences in surface modulus of a sample, and in DLFM phase, the contrast shows differences in

viscoelasticity. Figure 7.4 is also a good example for the observation of varying contrast. In these images, DLFM amplitude displays areas of surface adhesion (dark areas) and friction (light areas), whereas DLFM phase shows areas of elasticity (elastic vs. viscoelastic properties). Another interesting feature detected by DLFM is seen in Figure 7.5. In hexaniobate nanoscrolls, an interesting step-like morphology (telescoping) has been observed among several different nanoscroll samples which is perceived to be a result of the scrolling of uneven nanosheets.

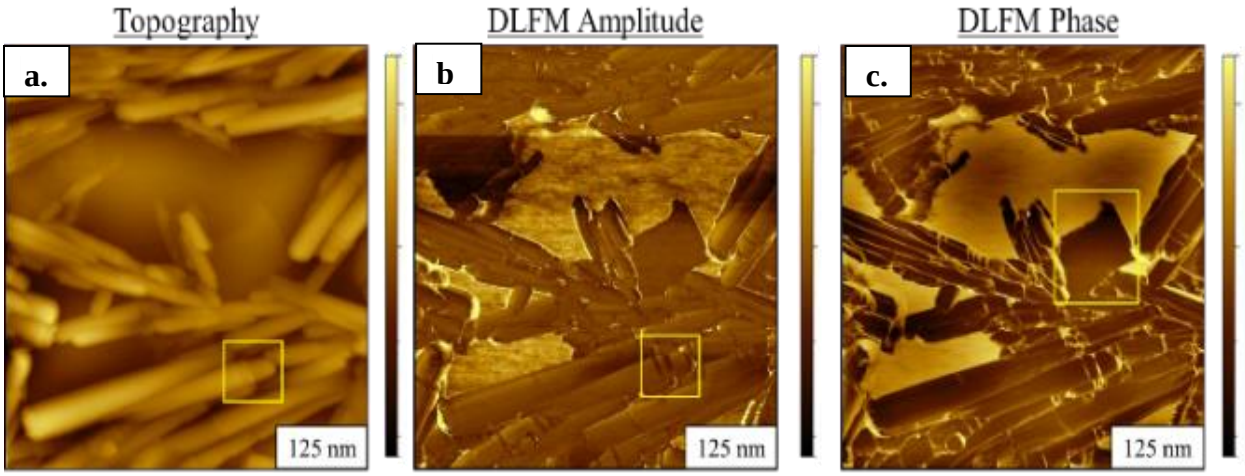

Figure 7.4. 2 x 2 μm^2 DLFM images of intercalated hexaniobate nanoscrolls. (a) Topography image showing the presence of a telescoping nanoscroll denoted by the yellow square (b) corresponding DLFM amplitude image showing surface modulus differences (c) corresponding phase image.

DLFM has shown promising results for the aforementioned nanocomposite structures. As a result, further work was continued to characterize nanocomposites quantitatively by investigating mechanical properties such as Young's Modulus on Ag-decorated nanosheets, Ag@hexaniobate nanopeapods, and amine-functionalized nanosheets. Figure 7.6 shows DLFM images of silver decorated nanosheets with their corresponding TEM images. It is interesting to see in the DLFM phase image (Figure 7.6f), features that resemble the silver nanoparticles atop the hexaniobate sheet as seen in the TEM images (Figure 7.6 a-c). These features can also be seen in Figure 7.7b and 7.7c when observing Ag@hexaniobate nanopeapods. Figure 7.8 displays amine-functionalized nanosheets. Under DLFM investigation, the nanosheets exhibit interesting

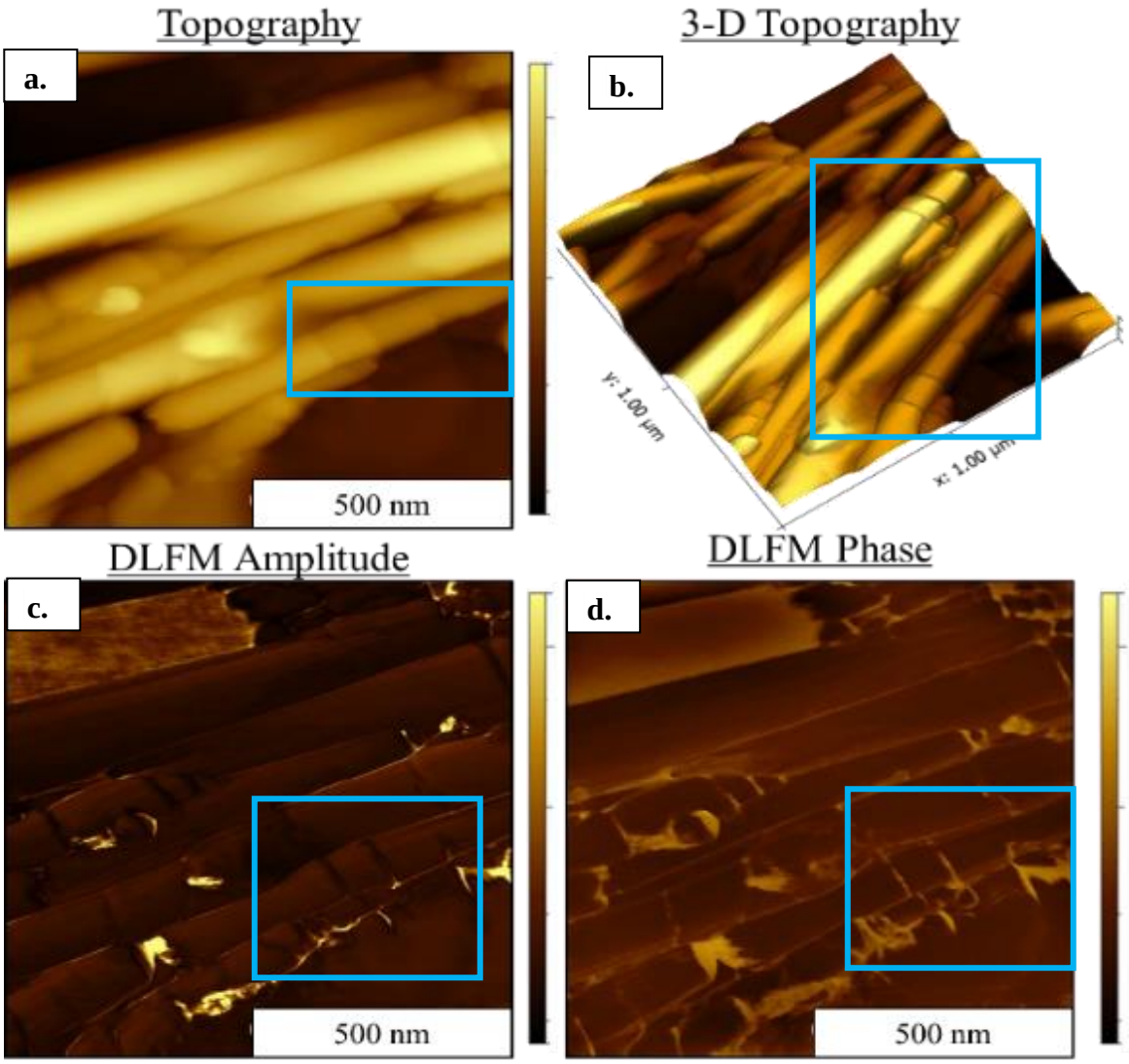

Figure 7.5. 1 x 1 µm^2 DLFM images of hexaniobate intercalated nanoscrolls showing telescoping effects. (a) Topography image showing the presence of a telescoping nanoscroll (b)corresponding 3D topography image (c) corresponding DLFM amplitude image (d) corresponding phase image.

features such as small islands on the surface of the sheets, along with great contrast that distinguishes the inhomogeneity of the individual sheets. Such observations are made possible due to the latitudinal torsional twisting of the AFM tip in DLFM mode which is not possible in conventional AFM imaging modes.

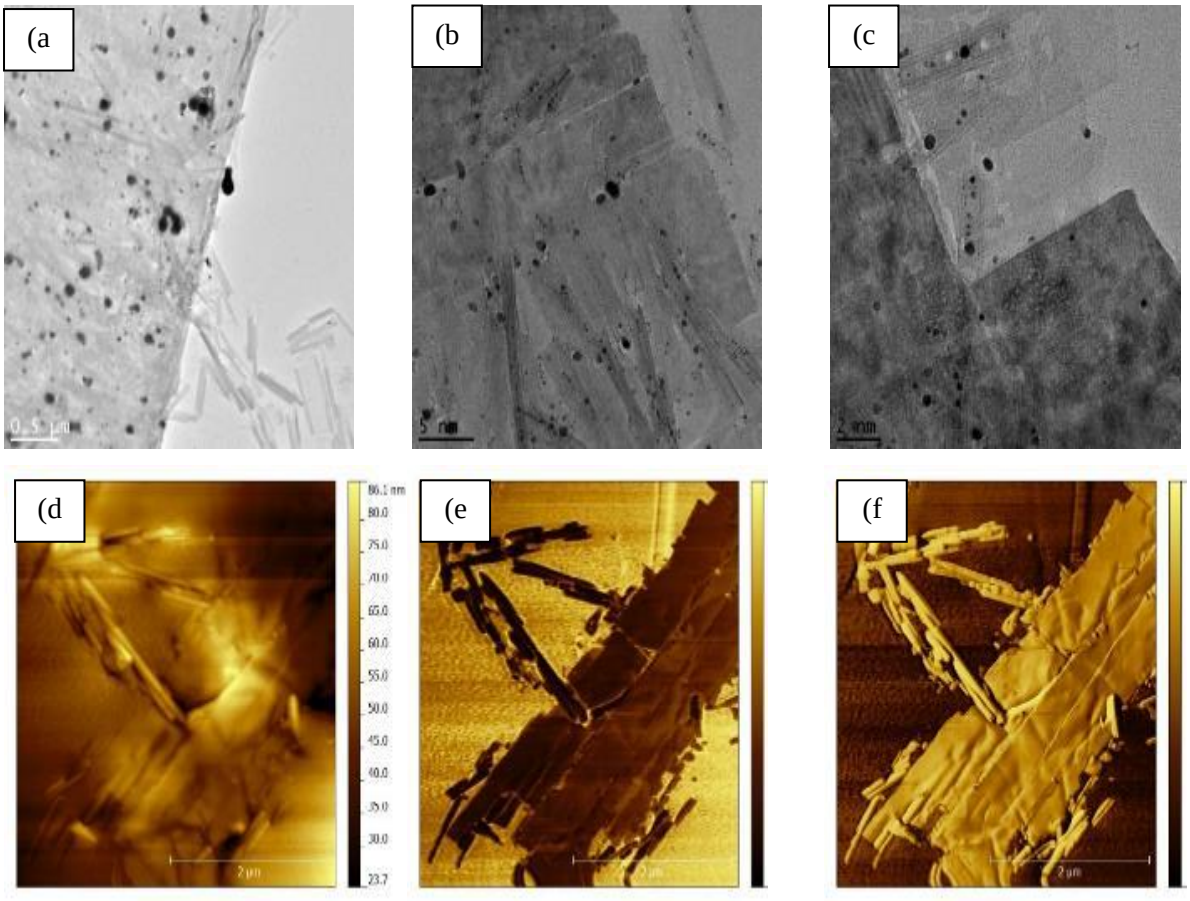

Figure 7.6. (a-c) Transmission Electron Microscopy images of Ag-decorated nanosheets and nanopeapods. (d) DLFM topography image of Ag decorated nanosheets and nanopeapods. (e) DLFM amplitude image corresponding to (d). (f) DLFM phase image corresponding to (d).

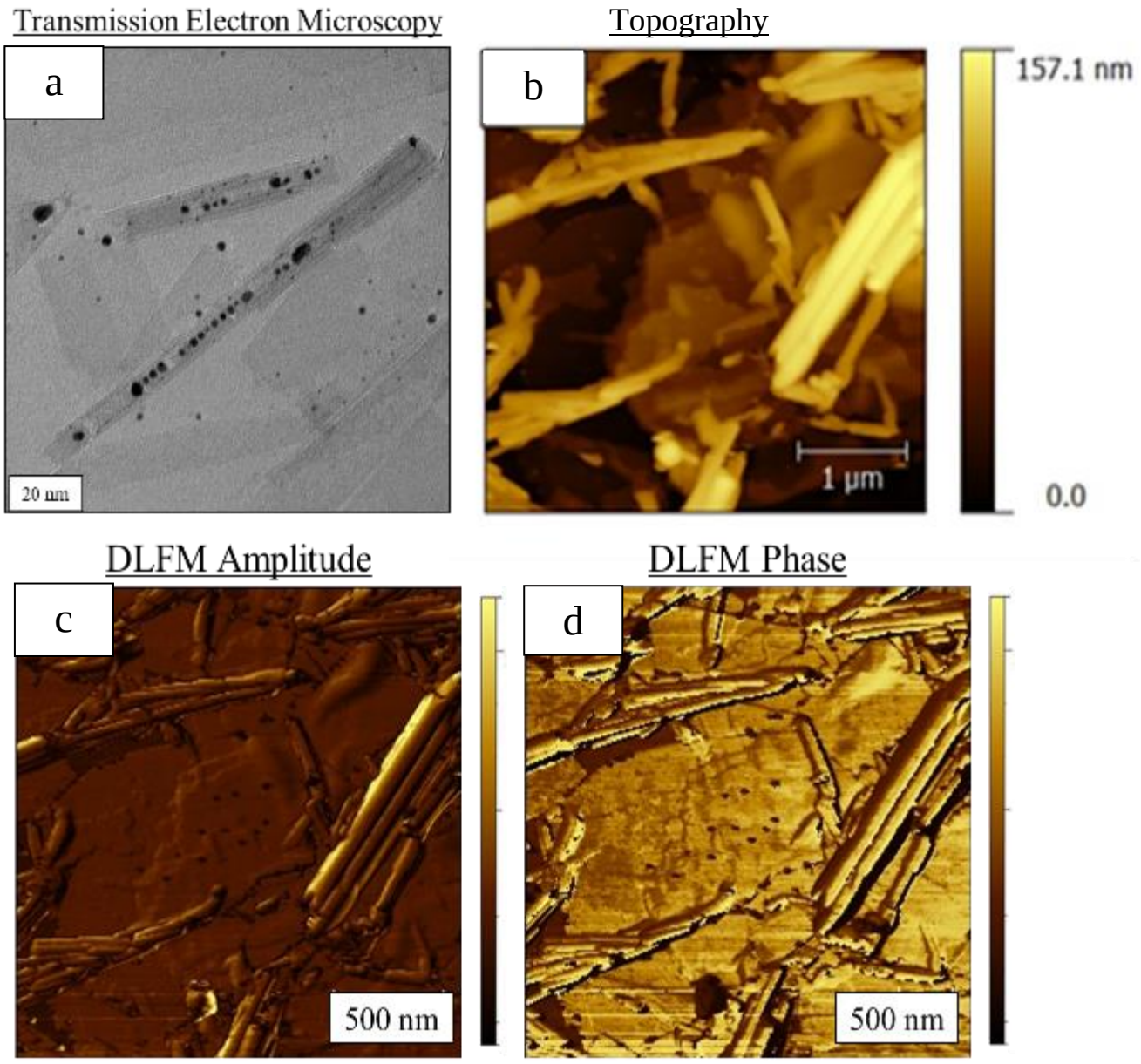

Figure 7.7. (a) TEM images of Ag-decorated nanosheets and nanopeapods. (d) DLFM topography image of Ag-decorated nanosheets and nanopeapods. (e) DLFM amplitude image corresponding to (d). (f) DLFM phase image corresponding to (d). AFM image size 2x2 µm^2.

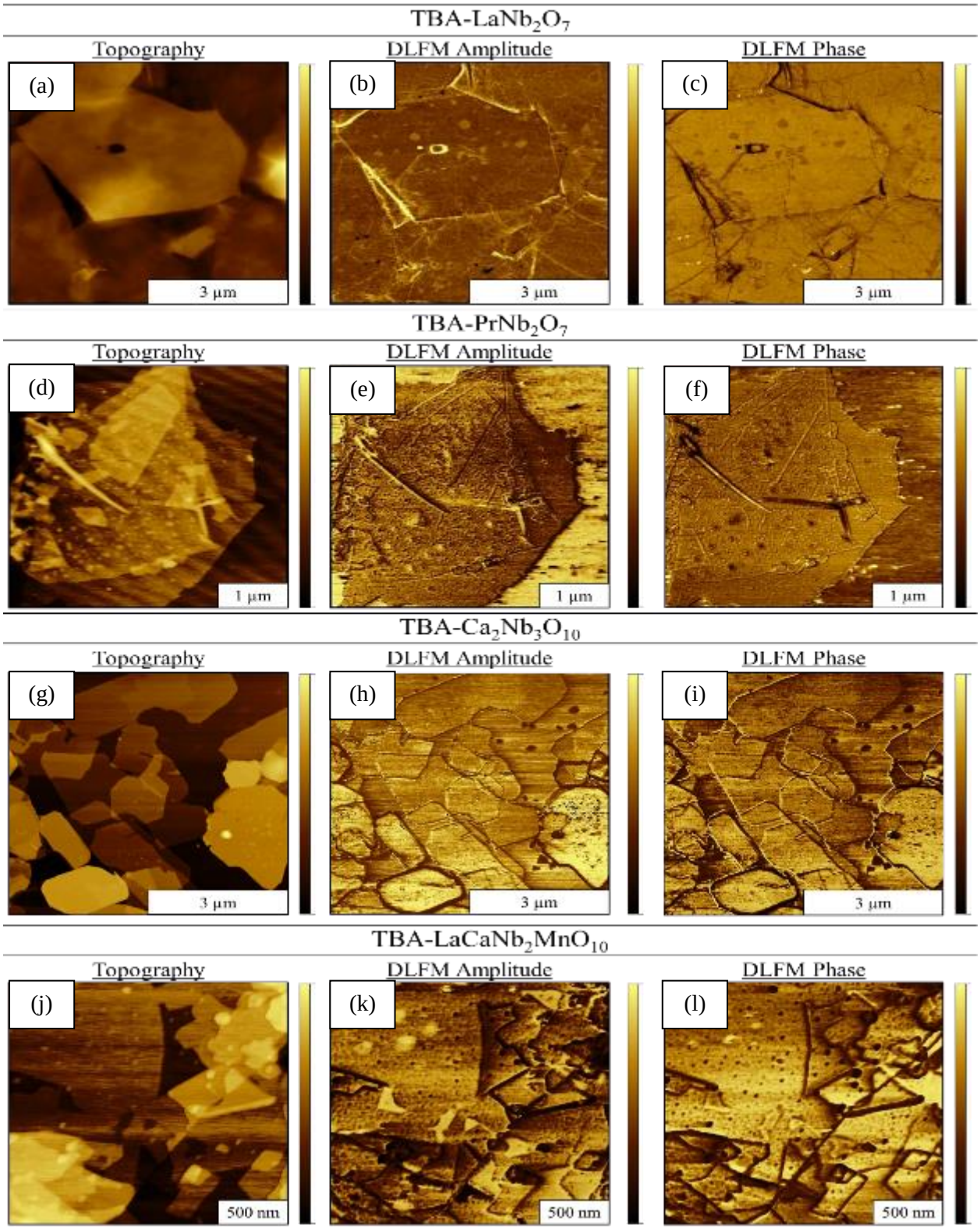

Figure 7.8. DLFM images of amine-functionalized nanosheets(a-c) 6x6 µm^2 images of TBA-$LaNb_2O_7$ nanosheets (d-f) 4x4 µm^2 images of TBA-$PrNb_2O_7$ nanosheets (g-i) 6x6 µm^2 images of TBA-$Ca_2Nb_3O_{10}$ nanosheets (j-l) 2x2 µm^2 images of TBA-$LaCaNb_2MnO_{10}$ nanosheets.

Measuring Mechanical Properties via DLFM

The mechanical properties of layered oxide nanocomposites are of interest because these measurements can help answer questions surrounding the scrolling phenomenon of hexaniobate and its respective nanocomposites along with studying the rigidity of functionalized nanosheets and other layered oxide nanocomposites. Furthermore, it may be possible to determine properties applicable to creating 3-dimensional nanoarchitectures for use in various nanomechanical materials and applications. Thus far, results for hexaniobate nanosheets before exfoliation, intercalated nanoscrolls, amine-functionalized nanosheets, silver-decorated nanosheets, and silver nanopeapods have been gathered from various force-distance curves acquired *in situ* (Figure 7.9) for quantitative measurements and are tabulated in Table 1. Variables determined from the force-distance curves were stiffness (rigidity of object), indentation (resistance to mechanical deformation), and Young's Modulus (ratio of stress to strain along an axis).[21]

Material	Stiffness (N/m)	Indentation (nm)	Young's Modulus (GPa)
$H_xK_{4-x}Nb_6O_{17}$ nanosheets	10(5) x 10^{-6}	16(2)	-110(4)
Hexaniobate nanoscrolls	11(1) x 10^{-6}	21(2)	-90(6)
Amine-functionalized nanosheets*	11(6) x 10^{-3}	11(1)	-110(3)
Ag decorated hexaniobate nanosheets	10(6) x 10^{-6}	18(1)	-140(5)
Ag@hexaniobate nanopeapods	10(6) x 10^{-6}	0.3(3)	-140(2)

Table 1. Stiffness, indentation, and elastic modulus are acquired simultaneously in real-time during scanning. While the XY scanner stops, the high-speed force-distance curves are taken with well-defined control of contact force and contact time between the tip.

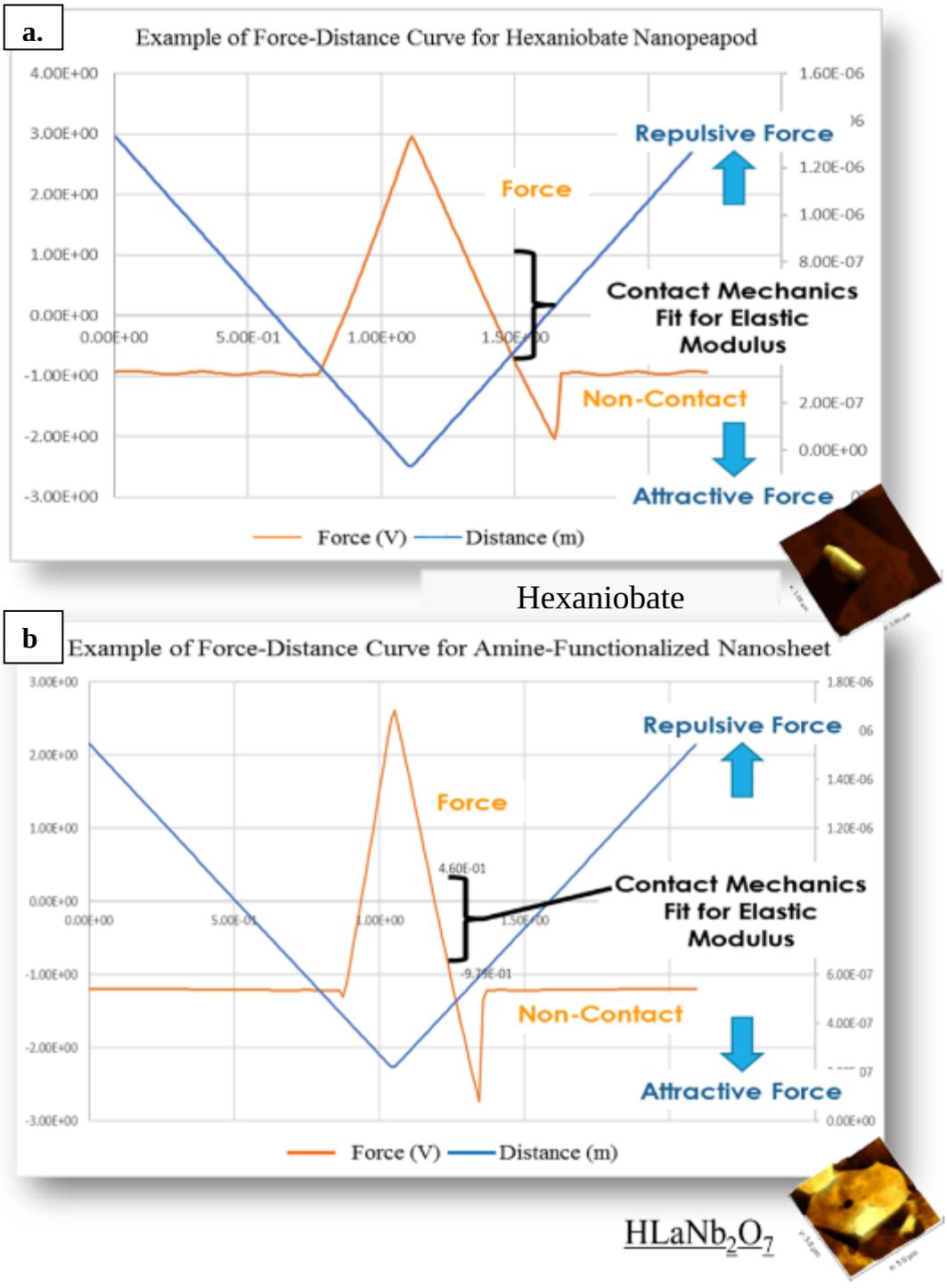

Figure 7.9. Representative force distance curves acquired from DLFM scans of (a)intercalated hexaniobate nanoscrolls and (b)amine functionalized nanosheets.

It is hypothesized that the surface functionalization of the amine-functionalized nanosheets compared to the other tested nanocomposites with TBAOH may be causing such an

outlier of a measurement regarding the stiffness measurement. If this is the case, it is possible that this would also provide a reason as to why the young's modulus measurement is also slightly larger. These materials were tested a significant number of times; however, more trials should be considered since this a novel method for these types of composites. Moreover, when considering the results obtained from the experiments in situ, the measurements generated were compared to the closest material that was tested similarly in literature.[22] Literature for similarly arranged nanocomposites have shown a Young's Modulus of ~140 GPa, as shown in graphene oxide scrolls such as those reported by K. Yao et al., showing some correlation to our results found thus far.[22] This is an ever-growing area of interest for our group, and it is my suggestion that this data be expound upon by testing other nanocomposites synthesized within our group to gain a better understanding of the qualitative data being acquired.

7.4 Conclusions

DLFM has allowed for a new characterization tool to use in conjunction with already existing characterization methods. With promising results found through DLFM, further work will be continued to characterize hexaniobate nanocomposites quantitatively by investigating mechanical properties such as Young's Modulus and frictional coefficients. Studies have already expanded into other hexaniobate nanopeapod systems such as Ag@hexaniobate nanosheets and nanopeapods (Figures 7.6 and 7.7) as well as other systems currently being developed within the group. These studies will aid in creating a library of characteristics to distinguish between varying nanomechanical properties of hexaniobate nanocomposites for further nanoscale applications.

7.5 References

(1) Withers, J. R.; Aston, D. E. Nanomechanical measurements with AFM in the elastic limit. *Adv. Colloid Interface Sci.* **2006**, *120* (1), 57–67 DOI: 10.1016/j.cis.2006.03.002.

(2) Hetherington, C. Aberration correction for TEM. *Mater. Today* **2004**, *7* (12), 50–55 DOI: 10.1016/S1369-7021(04)00571-1.
(3) Binnig, G.; Quate, C. F.; Gerber, C. Atomic Force Microscope. *Phys. Rev. Lett.* **1986**, *56* (9), 930–933.
(4) Stark, M.; Stark, R. W.; Heckl, W. M.; Guckenberger, R. Spectroscopy of the anharmonic cantilever oscillations in tapping-mode atomic-force microscopy. *Appl. Phys. Lett.* **2000**, *77* (20), 3293–3295 DOI: 10.1063/1.1325404.
(5) Salapaka, S. M.; Salapaka, M. V. Scanning probe microscopy. *IEEE Control Syst.* **2008**, *28* (2), 65–83.
(6) Kazushi Yamanaka and Eisuke Tomita. Lateral Force Modulation Atomic Force Microscope for Selective Imaging of Friction Forces. *Jpn. J. Appl. Phys.* **1995**, *34* (5S), 2879.
(7) Maivald, P.; Butt, H.; Gould, S.; Prater, C.; Drake, B.; Gurley, J.; Elings, V.; Hansma, P. Using force modulation to image surface elasticities with the atomic force microscope. *Nanotechnology* **1991**, *2* (2), 103.
(8) Syed Asif, S.; Wahl, K.; Colton, R.; Warren, O. Quantitative imaging of nanoscale mechanical properties using hybrid nanoindentation and force modulation. *J. Appl. Phys.* **2001**, *90* (3), 1192–1200.
(9) Elinski, M. B.; Menard, B. D.; Liu, Z.; Batteas, J. D. Adhesion and Friction at Graphene/Self-Assembled Monolayer Interfaces Investigated by Atomic Force Microscopy. *J. Phys. Chem. C* **2017**, *121* (10), 5635–5641 DOI: 10.1021/acs.jpcc.7b00012.
(10) Friedenberg, M. C.; Mate, C. M. Dynamic Viscoelastic Properties of Liquid Polymer Films Studied by Atomic Force Microscopy. *Langmuir* **1996**, *12* (25), 6138–6142 DOI: 10.1021/la960331i.
(11) Makoto Ashino and Alexander Schwarz and Hendrik Hölscher and Udo D Schwarz and Roland Wiesendanger. Interpretation of the atomic scale contrast obtained on graphite and single-walled carbon nanotubes in the dynamic mode of atomic force microscopy. *Nanotechnology* **2005**, *16* (3), S134.
(12) Giessibl, F. J. Advances in atomic force microscopy. *Rev. Mod. Phys.* **2003**, *75* (3), 949–983.
(13) http://www.parkafm.com/index.php/park-spm-modes/91-standard-imaging-mode/222-lateral-force-microscopy-lfm.
(14) Adireddy, S.; Yao, Y.; He, J.; Wiley, J. B. Rapid solvothermal fabrication of hexaniobate nanoscrolls. *Mater. Res. Bull.* **2013**, *48* (9), 3236–3241 DOI: 10.1016/j.materresbull.2013.04.090.
(15) Saupe, G. B.; Waraksa, C. C.; Kim, H.-N.; Han, Y. J.; Kaschak, D. M.; Skinner, D. M.; Mallouk, T. E. Nanoscale Tubules Formed by Exfoliation of Potassium Hexaniobate. *Chem. Mater.* **2000**, *12* (6), 1556–1562 DOI: 10.1021/cm981136n.
(16) Akbarian-Tefaghi, Sara, "Microwave-Assisted Topochemical Manipulation of Layered Oxide Perovskites: From Inorganic Layered Oxides to Inorganic-Organic Hybrid Perovskites and Functionalized Metal-Oxide Nanosheets" (2017). University of New Orleans Theses and Dissertations. 2287.
(17) Akbarian-Tefaghi, S.; Rostamzadeh, T.; Brown, T. T.; Davis-Wheeler, C.; Wiley, J. B. Rapid Exfoliation and Surface Tailoring of Perovskite Nanosheets via Microwave-Assisted Reactions. *ChemNanoMat* **2017**, *3* (8), 538–550 DOI: 10.1002/cnma.201700124.

(18) Akbarian-Tefaghi, S.; Teixeira Veiga, E.; Amand, G.; Wiley, J. B. Rapid Topochemical Modification of Layered Perovskites via Microwave Reactions. *Inorg. Chem.* **2016**, *55* (4), 1604–1612 DOI: 10.1021/acs.inorgchem.5b02514.
(19) Adireddy, Shivaprasad Reddy, "High Yield Solvothermal Synthesis of Hexaniobate Based Nanocomposites via the Capture of Preformed Nanoparticles in Scrolled Nanosheets" (2013). University of New Orleans Theses and Dissertations. Paper 1726.
(20) Klapetek, P.; Necas, D. Gwyddion, Czech Metrology Institute: Czech Republic, 2007.
(21) http://www-materials.eng.cam.ac.uk/mpsite/properties/non-IE/stiffness.html.
(22) Yao, K.; Manjare, M.; Barrett, C. A.; Yang, B.; Salguero, T. T.; Zhao, Y. Nanostructured Scrolls from Graphene Oxide for Microjet Engines. *J. Phys. Chem. Lett.* **2012**, *3* (16), 2204–2208 DOI: 10.1021/jz300749p.

Chapter 8 Concluding Remarks

This dissertation emphasizes the use of microwave-assisted synthetic methods to form hexaniobate nanoscrolls and nanopeapods as well as exploiting the various modes of atomic force microscopy (AFM) to investigate the topological and physical properties of such structures. The investigation of the protonation and scrolling processes was carried out via benchtop, solvothermal, and microwave approaches to determine which synthetic method proved to be most effective at synthesizing hexaniobate nanoscrolls. It was determined that microwave assisted approaches lead to the production of high quality intercalated nanoscrolls and hexaniobate nanopeapods in a rapid time frame (< 3 hours) with topological and morphological characteristics similar to nanocomposites synthesized via benchtop and solvothermal methods. Using microwave irradiation techniques provides a new method for fabricating nanopeapod structures with the advantage of rapid synthesis time, less product waste, the ability to combine nanoparticle and nanosheet components separately, and ease of expansion to other nanoparticle encapsulation systems. The effectiveness of this method is confirmed by TEM observations of microwave-assisted nanocomposites systems. These nanocomposites are important for future nanotechnology applications. Furthermore, these findings contribute to the already existing library of layered oxide nanocomposites previously synthesized by our group.

Atomic Force Microscopy (AFM) was used extensively as a characterization method for these nanomaterials both qualitatively and quantitatively. Due to the continued advancements of atomic force microscopes, techniques such as dynamic lateral force modulation (DLFM) and magnetic sampling modulation (MSM) have allowed for the investigation of physical and dynamic properties of various types of samples, including layered oxide nanocomposites as discussed in this work. Furthermore, atomic force microscopes can aid in the advancement of

knowledge surrounding the morphology of these materials via nanomanipulation and achieved with the AFM tip. For example, DLFM characterization allowed for the investigation of mechanical properties such as Young's Modulus and frictional coefficients with studies expanded into various hexaniobate nanopeapod systems These studies will aid in creating a library of characteristics to distinguish between varying nanomechanical properties of hexaniobate nanocomposites for further nanoscale applications. Moreover, magnetic sample modulation on functionalized metal oxide nanosheets provided interesting insight on the magnetic response of TBA^+-functionalized metal oxide nanosheets in the presence of an external vibrating magnetic field. Surface characteristics of the nanosheets were nicely resolved when observing the MSM amplitude and phase images. The MSM scanning probe technique will further add to the library of existing AFM techniques by providing a means for imaging hybrid magnetic samples that exhibit behaviors different from their bulk magnetic counterparts.

Overall, the material presented in this dissertation will add to our continued exploration of the inherent properties of layered oxide nanostructures. By applying AFM techniques to these systems, the quantitative data obtained from the structures will lead to a better understanding of those factors important in the formation of various nanomechanical architectures. Moreover, the use of microwave-assisted synthetic protocols will allow for rapid fabrication of said nanostructures which can be expanded to synthesize a wide array of these types of nanocomposites. It is expected that this area of research will continue to play a critical role in the future of materials studies, nanotechnology, and the study of magnetic behaviors of nanomaterials.

Vita

The author of this work was born and raised in North Baton Rouge, Louisiana. She attended Louisiana State University in Baton Rouge, LA where she obtained her Bachelor of Science degree in Chemistry in 2011. She then joined University of New Orleans as a Louisiana Board of Regents Graduate Fellow to pursue a PhD in Chemistry. She became a member of Professor John B. Wiley's group in 2012.